UNIVERSITY OF CALIFORNIA,
IRVINE

Novel Multimodal Bio-Signal Acquisition Systems for Adult and Embryonic Zebrafish

DISSERTATION

submitted in partial satisfaction of the requirements
for the degree of

DOCTOR OF PHILOSOPHY

in Biomedical Engineering

by

Ramses Seferino Trigo Torres

Dissertation Committee:
Professor Hung Cao, Chair
Professor Andrei Shkel
Professor James Brody

2024

DEDICATION

To

my wife, who has unwaveringly stood by my side throughout this entire journey,

my grandparents, who inspired me and motivated me to pursue this field,

my parents, who wholeheartedly supported me in pursuing my dreams,

and my brother, for his unwavering support.

TABLE OF CONTENTS

Page

LIST OF FIGURES vii

LIST OF TABLES viii

ACKNOWLEDGEMENTS ix

VITA x

ABSTRACT OF THE DISSERTATION xii

CHAPTER 1: Motivation 1
- 1.1 Cardiovascular Diseases 1
- 1.2 Contributions and Impact 2
- 1.3 Dissertation Outline 4

CHAPTER 2: Animal Models in Cardiovascular Research 6
- 2.1 Introduction 6
- 2.2 Popular Models for Cardiovascular Research 6
- 2.3 Why Zebrafish? 7

CHAPTER 3: Electrophysiology and Diagnostic Imaging Tests 14
- 3.1 Introduction 14
- 3.2 Electrocardiogram in Zebrafish 16
- 3.3 Diagnostic Imaging for Cardiovascular Studies 17
  - 3.3.1 Echocardiogram (ECHO) in Adult Zebrafish 17
  - 3.3.2 Heart Beating Videos in Embryonic Zebrafish 18
- 3.4 Machine Learning in Diagnostic Imaging in Zebrafish 19

CHAPTER 4: Consecutive Treatments of Methamphetamine Promote the Development of Cardiac Pathological Symptoms in Zebrafish 20
- 4.1 Introduction 20
- 4.2 Methodology 23
  - 4.2.1 Zebrafish Husbandry and Preliminary Surgical Procedures 23
  - 4.2.2 Drug Preparation and Methamphetamine Treatment 24
  - 4.2.3 ECG Recording Procedure and Instrumental Setup 25
  - 4.2.4 ECG Data Collection and Analysis 27
  - 4.2.5 Isolation of Zebrafish Cardiomyocytes 28
  - 4.2.6 Cloning, Cell Culture and Transfection 29
  - 4.2.7 GloSensor cAMP Assay 29
  - 4.2.8 FLIPR Calcium Assay 30
  - 4.2.9 Collagen Assay 31

4.2.10 Histochemical Staining and Immunofluorescent Staining for Collagen 31
4.2.11 Statistical Analysis 32
4.3 Results 32
4.3.1 Methamphetamine Induced Significant ECG Changes Over the Course of 2 Weeks 32
4.3.2 Methamphetamine Treatment Leads to Increased Expression of cAMP and Ca^{2+} in a TAAR1-mediated, Dose-Dependent Manner 36
4.3.3 Methamphetamine Treatment Produce Excessive Fibrosis in Zebrafish Cardiac Tissue 37
4.4 Discussion 39
4.5 Conclusion 47

CHAPTER 5: Development of Zebrafish ECG System for Extended Measurement for Drug Screening and Genetic Functional Analysis 48
5.1 Introduction 48
5.2 Materials and Methods 51
5.2.1 Mutant Tg(SCN5a-D1275N) and Zebrafish Husbandry 51
5.2.2 Design and Validation of the Zebra II System 52
5.2.3 Signal Processing and Statistics 57
5.3 Results and Discussion 58
5.3.1 Multiple Zebrafish ECG Acquisition with Zebra II 58
5.3.2 Investigation of Side Effects of Tricaine and Variable Temperature Cardiac Rhythm 62
5.3.3 Response Analysis to Drug Treatment in Real Time with the Zebra II System 63
5.3.4 Evaluation of High Sodium Intake in the Development of Sinus Arrest (SA) in Tg(SCN5A-D1275N) 65
5.3.5 Rescue of Arrhythmic Phenotypes Induced by High Sodium Intake in Tg(SCN5A-D1275N) Fish 68
5.4 Conclusion 69

CHAPTER 6: Zebra II as a Novel System to Record Electrophysiological Signals in Zebrafish 70
6.1 Introduction 70
6.2 Methods 74
6.2.1 Fish Husbandry 74
6.2.2 Fish Preparation and Amiodarone Treatement 74
6.2.3 Electrode Positioning and ECG Collection 74
6.2.4 Troubleshooting the Four Electrode Array Positioning System 74
6.2.5 Extracting and Analyzing Data 75
6.3 Results 75
6.4 Discussion 80

CHAPTER 7: Electrocardiogram Assessment in Doxorubicin Induced Cardiomyopathy in Adult Zebrafish 82

7.1 Introduction 82
7.2 Methodology 83
7.2.1 DOX Preparation 83
7.2.2 Zebrafish Selection and Sorting 83
7.2.3 Pre-Injection Preparation 84
7.2.4 IP DOX Injection Procedure 84
7.2.5 Post-Injection Fish Management 86
7.2.6 ECG Data Collection 86
7.2.7 Troubleshooting the Four-Electrode Array Positioning System 86
7.2.8 Extracting and Analyzing Data 87
7.3 Results 87
7.4 Discussion 93

CHAPTER 8: Deep Learning-Based Framework for Cardiac Function Assessment in Embryonic Zebrafish from Heart Beating Videos 96
8.1 Introduction 96
8.2 Methods 99
8.2.1 Experimental Animals 99
8.2.2 Video Imaging of Beating Zebrafish Hearts at the Embryonic Stage 99
8.2.3 Cardiac Function Assessment 100
8.2.4 Automated Quantification of Cardiovascular Parameters Using Image Processing 102
8.2.5 U-Net-Based Deep Learning Approach 103
8.2.5.1 Dataset 106
8.2.5.2 Preprocessing 106
8.2.5.3 Quantification of the Diameters of the Predicted Ventricle 106
8.2.5.4 Graphical User Interface (GUI) 107
8.5.6 Quantitative Comparison of Approaches 108
8.5.6.1 Pixel-Wise Accuracy 108
8.5.6.2 Dice Coefficient 108
8.5.6.3 Intersection Over Union 109
8.3 Results 109
8.3.1 Assessment of the Accuracy of the Framework with the Defined Metrics 109
8.3.2 Assessment of the Performance of the Framework for EF 110
8.4 Discussion 114
8.5 Conclusion 118

CHAPTER 9: Electrocardiogram and Video Assessment of Amiodarone Effects in the Developing Heart of Zebrafish Embryos 119
9.1 Introduction 119
9.2 Methodology 121
9.2.1 Embryo Preparation 121
9.2.2 Micropipette and Suction Electrode Preaparation 121

9.2.3 ECG and Video Recording 121
9.3 Results 123
9.4 Discussion 126
9.5 Conclusion 127

CHAPTER 10: Summary and Prospective 129
10.1 Summary of Contributions 129
10.2 Future Work 129

BIBLIOGRAPHY 131

LIST OF FIGURES

		Page
Figure 2.1	Key Features of Zebrafish	7
Figure 2.2	Zebrafish as a Model for Cardiovascular Research	9
Figure 2.3	Labeled Zebrafish Heart Structure	11
Figure 3.1	Illustration of Human Cardiac Nodal System and Purkinje Fibers	15
Figure 3.2	Electrode Positioning for Zebrafish ECG Recording	17
Figure 4.1	Zebrafish ECG Setup and Representative ECG Figures	26
Figure 4.2	Meth Induces a Biphasic and Depressive Effect on Cardiac Electrophysiology	33
Figure 4.3	Zebrafish Cardiomyocytes Exhibit a TAAR1-mediaated Increase in cAMP Expression and Ca^2 Concentration due to Meth Treatment	37
Figure 4.4	Meth Results in Increased Fibrotic Response in Zebrafish Cardiac Tissue	39
Figure 5.1	The Prolonged ECG System for Multiple Adult Zebrafish Acquisition	54
Figure 5.2	Investigation of Tricaine and Temperature to Reduce Cardiac Rhythm Side Effects	55
Figure 5.3	Demonstration of the Prolonged System Showing ECG Changes in Response to Different Amiodarone Concentrations	56
Figure 5.4	Evaluation of Sodium Sensitivity in the Development of Sinus Arrest In Tg(SCN5A-D127N)	59
Figure 5.5	Investigation of Methamphetamine (Meth)'s Efficacy to Rescue Phenotypes After Treatment with NaCl	59
Figure 6.1	Zebra II System	76
Figure 6.2	Electrode Positioning on Zebrafish	77
Figure 6.3	Effects of Acute Amiodarone Exposure (ECG Signals)	78
Figure 7.1	Three Different IP Methodologies for Zebrafish DIC Model	89
Figure 7.2	Zebrafish Survival Rate	90

Figure 7.3 Heart Rate, Heart Rate Variability and R-R Distances 92
Figure 7.4 ECG Change in Treated Fish from Day 1 to Day 7 93
Figure 8.1 A Frame in a Video Recorde From 3-dpf Zebrafish with Segmentation for Ventricle Border and Long and Short Axes 101
Figure 8.2 Ventricle Segmentation using Different Methods 103
Figure 8.3 The Process Flow and the U-net Architecture 105
Figure 8.4 The Proposed Model's Performance Plotted with the Metrics Commonly used in Semantic Image Segmentation 110
Figure 8.5 Accuracy of ZACAF 112
Figure 8.6 Validation of U-net Image Segmentation Framework 113
Figure 8.7 Comparison of the Shape and Size of Wildtype 116
Figure 9.1 Suction Electrode Positioning in Embryonic Zebrafish 123
Figure 9.2 ECG Graphs for 10 Second Lapse for Treated and Untreated larvae with PQRST Complex Labels 125
Figure 9.3 Heart Border Labeling from Video Recording of the Heart Beating 126

LIST OF TABLES

Page

Table 2.1 Comparison of features between mammalian, invertebrate and zebrafish models for cardiovascular research. 9
Table 5.1 Comparison of WT and Tg(SCN5A-D127N fish with NaCl Treatment 67

ACKNOWLEDGEMENTS

To my wife, Monica, for being my anchor throughout this entire journey, for her unwavering love and support, boundless patience, and encouraging words.

To my grandparents, Seferino, Urbano, Esther, and Gloria, who have been my greatest inspiration and motivation for pursuing a career in the biomedical field. Thank you for your encouragement over the years and for your deepest wish for me to become "your doctor".

To my father, Seferino, my mother, Helia, and my brother, Gabriel, for their unwavering support and love, encouraging me to go abroad to pursue my dreams.

I would like to express my deepest gratitude to my advisor and mentor, Professor Hung Cao, for his invaluable support and guidance in my growth as a researcher and entrepreneur in science. My heartfelt thanks also go to all my friends at The Hero Lab, former and current, who have been a part of this journey. Special thanks to Dr. Jimmy Zhang and Dr. Xing (Chris) Xia for being such wonderful colleagues in the lab and dear friends outside of it. To my fellow "Musketeers," Mohamed Benomar El Kati and Mao-Hsiang (Alex) Huang, thank you for your unwavering support during the final stretch of my Ph.D. and for being such great friends both in and out of the lab. I would also like to acknowledge and thank my committee members, Professor Andrei Shkel and Professor James Brody, for their advice and support.

I would like to extend my deepest gratitude to Director Luisa Kregel, Director of the Mexico Graduate Research Education Program (MGREP), for guiding me through the UC System and for her unwavering support, which has greatly contributed to my success. My heartfelt thanks also go to all my friends from MGREP, who have been like family to me over the years.

To Dr. Michael P. H. Lau, who, along with Professor Hung Cao, has guided me through the entrepreneurship path by sharing his knowledge, experience, and encouraging words.

Lastly, I would like to thank the Consejo Nacional de Humanidades, Ciencia y Tecnología (Conahcyt) for funding my Ph.D. through their International Ph.D. Fellowship. I also appreciate Plos One for granting permission to include Chapter 4 of this dissertation, which is a reprint of material from [1]. The co-authors for this publication are Jimmy Zhang, Anh H. Nguyen, Daniel Jilani, Lauren Shmiess-Heine, Tai Le, Xing Xia, and Hung Cao. Thanks to Elsevier for permitting the inclusion of Chapters 5 and 8, which reprint material from [2] and [3] respectively. The co-authors for [2] are Tai Le, Jimmy Zhang, Anh H. Nguyen, Khuong Vo, Nikil Dutt, Juhyun Lee, Yonghe Ding, Xiaolei Xu, Michael P. H. Lau, and Hung Cao. The co-authors for [3] are Amir Mohammed Naderi, Haisong Bu, Jingcheng Su, Mao-Hsiang Huang, Khuong Vo, J.-C. Chiao, Juhyun Lee, Michael P. H. Lau, Xiaolei Xu, and Hung Cao. Thanks to JoVE for allowing the inclusion of Chapter 6, which reprints material from [4]. The co-authors for this publication are Mao-Hsiang Huang, Mohamed Benomar, Tai Le, Tim Etchells, Xiaolei Xu, Michael P. H. Lau, and Hung Cao.

VITA

Ramses Seferino Trigo Torres

EDUCATION

Doctor of Philosophy (Ph.D.) in Biomedical Engineering **2024**
University of California, Irvine *Irvine, California, United States*

Master of Science (M.Sc.) in Biomedical Engineering **2019**
University of California, Irvine *Irvine, California, United States*

Bachelor of Science (B.Sc.) in Mechanical Engineering **2016**
Minor in Automotive Design
Cetys Universidad Campus Mexicali *Mexicali, Baja California, Mexico*

ACADEMIC EXPERIENCE

Laboratory Manager – The Hero Laboratory **January 2021 – September 2024**
University of California, Irvine *Irvine, California, United States*

Graduate Student Researcher **August 2017 – September 2024**
University of California, Irvine *Irvine, California, United States*

Teaching Assistant – BME 60A **January 2024 – March 2024**
University of California, Irvine *Irvine, California, United States*

Graduate Interconnect Peer Mentor **February 2018 – December 2023**
University of California, Irvine *Irvine, California, United States*

Teaching Assistant – BME 60C **January 2020 – March 2020**
University of California, Irvine *Irvine, California, United States*

INDUSTRY EXPERIENCE

Design Engineering Lead **April 2023 – September 2024**
Sensoriis, Inc *Irvine, California, United States*

Electrical Engineer Intern **June 2021 – September 2021**
Sensoriis, Inc *Irvine, California, United States*

Mechanical Design Engineer **December 2016 – August 2017**
Hielo Cachanilla *Mexicali, Baja California, Mexico*

Manufacturing Engineer Jr. **June 2015 – February 2016**
Emerson Ascotech *Mexicali, Baja California, Mexico*

Design Engineering Intern **June 2014 – October 2014**
Honeywell Aerospace *Mexicali, Baja California, Mexico*

FIELD OF STUDY

Novel multimodal bio-signal acquisition systems for zebrafish.

PUBLICATIONS

1. **Torres, R. S. T.**, Huang, M.-H., Benomar, M., Le, T., Etchells, T., Xu, X., Lau, M. P. H., & Cao, H. (2024). Zebra II as A Novel System to Record Electrophysiological Signals in Zebrafish. *JoVE*(210), e67066. https://doi.org/doi:10.3791/67066
2. Huang, M. H., Xia, X., Benomar, M., Marsh, P., **Torres, R. S. T.**, Chen, J. T. J., Shahverdi, K., Tran, I., Nguyen, H. A., Chiao, J. C., & Cao, H. (2024). Boosting Stability and Sensing Range in Electrodeposited Iridium Oxide pH Sensors. *IEEE Transactions on Instrumentation and Measurement*, *73*, 1-8. https://doi.org/10.1109/TIM.2024.3428632
3. Zhang, J., Nguyen, A. H., Jilani, D., **Trigo Torres, R. S.**, Schmiess-Heine, L., Le, T., Xia, X., & Cao, H. (2023). Consecutive treatments of methamphetamine promote the development of cardiac pathological symptoms in zebrafish. *PLOS ONE*, *18*(11), e0294322. https://doi.org/10.1371/journal.pone.0294322
4. Xia, X., Vishwanath, M., Zhang, J., Sarafan, S., **Trigo Torres, R. S.**, Le, T., Lau, M. P. H., Nguyen, A. H., & Cao, H. (2022). Microelectrode array membranes to simultaneously assess cardiac and neurological signals of xenopus laevis under chemical exposures and environmental changes. *Biosensors and Bioelectronics*, *210*, 114292. https://doi.org/https://doi.org/10.1016/j.bios.2022.114292
5. Le, T., Zhang, J., Nguyen, A. H., **Trigo Torres, R. S.**, Vo, K., Dutt, N., Lee, J., Ding, Y., Xu, X., Lau, M. P. H., & Cao, H. (2022). A novel wireless ECG system for prolonged monitoring of multiple zebrafish for heart disease and drug screening studies. *Biosensors and Bioelectronics*, *197*, 113808. https://doi.org/https://doi.org/10.1016/j.bios.2021.113808
6. Naderi, A. M., Bu, H., Su, J., Huang, M.-H., Vo, K., **Trigo Torres, R. S.**, Chiao, J. C., Lee, J., Lau, M. P. H., Xu, X., & Cao, H. (2021). Deep learning-based framework for cardiac function assessment in embryonic zebrafish from heart beating videos. *Computers in Biology and Medicine*, *135*, 104565. https://doi.org/https://doi.org/10.1016/j.compbiomed.2021.104565

ABSTRACT OF THE DISSERTATION

Novel Multimodal Bio-Signal Acquisition Systems for Adult and Embryonic Zebrafish

by

Ramses Seferino Trigo Torres

Doctor of Philosophy in Biomedical Engineering

University of California, Irvine, 2024

Professor Hung Cao, Chair

Cardiovascular diseases remain the leading cause of death worldwide, highlighting the urgent need for research to address the various pathologies within the cardiovascular system. The zebrafish (Danio rerio) serves as a compelling model for cardiovascular research due to its genetic similarity to humans, extensive genomic knowledge, ease of maintenance, and remarkable regenerative abilities. Consequently, the zebrafish model is valuable for investigating a range of cardiovascular conditions, including drug screening, electrophysiological analysis, genetic characterization, and the development of future cardiac therapies.

This dissertation presents the application of two novel multimodal methodologies for studying cardiac disease and drug screening in both adult and embryonic zebrafish models. A cutting-edge electrocardiogram (ECG) system was developed, capable of simultaneously recording four ECG signals from four adult zebrafish simultaneously. This system was validated through dose-response experiments, the phenotyping of mutations related to electrophysiology, and drug screening. The research included an analysis of how varying doses of Doxorubicin influence abnormal electrophysiological phenotypes, as well as a study

on the impact of different levels of Amiodarone exposure on the electrophysiological parameters of healthy adult zebrafish. Additionally, this dissertation shows a novel approach combining simultaneous ECG and video recording in embryonic zebrafish to assess various cardiac parameters, providing a more comprehensive understanding of the effects of acute Amiodarone exposure on heart development. Overall, the work presented in this dissertation explores the need and advantages of multimodal bio-signal acquisition systems.

CHAPTER 1

Motivation

1.1 Cardiovascular Diseases.

Despite extensive research and medical expenditures, cardiovascular disease remains the leading cause of mortality and morbidity in the modern world [5]. Despite substantial efforts to comprehend and combat cardiovascular diseases (CVDs), they continue to be the leading cause of death both in the US and globally. According to the latest report from the American Heart Association (AHA), cardiovascular diseases were responsible for nearly 860,000 deaths in the US. Additionally, CVDs resulted in an estimated $351.2 billion in healthcare costs [6, 7]. In Europe, CVDs accounted for approximately 40% of all deaths [8]. While the treatment efforts for CVDs are well documented in developed countries, data shows that 80% of global CVD-related deaths occur in developing nations [9]. Extensive research has identified the risk factors contributing to the onset of CVDs, including non-modifiable factors such as age, sex, and race, as well as modifiable factors like blood pressure, cholesterol levels, and smoking [10]. Preventative strategies have been developed to address these modifiable risks, including dietary changes, regular exercise, surgical interventions, and medications to regulate blood pressure and cholesterol levels [11].

However, the effectiveness of current treatments remains limited. While social disparities and gaps in preventing or modifying cardiovascular risk factors have been acknowledged, a critical issue that often goes unaddressed is the long-term outlook for CVDs, including the high incidence of recurring cardiovascular events [12, 13]. Typically, medications like statins and beta-blockers are prescribed following palliative interventions to enhance patient outcomes. However, these treatments do not fully address the complex nature of CVDs and

may even introduce new challenges [14, 15]. For instance, studies have shown that beta-blockers can cause side effects such as hypotension, bradycardia, and cardiogenic shock [16]. Therefore, a more comprehensive approach is needed to tackle cardiovascular issues from multiple angles.

For instance, myocardial infarction is fundamentally defined as ischemic damage to the heart muscle due to a blockage in one or more coronary arteries. However, this straightforward definition oversimplifies the complex, multifactorial nature of its pathology. The American Heart Association has developed comprehensive guidelines for diagnosing myocardial infarction, which involve categorizing myocardial infarctions based on their underlying causes and identifying various symptoms such as cardiac troponin levels indicating tissue injury, ischemic ECG changes (e.g., ST segment deviations, pathological Q waves), and abnormal wall motion detected via echocardiography [17]. Furthermore, this universal definition has been revised multiple times, underscoring both the advances in cardiovascular research and the need for further clarity regarding the complex nature of myocardial infarctions. Similar challenges exist with other cardiovascular diseases, which are often interrelated, highlighting the importance of understanding the multifactorial aspects of cardiovascular conditions.

1.2 Contributions and Impact.

This doctoral research focused on investigating various cardiovascular pathologies and drug screening using the zebrafish model, with the goal of developing a new high-throughput research platform. This platform aims to reduce the learning curve for new researchers while improving the quality of studies. The zebrafish model offers several significant advantages, including genetic similarities to humans, the presence of orthologous genes in

both species, and ease of maintenance. These advantages are further enhanced when using the embryonic model, as zebrafish embryos are transparent from 0 hours post-fertilization (hpf), allowing researchers to observe the development of internal organs in real-time. To leverage these benefits, multiple experimental approaches were designed and implemented to enhance our understanding of specific applications, as detailed below:

- Comprehensive analysis of the effects of Methamphetamine on cardiac electrophysiological dysfunction. Refer to Chapter 4 and the journal article [1].
- Development of an ECG system designed to capture signals from zebrafish for extended drug dose-response testing and genetic functional analysis of mutations in the SCN5A gene, which is crucial for cardiac electrophysiology. Refer to Chapter 5 and the journal article [2].
- Fabrication of the next-generation ECG system for extended drug dose-response testing, incorporating innovative features such as multi-point ECG recording probes, four individual chambers for simultaneous zebrafish recordings, and capabilities for both in-device and cloud-based data recording and analysis. Refer to Chapter 6 and the journal article [4].
- Comprehensive analysis of the cardiac electrophysiological dysfunctions resulting from acute Doxorubicin exposure, using three distinct intraperitoneal (IP) injection methodologies. Refer to Chapter 7.
- Development of a deep learning-based framework for cardiac function assessment for embryonic zebrafish using heart beating videos. Refer to Chapter 8 and the journal article [3].

- Comprehensive study of acute Amiodarone exposure on the developing hearts of embryonic zebrafish, utilizing a multimodal framework that combines simultaneous ECG recording and cardiac function assessment through real-time heart beating videos. Refer to Chapter 9.

1.3 Dissertation Outline.

The primary aim of this dissertation is to explore the benefits of novel multimodal methodologies for cardiovascular research using both adult and embryonic zebrafish models. This work involves analyzing various approaches and integrating them into a platform designed to streamline the research process. **Chapter 2** reviews the existing literature on the use of animal models in cardiovascular research, with a particular focus on the advantages of the zebrafish model in this field. **Chapter 3** delves into the concept of electrocardiograms (ECG), a key element of this dissertation, and discusses the two diagnostic imaging tools employed in cardiovascular research. It also explains how these tools, combined with machine learning, are used for cardiac assessment in zebrafish studies. **Chapter 4** examines the impact of drug exposure on cardiac physiology, specifically focusing on Methamphetamine. The chapter reports electrophysiological abnormalities and investigates the underlying mechanisms, such as the GPCR pathway, while also highlighting traditional ECG recording methods in zebrafish. In **Chapter 5**, the first generation of an in-house developed ECG acquisition system for multiple zebrafish is introduced. This chapter covers an extensive drug dose-response analysis and the characterization of the Tg(SCN5A-D1275N) mutation, which is relevant to arrhythmic diseases. **Chapter 6** presents the second generation of our in-house ECG acquisition system, Zebra II, which builds on the previous model with additional features like multi-point ECG recording probes, four individual

chambers for simultaneous zebrafish recordings, and capabilities for both in-device and cloud-based data recording and analysis. **Chapter 7** details an in-depth study assessing the effects of acute Doxorubicin exposure via intraperitoneal (IP) injection through ECG, along with a comparison of three different IP injection methodologies.

Chapter 8 introduces an in-house deep learning-based framework for cardiac function assessment in embryonic zebrafish using heart beating videos. **Chapter 9** applies the framework from Chapter 8, showcasing a new approach that combines ECG and real-time heart beating videos for a novel multimodal method of cardiac function assessment. Finally, **Chapter 10** summarizes the findings from the studies outlined in the previous chapters, highlighting key discoveries from each work. It also discusses the next steps for the third-generation device in the Zebra II project and the development of the first-generation device for the work detailed in Chapter 9.

CHAPTER 2

Animal Models in Cardiovascular Research

2.1 Introduction.

This chapter will examine the various animal models employed in cardiovascular research, with a focus on the most widely used models. An in-depth discussion will be dedicated to the zebrafish model, covering its advantages, disadvantages, and significant applications in cardiovascular studies.

2.2 Popular Models for Cardiovascular Research.

In cardiovascular research, the most commonly utilized animal models are mammalian, including mice, rats, pigs, and other large animals. These models are preferred due to their anatomical, physiological, and pathological similarities to humans, particularly concerning the cardiovascular system [18]. Additionally, small mammalian models have benefitted from the development of various genetic engineering tools, making them popular in studies involving genetic mutations [19]. Research using these animal models often combines treatment procedures, such as drug administration and mechanical injury, followed by genetic analysis. A frequent approach involves creating mutant lines to investigate how specific genes influence wound healing or regeneration processes after physical injury, such as left anterior descending (LAD) artery ligation [20]. These studies have shed light on the molecular pathways most critical for treating cardiovascular diseases. Mammalian models are also extensively used in drug discovery and screening, as their characteristics make them suitable substitutes for human drug testing [21].

However, it is essential to recognize that mammalian models, even small ones like mice and rats, present challenges due to their size, maintenance requirements, and relatively low fecundity [22]. Consequently, exploring alternative animal models is crucial.

2.3 Why Zebrafish?

The zebrafish (Danio rerio), a small freshwater fish native to South Asia, has become an invaluable model in biological research due to its numerous advantageous traits. Initially introduced in the 1950s, zebrafish were predominantly used in toxicology studies related to drug and natural contaminant exposure [23-25]. However, advancements in genetics have significantly increased their popularity, particularly after the sequencing of the zebrafish genome revealed substantial similarities with the human genome. Additional attributes, such as comparable morphology and physiology, along with the zebrafish's innate ability to regenerate certain organs like the heart and brain, have further solidified its role in research, as illustrated in Figure 2.1. These unique characteristics position zebrafish as a vital vertebrate model for advancing cardiovascular research and developing treatments for cardiovascular diseases.

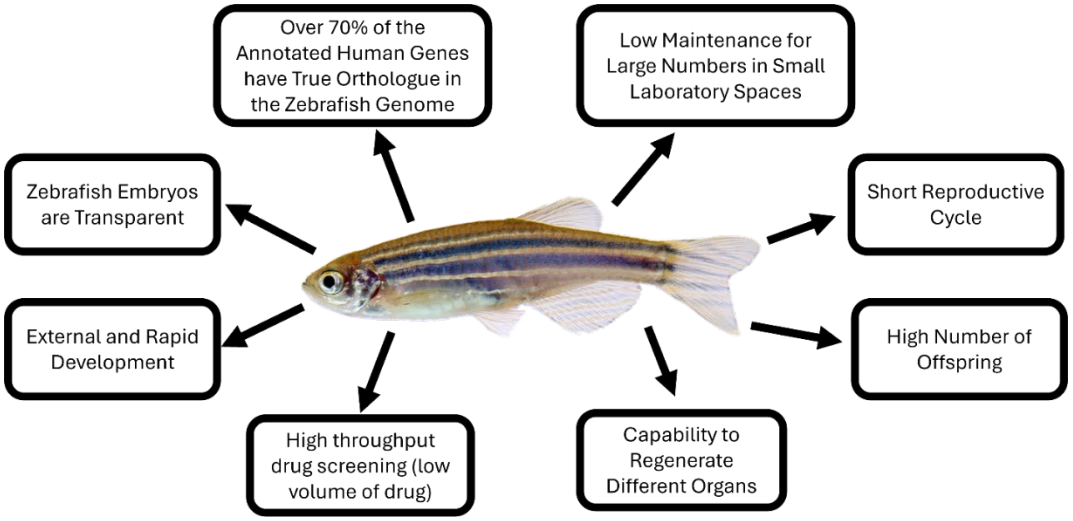

Figure 2.1. Key Features of the Zebrafish Model for Cardiovascular, Drug Screening, and Genetic Research.

The significance of the zebrafish model gained broader recognition in 1981 when pioneering molecular biologist George Streisinger published his groundbreaking work on creating homozygous clones of zebrafish [26].Streisinger, initially captivated by the rapid embryonic development of zebrafish, developed these clones to study mutations relevant to neuronal development, which was the primary focus of his research. In his publication, he highlighted several advantages of zebrafish embryos, including their short generation time of 3-4 months, high egg production, small size that facilitates easy maintenance, and the transparency of their egg sacs, which allows for easy observation of embryonic development. Following Streisinger's work, the zebrafish model attracted interest from other researchers, particularly those who had previously worked with developmental models like fruit flies [27]. Since then, knowledge surrounding zebrafish genetics has expanded significantly. The zebrafish genome sequencing project, initiated in 2001, revealed that approximately 70% of human genes in the reference genome have at least one zebrafish orthologue, highlighting the zebrafish model's relevance in studying human-associated genetics and diseases [28]. As a result, zebrafish research has seen substantial growth, with over 1,300 laboratories worldwide utilizing zebrafish in various studies by 2019, according to the ZFIN database [27].

Over the past few decades, zebrafish have emerged as a leading animal model, offering significant advantages in cardiovascular research and understanding disease mechanisms [29, 30]. As a model for studying human cardiac pathologies, zebrafish have provided crucial insights into the mechanisms of heart regeneration and development down to the molecular level [29]. The zebrafish model is particularly well-suited for studying the complexities of cardiovascular development and disease, as shown in Figure 2.2 [31].

Feature	Mammals	Invertebrates (i.e. Drosophila, C. Elegans)	Zebrafish
Morphological Homology to Humans	High	Low	Medium
Fecundity	Low	High	High
Size	Large (> 5cm)	Small (<1 cm)	Medium (2-5 cm)
Maintenance & Ethics	High	Low/Null (No Regulatory Approval)	Medium
Experimental Duration	Long (>2 years)	Short (< 1 month)	Medium (6-12 months)
Time to Maturity	Long (>2-3 months)	Short (<3 days)	Long (3 months)

Table 2.1. Comparison of features between mammalian, invertebrate and zebrafish models for cardiovascular research.

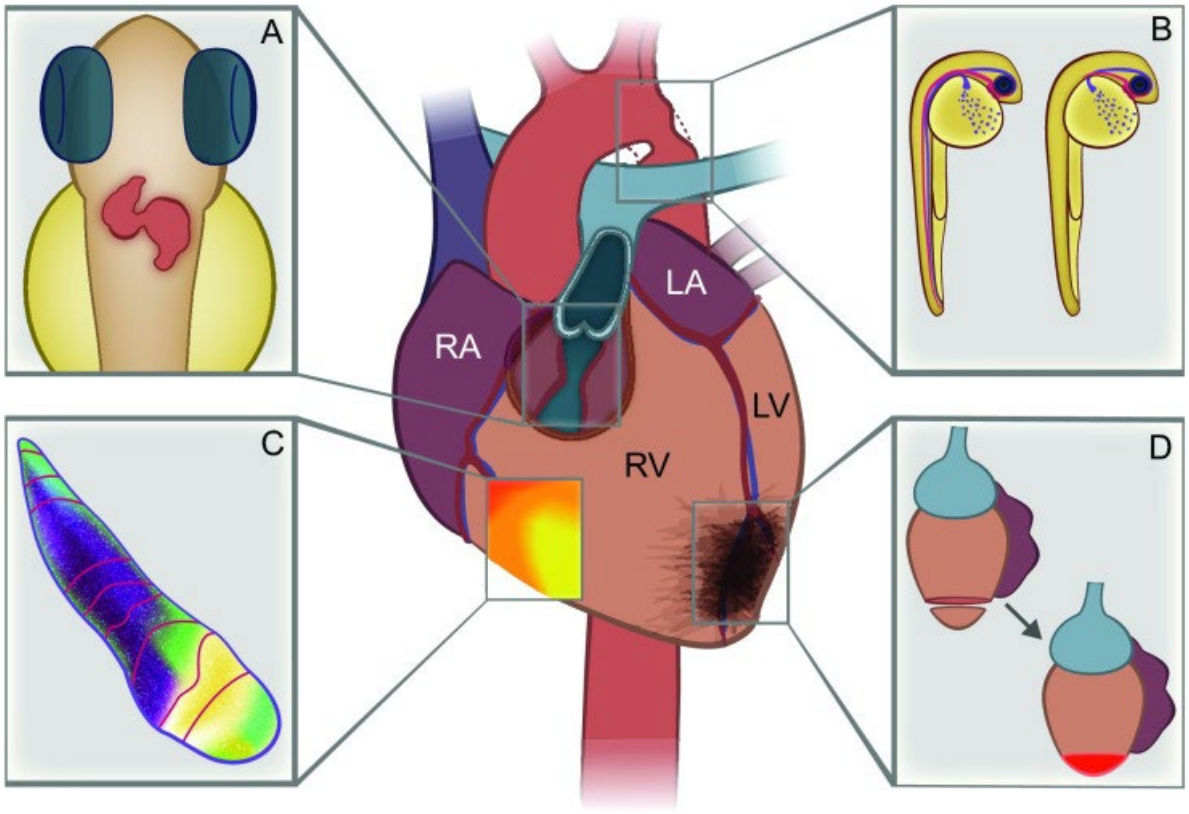

Figure 2.2. Zebrafish as a Model for Cardiovascular Research. The middle panel features a human heart, highlighting its four chambers: the Right Atrium (RA), Left Atrium (LA), Right Ventricle (RV), and Left Ventricle (LV). Despite structural differences, zebrafish hearts share key functional similarities with human hearts, making them valuable for cardiovascular research. (A) Illustrates the zebrafish heart, which, although simpler with only a single atrium and ventricle, offers significant insights due to its physiological parallels with the human heart. (B) Presents a comparison of cardiac

disease models in zebrafish. On the left is a wild-type zebrafish (with no mutations), and on the right is a zebrafish with a gridlock mutation, analogous to human aortic coarctation, demonstrating the utility of zebrafish in modeling human cardiovascular diseases. (C) Depicts voltage mapping performed on zebrafish, a critical technique for studying arrhythmic disorders, illustrating how electrophysiological properties can be investigated in this model. (D) Highlights the remarkable regenerative capacity of the zebrafish heart, an essential feature for exploring potential treatments for various cardiac conditions in humans. This regenerative ability provides a unique opportunity to study the mechanisms underlying heart repair and recovery. Reproduced from [32] under the CC-BY license.

The primary benefits of using zebrafish as a cardiac model include their small size, rapid embryonic development, optical transparency of embryos, high genetic homology with humans, and the availability of transgenic models [33]. These advantages, along with others, make zebrafish an excellent model for understanding vertebrate development and organogenesis [34]. In direct comparison to the mouse model, zebrafish possess a unique ability to regenerate their hearts indefinitely, provided the injury does not exceed 25% of the total heart area. In contrast, intrinsic cardiac regeneration in mice is limited to about seven days after birth [35]. The zebrafish model has become a cornerstone in regenerative studies, initially studied through fin amputation, which established a foundational understanding of zebrafish regeneration. After injury, the site is covered by epidermal tissue, and a regenerative blastema—a diverse group of cells that form the precursor tissue for regeneration—develops to facilitate wound healing [36]. This process is similar to the wound healing mechanisms found in humans and other mammals [37]. With the advent of genetic engineering tools, researchers have identified genes that play critical roles in the regenerative process, many of which originate from embryonic morphogenic pathways. This suggests that regenerative activity in zebrafish may be linked to processes commonly observed during embryonic development [38]. Additionally, these studies have shown that cells can dedifferentiate and redifferentiate into the appropriate cell types necessary for

regeneration. For example, Singh et al. demonstrated that fin osteoblasts could regenerate even after all resident osteoblasts were ablated [39].

These regenerative principles also apply to zebrafish heart regeneration. Research by Kikuchi et al. revealed that the zebrafish heart regenerates through the proliferation of cardiomyocytes expressing gata4, a gene essential for embryonic heart development [40]. Furthermore, Jopling et al. found that cardiomyocytes dedifferentiate during the regeneration process, indicated by the disappearance of muscle fiber structure [41].

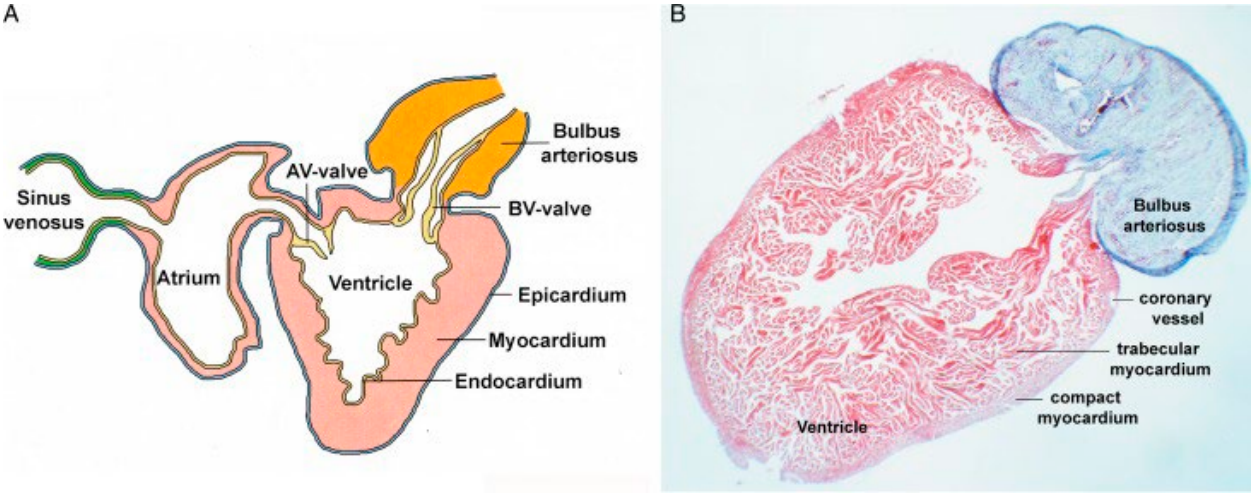

Figure 2.3. Labeled Zebrafish Heart Structure. (A) Presents a schematic of the zebrafish heart, highlighting its simple yet functional anatomy. The zebrafish heart consists of a single atrium and a single ventricle. The Sinus Venosus, analogous to the Vena Cava in humans, collects deoxygenated blood before it enters the atrium. Blood is then pumped from the ventricle into the Bulbus Arteriosus, which functions similarly to the human aorta, distributing blood throughout the body. (B) Showcases a trichrome-stained section of zebrafish cardiac tissue, providing a clear visual distinction between the different tissue types. Myocardial tissue, responsible for the heart's contractile function, is stained red, while non-myocardial tissue is stained blue. This staining technique allows for detailed examination of the heart's structural composition, aiding in the study of cardiac function and pathology in zebrafish as a model for human cardiovascular research. Reproduced [42] from under the CC-BY license.

However, further research is required to clarify the complex mechanisms driving this process, including the specific regeneration pathways and the triggers during wound healing and regeneration. In addition to their regenerative capabilities, zebrafish remain relevant for drug testing and discovery studies, stemming from their initial use in toxicology research.

The zebrafish model serves as an optimal balance between ease of experimentation and relevance to human drug discovery. Compared to conventional mammalian models like mice and rats, zebrafish offer higher fecundity and lower maintenance costs, making them ideal for high-throughput drug screening [43]. Moreover, compared to common invertebrate models like Drosophila and C. elegans, zebrafish possess morphology and physiology more akin to humans. Although the validity of using animal models for human applications has been debated, studies have shown that zebrafish exhibit qualities closely resembling those in humans. For instance, receptors commonly targeted by drugs, such as the glucocorticoid receptor, share up to 90% structural homology between zebrafish and human variants [44], which can be attributed to the genetic similarities between the two species.

Researchers have also tested whether administering certain drugs to zebrafish produces similar effects as in humans. For example, Milan et al. conducted a drug screen to observe changes in heart rate in zebrafish [45]. Their results showed that of the 23 drugs known to disrupt heart repolarization in humans, 22 induced similar effects in zebrafish, manifesting as signs of bradycardia. The comparable morphology between zebrafish and humans further supports the zebrafish model's rise in drug discovery. Genetically engineering zebrafish lines has become relatively straightforward, enabling researchers to study zebrafish's morphological features and development. Studies by de Pater et al. and Lazic et al. demonstrated that zebrafish heart development occurs in two distinct phases, analogous to the two heart fields found during human heart development [46, 47]. Additionally, orthologous genetic pathways govern heart development in both species, underscoring the zebrafish model's potential for evaluating drug functionality [32]. Consequently, the

zebrafish model remains one of the most popular animal models for drug screening, particularly in cardiovascular research.

CHAPTER 3

Electrophysiology and Diagnostic Imaging Tests

3.1 Introduction.

Cardiac electrophysiology is a critical aspect of maintaining proper cardiac function, defined by the initiation and propagation of electrical signals within the heart. These signals ensure the coordinated contraction of the heart's chambers, which is essential for effective blood circulation. In humans, this cascade of electrical signals is orchestrated by a network of cardiac nodal cells distributed throughout the heart, as illustrated in Figure 3.1. This intrinsic conduction system originates with pacemaker cells, which spontaneously generate electrical impulses [48]. These impulses first cause the atria to contract, pushing blood into the ventricles. The signal then travels through the atrioventricular (AV) node, where it is briefly delayed to ensure complete ventricular filling [49]. After passing through the AV node, the signal moves along the bundle branches within the ventricles and subsequently disperses through the Purkinje fibers, which cover the entire ventricular wall. This sequence triggers ventricular contraction, propelling blood into systemic or pulmonary circulation. The precise timing and coordination of these electrical signals are vital for normal cardiac function. Any disruption in this rhythm can significantly impair heart function and lead to various cardiovascular diseases. This chapter will provide an overview of the development and application of the electrocardiogram (ECG), a tool used to detect and analyze heart rhythm, highlighting its importance in diagnosing and understanding cardiac electrophysiology.

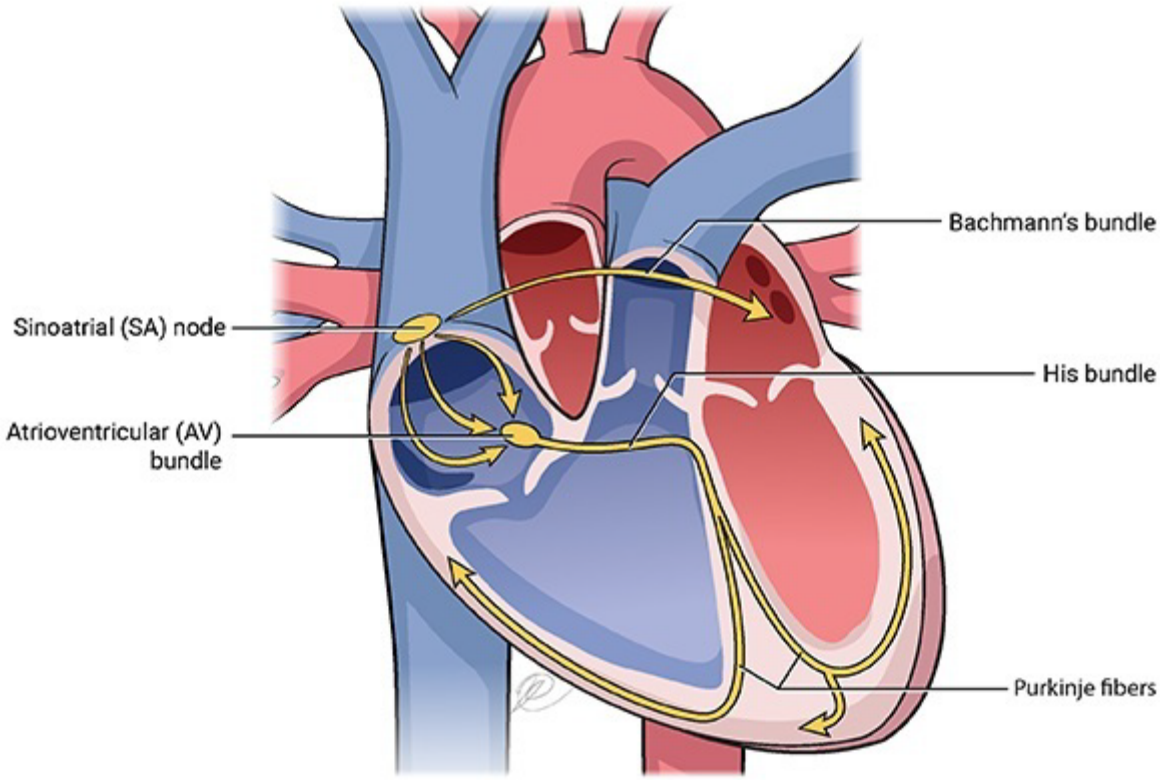

Figure 3.1. Illustration of Human Cardiac Nodal System and Purkinje Fibers. The sinoatrial (SA) node, located within the right atrial wall, serves as the primary initiator of the heart's electrical conduction system. Once the SA node generates an impulse, the signal spreads across the atria, leading to atrial contraction. The electrical impulse then travels to the atrioventricular (AV) node, situated between the atria and ventricles, where it is momentarily delayed allowing complete ventricular filling. From the AV node, the signal is transmitted through the His bundle and dispersed via the Purkinje fibers, which extend throughout the ventricular myocardium, ensuring coordinated ventricular contraction. Source: US National Library of Medicine.

Besides electrophysiology, modern technology has permitted physicians to incorporate imaging diagnostic tools that have presented a huge advantages during clinical diagnosis. Cardiac imaging, testing, and diagnostic procedures are essential tools in cardiology, crucial for the early detection, precise diagnosis, and effective management of heart diseases. While these procedures do carry some inherent risks, as with any medical intervention, their benefits—such as improved patient outcomes and timely treatment—far outweigh the potential drawbacks. Some examples include echocardiography (ECHO), Computed Tomography (CT), Magnetic Resonance Imaging (MRI), and others.

3.2 Electrocardiogram in Zebrafish.

As the zebrafish model gained prominence in cardiovascular research, scientists began to delve into the electrophysiology of the zebrafish heart. Despite its simpler anatomy compared to the human heart, the zebrafish heart produces an electrocardiogram (ECG) that closely resembles the human ECG, retaining the characteristic PQRST waveforms [50]. Additionally, the heart rate of zebrafish is comparable to that of humans, making it more similar than the commonly used mouse model [51]. The QT interval, a critical measure in cardiac electrophysiology, is also similar between zebrafish and humans. These parallels have established the zebrafish as a compelling model for drug studies, particularly those with cardiovascular implications. When combined with the ability to create specific mutant lines, the zebrafish model becomes an ideal platform for drug screening, toxicology, and the discovery of novel mechanisms of action [44]. For instance, research has shown that glucocorticoids can alleviate symptoms of prolonged QT syndrome caused by mutations in the potassium ion channel in zebrafish [52]. However, despite these notable similarities, researchers have identified significant differences between zebrafish and human ECGs that must be considered when setting up experiments and interpreting results. For example, Zhao et al. found that the polarity of ECG leads must be reversed when recording from zebrafish compared to humans [53]. Specifically, the zebrafish equivalent of lead II, known as reverse lead II, requires placing the negative electrode near the abdomen (analogous to the left leg in humans) and the positive electrode slightly anterior to the heart—opposite of the typical human ECG electrode placement. This reversal suggests that zebrafish have different depolarization and repolarization gradients than humans, a factor that must be accounted for during zebrafish ECG acquisition and analysis.

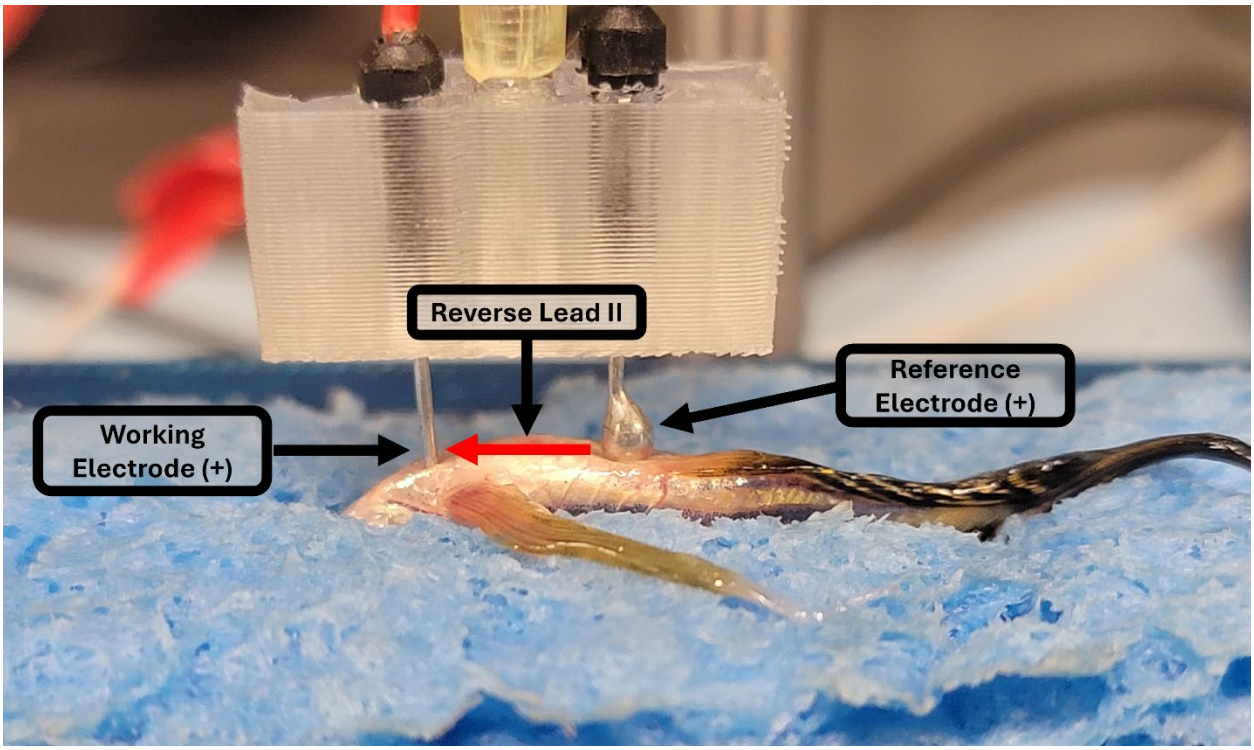

Figure 3.2. Electrode Positioning for Zebrafish ECG Recording. In zebrafish ECG recording, the positive (working) electrode is placed over the chest region, while the negative (reference) electrode is positioned on the lower abdomen. This electrode configuration creates a Reverse Lead II, as indicated by the red arrow along the ventral side of the fish. The orientation of this lead is opposite to that of Lead II in human ECG. This reversal is intentionally implemented to produce upright waveforms that closely resemble those found in human ECG, ensuring more accurate and comparable data between the two species.

3.3 Diagnostic Imaging for Cardiovascular Studies.

3.3.1 Echocardiogram (ECHO) in Adult Zebrafish. Embryonic zebrafish provide a powerful model for studying cardiac developmental processes, largely due to their optical transparency, which allows for direct visualization of the heart. However, as zebrafish mature, their body transparency diminishes, presenting a significant challenge for using this model to study adult-onset cardiovascular disorders. One of the primary limitations has been the lack of tools for in vivo assessment of the mature zebrafish heart. Despite this, recent studies have shown that adult zebrafish can undergo significant ventricular remodeling in response to environmental stressors [54, 55]. These findings highlight the untapped potential of adult zebrafish as a model for investigating a

wide range of human heart disorders, including heritable and acquired cardiomyopathies, as well as post-infarction myocardial regeneration.

Echocardiography, a non-invasive, ultrasound-based imaging technique, is widely used in clinical settings and mammalian animal models to evaluate cardiac function in vivo [56-60]. It allows for serial assessment of cardiac structure and function, making it an essential tool in cardiovascular research. While applying echocardiography to an aquatic organism like the adult zebrafish—whose size ranges from 20-40 mm in length—presents unique challenges, recent advances in high-frequency ultrasound technology (up to 70 MHz, with 30 μm axial resolution) have made it feasible. However, the application of high-frequency echocardiography in zebrafish is still in its early stages, and there is a critical need for standardized protocols for image acquisition and data analysis. Addressing this gap will enhance the reliability and reproducibility of research using adult zebrafish as a model for human cardiovascular diseases [54].

3.3.2 Heart Beating Videos in Embryonic Zebrafish. Embryonic zebrafish, up to approximately three days post-fertilization (dpf), offer a unique advantage in cardiovascular research due to their transparency, which allows for clear visualization of internal organs, including the heart and vascular system. This transparency makes it possible to capture bright field microscopic videos that can be used to quantify cardiac function and morphology during this early developmental stage [55]. Typically, two-dimensional (2D) videos are recorded for cardiovascular analysis, where the continuous motion of the ventricular wall throughout the cardiac cycle is tracked. This is done by identifying a linear region of interest along the ventricle's borders [55]. Structural analysis of the zebrafish heart during this stage often involves capturing 2D images at specific time points to measure the dimensions of the cardiac chambers. However, traditional methods require researchers to manually label the ventricle, identify the End Systolic (ES) and End Diastolic (ED) frames, and then calculate

parameters such as ejection fraction (EF) and heart rate (HR). To date, most reported studies have focused primarily on the simple detection of heart rate, often using techniques like edge tracing [56]. While these methods provide valuable insights, there remains a need for more advanced and automated approaches to streamline the analysis of cardiac function in embryonic zebrafish[3].

3.4 Machine Learning in Diagnostic Imaging in Zebrafish.

Machine learning is a computational approach that uses statistical models to enable computer systems to perform specific tasks effectively by identifying patterns and making inferences without the need for explicit instructions. This technology has been widely applied across various fields, including image recognition. In 2005, machine learning was first introduced into zebrafish research to analyze zebrafish transcriptomics using support vector machines [57]. Since then, its applications have expanded to include behavioral analysis[58, 59] and image processing [60-62]

A notable recent advancement by Cordero-Maldonado et al. demonstrated that combining machine learning with robotic manipulation can facilitate high-throughput microinjections into zebrafish eggs, precisely targeting specific sites[63]. This integration of automated imaging, quantification, and machine learning is poised to significantly enhance large-scale, high-throughput zebrafish screening, particularly in drug discovery research. The appeal of machine learning lies in its superior efficiency and accuracy. However, the development of analysis pipelines is often tailored to a single purpose, requiring specialized expertise in computer science, which can be costly. As a result, small-to-medium-sized laboratories may find it challenging to adopt these systems, limiting their widespread use in zebrafish research [64].

CHAPTER 4

Consecutive Treatments of Methamphetamine Promote the Development of Cardiac Pathological Symptoms in Zebrafish

4.1 Introduction.

Methamphetamines are sympathomimetic amines with a range of adverse effects upon multiple organ systems. Based around a phenylethylamine core, methamphetamine (Meth) and its analog, *d*-amphetamine, have high affinity with transporters associated with catecholamine signaling, significantly increasing the number of neurotransmitters such as dopamine and norepinephrine [65]. Unlike Meth, *d*-amphetamine has been prescribed as medication to treat neurological disorders such as attention deficit hyperactivity disorder (ADHD) and narcolepsy [66]. A possible reason for limited legal Meth use is the addition of the *N*-methyl group compared to amphetamine, which has been shown to confer better penetration through the blood-brain barrier for Meth, leading to stronger and more addictive responses [67]. Meth has been shown to induce heightened catecholamine response by promoting catecholamine release, preventing their reuptake, and destabilizing their levels [68, 69]. Thus, Meth is responsible for numerous neurotoxic symptoms, including potential neuronal apoptosis, decreased immune response, and associated memory deterioration [69-72]. Given that the elucidation of the direct mechanism of Meth was on neurological response, the major focus in researching treatments for Meth-related abuse has been associated with neurological modulation. Therefore, less attention was given to researching the direct mechanism of Meth in other physiological systems, such as the cardiovascular system.

Cardiotoxicity is one of the most adverse consequences of Meth abuse, leading to a notable increase of morbidity and mortality [65]. Cardiovascular complications are the second leading cause of death in Meth abusers. Cardiotoxicity can appear early in the course of the drug use and cause numerous significant effects, such as pulmonary hypertension, atherosclerosis, cardiac arrhythmias, acute coronary syndrome, and other associated cardiomyopathies [73]. Furthermore, a Meth 'binge' study in rats to determine long-term effects discovered that Meth decreased the sensitivity of nervous and cardiovascular physiology through successive treatments, implying the potential remodeling of electrophysiological responses through chronic Meth abuse [74]. Previous human case studies have determined that Meth abusers experienced increased ventricular tachycardia and QTc prolongation [75, 76]. However, case studies are generally retrospective, and there is a scarcity in animal studies regarding the effect of Meth on the actual initiation of arrhythmic symptoms [65]. Moreover, data on the underlying mechanism of cardiac dysfunction during drug abuse and the susceptibility of long-term cardiotoxic development are limited.

Despite the prevailing issue of Meth abuse, studies have shown that cardiac pathology induced by Meth can be attenuated and even reversed through the discontinuation of Meth use and the initiation of subsequent treatment [77]. A study in rats regarding the administration of Meth and eventual withdrawal revealed that the rats were able to recover from myocardial pathologic symptoms such as atrophy, fibrosis, and edema starting from 3 weeks after discontinued Meth administration [78]. A human case study indicated that attenuation of Meth use and subsequent therapy led to recovery from ventricular hypertrophy and ECG ST deviations [79]. While evidence of recovery from Meth abuse is

promising for the development of future treatments, it is essential to conduct research to understand the specific mechanisms underlying Meth-induced cardiovascular pathologies. Therefore, a better understanding of the cardiac dynamics of Meth abuse in zebrafish, a relevant model for human cardiac studies, may be vital for the future Meth-associated research.

In neurological studies associated with Meth, the drug-induced effect of G protein-coupled receptors (GPCRs) on subsequent neuropathology has been frequently investigated due to the receptors' association with neurotransmitters, hormones, and other neuromodulatory responses [80]. cAMP, a prominent secondary messenger within the GPCR signaling pathway, tends to be upregulated due to drug exposure, and it has been shown to influence sensitization and addiction to psychostimulant drugs [81]. However, given the ubiquity of GPCRs in numerous physiological systems, the effects of GPCRs on other symptoms of drug toxicity have also been explored. GPCRs have been demonstrated to be influential in the development of cardiovascular diseases. Studies have found that GPCRs induced increased Ca^{2+} release and myocardial contractility, leading to a higher susceptibility to hypertrophy and cardiomyopathy [82]. GPCRs have also demonstrated the ability to modulate remodeling processes within the biological system, including epithelial-mesenchymal transition (EMT) and collagen deposition [83]. For example, TAAR1, a prominent GPCR targeted by Meth, was determined to be an integral player in the psychostimulant activity and addictive response of Meth [84]. However, TAAR1 has also been found outside of the neurological system, including the heart [85]. Therefore, cAMP and GPCRs may play a crucial role in the further elucidation of the effects of Meth on cardiac electrophysiology.

Although current research has not fully proven whether the single ventricular heart of zebrafish is comparable to the more complex ventricular conduction system found in higher vertebrates, zebrafish have been proposed as a versatile model system for researching biological applications due to similarities with humans pertaining to cardiac physiology. Zebrafish has also emerged as a high-throughput and low-cost animal research model that has been used for phenotype-driven drug screenings for new insights into chemical toxicity due to similar drug metabolism and genetic homology [44]. Our lab previously developed a method for measuring *in vivo* surface electrocardiography for adult zebrafish. This method was targeted for studies regarding irregular heartbeats and QT dysregulation, and the acquired results displayed remarkable electrophysiological similarities between zebrafish and humans [86]. As such, *in vivo* ECG for adult zebrafish would be a powerful tool for studies involving Meth-induced cardiac toxicity. In this study, we first demonstrate the potential of zebrafish ECG in the diagnosis of Meth-induced cardiotoxicity. We then sought to explain the results by conducting molecular analysis of the GPCR pathway within heart tissue, including the effect on fibrotic and Ca^{2+} dysregulation, which attribute to cardiac toxicity. With the implementation of our ECG system in Meth studies, we hope to provide a new insight into the mechanisms of Meth-induced cardiotoxicity, further uncovering the multifactorial nature of Meth and assisting in the development of novel treatment methods.

4.2 Methodology.

4.2.1 Zebrafish Husbandy and Preliminary Surgical Procedures. Wild-type zebrafish were housed in a custom built circulating fish rack system. The fish tanks were maintained at 28° C, ~pH 7.0, and these parameters were checked at least once daily. The system was equipped with four filters, a UV, carbon, and two particle filters. Zebrafish were kept under the 14:10

hour light/dark cycle. Zebrafish (AB-wild type strain) were approximately 6–12 months old at the onset of the experiment. Prior to Meth treatment, zebrafish underwent open chest surgery to improve subsequent ECG signal acquisition. Fish were first anesthetized with tricaine (200 mg/L) via immersion for approximately 5 minutes or until no opercular movement has been observed. Under a stereo microscope, scales (above the coelomic cavity and the posterior site above the tail) were removed with forceps, exposing flesh, to allow more direct electrode contact. A small incision, ~2–3 mm, was made on the ventral surface of the fish above the heart. The incision cut through the chest wall and the heart was visible afterward. The fish were recovered in fresh fish water for a few minutes. The incision was not closed via suture, staple, clips, or glue as the chest wall and scales have been observed to regrow within 4 weeks. The zebrafish groups were then housed in separate tanks throughout the duration of the study. All zebrafish were checked every day for the first week and then at least 3 days/week in the second week until the experiment was concluded. Observations were made to see whether the fish displayed some abnormal activities (e.g., erratic swimming, strained breathing, bloating). The fish would be removed from the study if any abnormal activity was detected. In rare cases where extreme behavior/distress was seen, the fish would be euthanized. Euthanasia was conducted by immersing the fish in tricaine (250 mg/L) for at least 30 min after the last observed opercular movement. All fish carcasses will be frozen post-euthanasia. All zebrafish procedures were conducted in accordance to IACUC guidelines (#AUP-21-066 at University of California, Irvine).

4.2.2 Drug Preparation and Methamphetamine Treatment. The Meth solution for treatment (200 μM) was prepared by mixing the specified amount of Meth stock into regular fish water obtained from the fish rack system. Solutions were prepared fresh for each day of treatment.

The Meth stock (1 mg/mL) was obtained from Sigma-Aldrich (MDL MFCD00056130). The solution (10 mL) was then placed in a small custom polydimethylsiloxane (PDMS) chamber suitable for housing one zebrafish. PDMS is a flexible and biocompatible polymer most commonly used in biosensors and implants [87]. Untreated fish were placed in the same custom chamber with regular fish water. Each zebrafish was treated in the designated treatment for 20 minutes before ECG recording, as determined in a previous study [88]. This treatment was conducted 3 times a week over a period of two weeks, following similar studies.

4.2.3 ECG Recording Procedure and Instrumental Setup. ECG was obtained using the instrumental setup depicted in Figure 4.1A. Prior to placing the fish in the designated zebrafish station, the fish was first anesthetized in tricaine (200 mg/L) for approximately 5 minutes until the fish became unresponsive to external stimulus. Then, the fish was placed ventral side up in a precut crevice in the middle of the sponge. The sponge was then placed on a glass platform with the pin electrodes as positioned in Fig 4A, where the green working electrode was placed near the open incision on the chest while the yellow reference electrode was placed near the lower abdomen. Each fish underwent recording for approximately 1 minute before placing in regular fish water for recovery from anesthesia. Treatment concentrations and durations were approved by University of California-Irvine's IACUC.

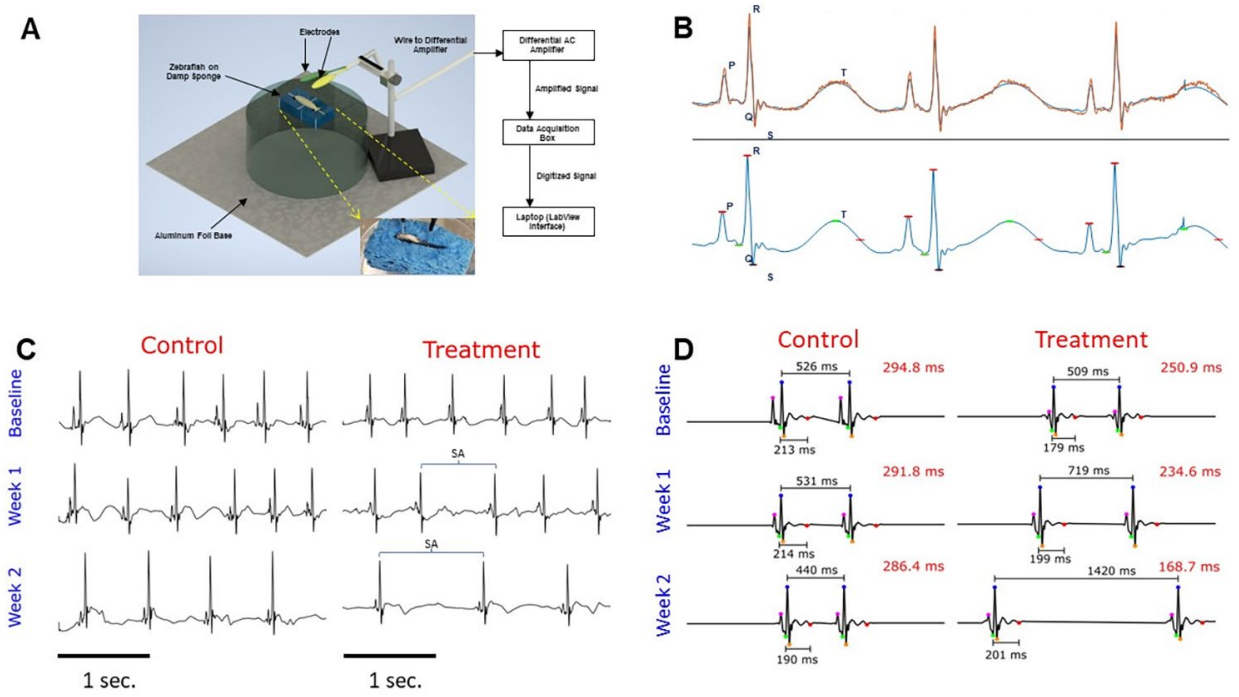

Figure 4.1 Zebrafish ECG Setup and Representative ECG Figures. (A) The main figure depicts the general layout of zebrafish and electrodes during ECG recording. The working electrode is shown in green and contacts the chest cavity. The reference electrode is shown in yellow and contacts near the tail. This electrode setup connects with instruments outlined in the block diagram on the right, where signals are processed and displayed on the laptop. The inset provides a closer view of the positioning of electrodes on the zebrafish during recording. (B) Representations of ECG signal processing with labeled waveforms utilizing custom MATLAB software. The top displays the orange raw signal, while the bottom displays the blue processed signal. (C) These ECG signal figures were processed from both untreated (control, n = 6) and Meth-treated (treatment, n = 8) fish, taken during baseline, week 1, and week 2 of the study. The ECG waveforms (PQRST) were labelled on the first cycle of each figure. These figures depict that Meth treatment has significantly decreased heart rate over the duration of the study compared to no treatment. Additionally, Meth-treated zebrafish exhibited more pronounced bradyarrhythmia, as indicated by the blue brackets spanning across the occurrence of the bradyarrhythmia. Note that while control fish also exhibit bradyarrhythmia, the occurrences in Meth-treated fish were more pronounced. Figures shown represent 3 seconds of recording. Scale bar depicts 1 second. (D) These figures were produced by averaging all ECG segments from each recording, extrapolating the ECG waveforms in order to determine the T wave. The waveforms are depicted as follows: Magenta = P; Green = Q; Blue = R; Orange = S; and Red = end of T wave. The RR and QT intervals are labelled for all waveforms, and the calculated QTc interval is shown on the top right of each figure. In comparison between untreated (control, n = 6) and Meth-treated (treatment, n = 8) fish, treated fish exhibited progressively lower QTc throughout the duration of the experiment, likely due to decreasing heart rate (depicted as increasing RR interval).

The design of the recording system was modified from the initial design as described in the study by Yu *et al.* [89]. The pin electrodes were derived from isolating ends of jumper wires (Austor Part AMA-18-580) and stripping the outer insulator layer of the wire about 2 cm

from the metal tip of the wires. The exposed copper wires underneath were then soldered to improve signal integrity and electrode longevity. The pin electrodes were embedded in a PDMS mold and were attached to alligator clips at the end of a cable wire leading to the differential AC amplifier (A-M Systems Model 1700). The AC amplifier bandpass filter settings were set to 1–1000 Hz. The signal from the zebrafish underwent 10000x amplification before undergoing digitalization with the data acquisition box (National Instruments Model USB-6001). The signal was then transmitted to a laptop (Dell Latitude E5470), where the processed ECG signal was displayed using the LabView interface. ECG signals were saved as text files using the LabView interface, where they can be accessed and visualized through MATLAB.

4.2.4 ECG Data Collection and Analysis. Before applying signal processing, the ECG signal was manually inspected and trimmed to remove segments with significant noise such as muscle twitching or electrical interference. A highpass and lowpass filter with 15 Hz and 70 Hz cut-off frequencies were applied to the ECG signal to remove respiratory, motion, and electrical artifacts. To accentuate the R wave morphology, a ricker wavelet with a central frequency of 25 Hz was convolved with the filtered signal. To better detect the R waves, the difference between adjacent samples was derived, squared, and smoothed using a 15-point moving average filter:

$$Y = \Phi((X_n - X_{n-1})^2) \quad (1)$$

where X_n is the ECG indexed by n, ϕ is the moving average filter, and Y is the resulting residual signal. A peak-finding algorithm was applied to the residual signal to determine the locations of the R waves in the ECG, and corrections were applied for mapping inaccuracies. The P, Q, and S waves were detected by identifying the highest maxima and lowest minima

preceding and following the R wave. Given the energy of the T wave was usually weak compared to the noise, the PQRST waveforms of the entire segment were averaged in order to extrapolate the general morphology of the PQRST, which produces an identifiable T wave. The T wave was identified as the highest point within a time range 125 to 175 milliseconds (ms) following the R wave, based on previous work [2]. These annotations were manually inspected and corrected after automatic detection. Annotated ECG signals with waveform detections are shown in Figure 4.1B. After annotating all of the waveforms in the signals, parameters including the heart rate (HR), heart rate variation (HRV), QRS interval, PR interval, and QTc interval were derived. The heart rate (in beats per minute) was calculated from the determined RR interval based on the following formula:

$$\mathrm{HR} = \frac{60}{1000\ (RR)} \tag{2}$$

where RR is in ms.

The HRV, in ms, was determined by the root mean square of successive differences between normal heartbeats (RMSSD), given by the formula:

$$HRV = \sqrt{\frac{\sum_{i=1}^{N-1}(RR_{i+1} - RR_i)^2}{N-1}} \tag{3}$$

where *N* represents the number of ECG cycles within each recording.

The corrected QT interval (QTc), in ms, was determined as shown in previous literature [90]:

$$QTc = \frac{QT}{\sqrt{RR}} \tag{4}$$

4.2.5 Isolation of Zebrafish Cardiomyocytes. Zebrafish cardiomyocytes were isolated according to the protocol presented by Sander *et al* [91]. Briefly, 6 zebrafish hearts were first excised from anesthetized fish via incision with a pair of forceps. After incubating in heparin buffer immediately after excision, the hearts were placed in a digestion buffer (1x PBS, 10

mM HEPES, 30 mM taurine, 5.5 mM glucose, 10 mM BDM (butanedione monoxime, a contraction inhibitor), 12.5 μM $CaCl_2$, 5 mg/mL collagenases II and IV) for 2 hours in a thermomixer set at 32°C and 800 rpm. The digested tissue was then washed with a sequential series of stopping buffers (1x PBS, 10 mM HEPES, 30 mM taurine, 5.5 mM glucose, 10 mM BDM, 5–10% FBS, 12.5–1000 μM $CaCl_2$). After washing, the isolated cardiomyocytes were plated on 2 wells in a 96-well plate. The plating medium consisted of DMEM with 2 mM glutamine, 5 mM BDM, 5% FBS, 100 U/mL penicillin-streptomycin, and 1:500 Normocin (InvivoGen).

4.2.6 Cloning, Cell Culture and Transfection. Rat *TAAR1* gene was amplified from total cDNA using the set of primers: (BamHI)ACCATG**G**CATCTTTGCCACAATAGCGC and (NotI)ACAAAAATAACTTAGACCTAGATGAATCT. After amplification, the *TAAR1* gene was cloned into pcDNA3.1 Zeo (+) (Invitrogen) and transformed in E. coli DH5α. The cloned plasmid product was sequenced (Sanger method) using the Sanger Sequencing Kit (Applied Biosystems). For transient expression, the plasmid (10 μg) was transfected to human embryonic kidney cells (HEK293) transiently expressing the recombinant TAAR1 protein. The HEK293 cells were maintained in DMEM containing 10% FBS and 1% penicillin/streptomycin at 37°C in a 5% CO_2 incubator. After 24 h, the cells were maintained in the media containing zeocin (100 μg/mL) for a stable expression of *TAAR1* in HEK293 cells. The transfected HEK293 cells were used in the subsequent cAMP assay and calcium assay.

4.2.7 GloSensor cAMP Assay. The HEK293 and isolated zebrafish cardiomyocytes were cultured in DMEM (10% FBS and 1% PS) in a poly-D-lysine pre-coated 96 well microplate and incubated in the CO_2 incubator at 37°C. 0.2 mL of cardiomyocyte selective growth

supplement (Sciencell) was added to the cardiomyocyte culture. The pGloSensor-22F-cAMP plasmid (10 μg was transfected into HEK293 cells and isolated zebrafish cardiomyocytes (1.5×10^4 cells) using the Lipofectamine 3000 reagent as the manufacturer described. 48 hours after transfection, cells expressing the plasmid (15,000 cells/well) were collected. The desiderated cell number was incubated in equilibration medium containing a 2% (v/v) GloSensor cAMP reagent (Luciferin) stock solution, 10% FBS and 88% CO_2-independent medium in 2 hours at 37°C according to the manufacturer's instructions. The cells were dispensed in wells of 96-well plate and a basal signal was obtained before treating with Meth with doses from 10^{-10} to 10^{-2} M was added at room temperature (~25°C) before luminescence detection. The original cell population isolated from the zebrafish heart was separated into the respective groups for treatment with different doses. EPPTB (0.1 μM) was also utilized as a selective TAAR1 and GPCR antagonist in this assay [92]. Therefore, according to the proposed pathway seen in Figure 4.3A, EPPTB would inhibit cAMP expression.

4.2.8 FLIPR Calcium Asssay. Two days after transfection, cells were washed with FLIPR buffer (1x HBSS, 20 mM HEPES, 2.5 mM probenecid, pH 7.4), loaded with the calcium-sensitive fluorophore Fluo-3 (ThermoFisher) for 1.5 h at 37°C, 5% CO_2. During the incubation, two separate 96-well polypropylene compound plates were prepared. Meth was prepared with 10-point concentration-response curve dissolved in the buffer. EPPTB was prepared in 1% DMSO in FLIPR buffer. After the incubation with Fluo-3 dyes on the assay plate, different Meth doses were added to the assay plate and incubated for 15 min at 37°C. Subsequently, the assay plate was read with a Fluorescent Imaging Plate Reader (FLIPR) Tetra (Molecular Devices). Data of calcium-responsive changes in fluorescence were

collected every second over a 60-second time period. Regarding the antagonist assay, the assay plate with EPPTB were incubated for 15 min before monitoring fluorescence.

4.2.9 Collagen Assay. The level of collagen in tissues was measured by the collagen assay kit (Sigma Aldrich) following standard protocol. Briefly, collagen in samples was first enzymatically digested into collagen peptides in master reaction mix including 35 µL buffer and 0.5 µl Collagen I. The reaction mix was incubated at 37°C for 60 min. Subsequently, 40 µL of Dye Reagent to wells and incubated at 37°C for 10 min. The collagen levels are determined by reading fluorescence at 465 nm.

4.2.10 Histochemical Staining and Immunofluorescent Staining for Collagen. After treatment of Meth, zebrafish hearts were isolated as described in previous literature [91]. Briefly, the fish were anesthetized by tricaine before undergoing chest incisions. The heart was then located and excised, which were then placed in a solution of perfusion buffer (10 mM HEPES, 30 mM taurine, 5.5 mM glucose and 10 mM BDM in 1x PBS solution). After excision of all hearts, they were subsequently fixed by 4% formaldehyde and cryo-sectioned with a cryostat. The tissue slices were placed onto frosted microscope slides (Thermofisher Scientific) and underwent Masson's Trichrome staining (following the provided protocol from American Master Tech, TKMTR2). Myocardial tissue is stained red, and collagenous tissue is stained blue. For immunofluorescence, mouse anti-collagen I antibody (Novus Biologicals) and rabbit anti-collagen III antibody were incubated overnight on cryosections of cardiac tissues, followed by staining for 2 h with goat-anti mouse IgG conjugated Alexa 568 (Abcam) and donkey-anti rabbit IgG conjugated FITC (Thermo Fisher). Sections were mounted in Antifade Mounting Medium with 4′,6-diamidino-2-phenylindole (DAPI)

(Thermo Fisher) and mounted in Antifade Mounting Medium. Fluorescent imaging was taken with the Keyence Digital Microscope (BZ-X800) system.

4.2.11 Statistical Analysis. Statistical analysis was conducted via the JMP Suite, a statistical data analysis tool derived from SAS. All parameters derived from data analysis (*i.e.*, HR, HRV, QRS, PR, QTc) were averaged within each experimental group. Statistical significance was determined by the one-way ANOVA test between experimental groups with significance level $p<0.05$. Data in figures were plotted as mean ± standard error (SE).

Outputs of the cAMP and calcium assays were expressed as relative luminescence units (RLU) and relative fluorescent units (RFU), respectively. A non-linear regression (Prism 8.0 GraphPAD Software, San Diego, CA, USA) was used to quantify methamphetamine potency for EC50 value calculations. EC50 is the concentration of agonists required to produce 50% of the maximum effect. The maximum effect obtained in the cAMP and calcium assays were approximately 1400000 RLU and 12000 RFU, respectively. Each concentration was tested three times in triplicate, and the values were given as mean ± SE. Significance was determined via the Student's T-test.

4.3 Results.

4.3.1 Methamphetamine Induced Significant ECG Changes Over the Course of 2 Weeks. Using the ECG setup designed in our lab (Figure 4.1A), we acquired ECG signals over a two-week period. The control (n = 6) and Meth-treated (n = 8) groups were immersed in the designated solutions for 20 minutes for 3 instances per week, and their ECG were subsequently acquired after treatment. The raw signals were then processed to eliminate external noise, and the PQRST waveforms were labelled on the processed ECG signals. Representative raw signals (orange) and annotated processed signals (blue) are displayed in Figure 4.1B. Relevant ECG

parameters including HR, HRV, QRS, QTc, and PR intervals were then quantified. The day number was defined as follows: day 1 corresponded to the first day of Meth treatment, and subsequent days were numbered accordingly. Figure 4.1C & 4.1D comprise ECG diagrams obtained during baseline, week 1, and week 2 of the treatment regimen. Figure 4.1C represents individual ECG signals after filtering and smoothing. Figure 4.1D represents the averaged outcome of all ECG signals for the specific experimental group and time period, developed for the detection of the T wave. The representative ECG figures indicate a progressive decrease in heart rate for the Meth-treated group with instances of sinus arrest highlighted by blue brackets (Figure 4.1C). The QTc interval also displayed a decrease in the treated group (Figure 4.1D). Calculated ECG parameters are displayed in Figure 4.2. All ECG parameters were verified to display no significant differences during baseline measurement between the experimental groups. Two trials were conducted, and the results of the second trial are presented in Supplemental Figure 4.1. Additionally, the results also indicate that there were no significant differences in QRS duration between the Meth-treated fish and the untreated (control) fish throughout the duration of the study (Figure 4.2E).

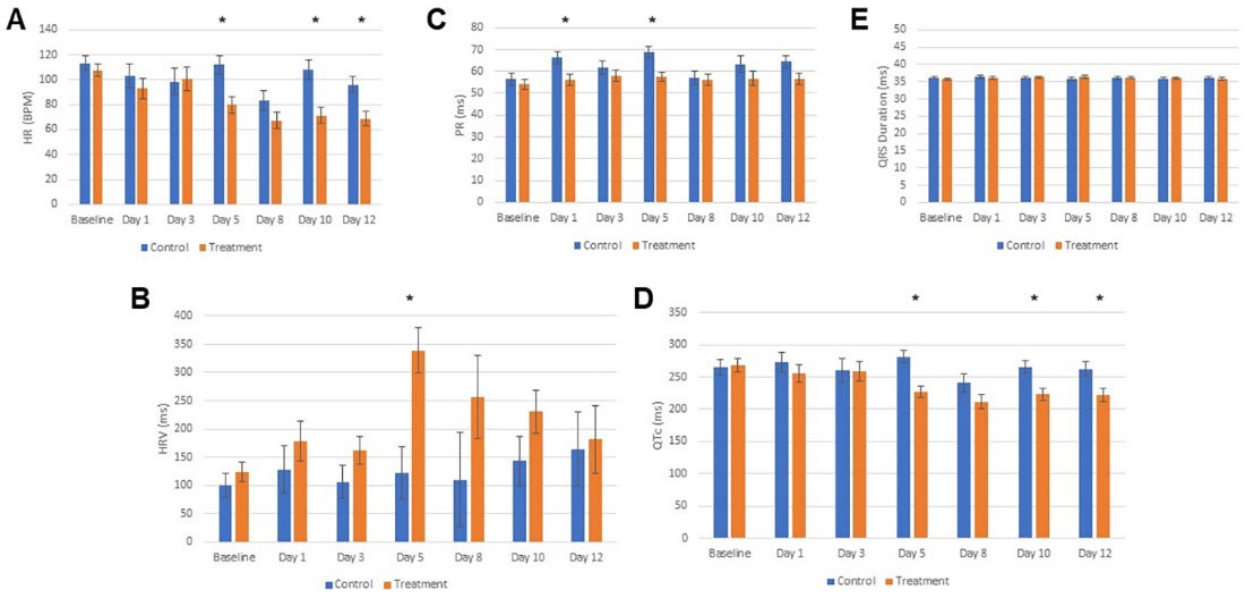

Figure 4.2 Meth Induces a Biphasic and Depressive Effect on Cardiac Electrophysiology.
Tabulated averages from all ECG data acquired from both untreated (control, n = 6) and Meth-treated (treatment, n = 8) groups across the 2-week study. (A) Meth-treated fish displayed decreased heart rate compared to the untreated fish starting from the end of the week 1. (B) Meth-treated fish exhibited a biphasic trend in heart rate variation (HRV) throughout the duration of treatment, reaching a peak at the end of week 1 before decreasing during week 2. (C) Meth treatment induced a significant decrease in PR interval during week 1 but not week 2 of treatment. (D) Meth treatment induced a significant decrease in QTc during the end of week 1 before maintaining the depressed QTc throughout week 2. (E) Meth treatment did not exhibit a change in QRS duration. * denotes $p<0.05$.

The heart rate (HR) for treated fish decreased throughout the course of the treatment, exhibiting signs of bradyarrhythmia (Figure 4.1C). In the first trial, the HR presented significant differences at the end of the first week of the treatment (Figure 4.2A). The HRs on day 5 ($p = 0.008$) were 79.77 BPM (95% CI, 65.43–94.11) and 111.9 BPM (95% CI, 95.31–128.4) for treated and untreated fish, respectively. The HR stabilized in the second week (days 10 ($p = 0.004$) and 12 ($p = 0.012$)), displaying a consistent decrease through the remainder of the study. The HRs for treated fish were 71.17 BPM (95% CI, 56.71–85.63) for day 10 and 68.99 BPM (95% CI, 55.55–82.44) for day 12. These were in contrast with the HRs seen in untreated fish, which displayed 107.9 BPM (95% CI, 91.21–124.6) and 95.89 BPM (95% CI, 81.37–110.4) for days 10–12, respectively. In the second trial, the HR for treated fish displayed a significant decrease on the third day of treatment and remained lower than those of untreated fish throughout the course of the experiment (Supplemental Figure 4.1A).

Throughout the course of the study, the heart rate variation (HRV) displayed a biphasic trend for the treated fish (Figure 4.2B). The HRV between Meth-treated fish and control fish exhibited no differences on days 1 and 3, but Meth seemed to have induced an increase in HRV during the first week of treatment. Treated fish exhibited a significant increase in HRV during day 5 ($p = 0.004$), reaching up to 338.6 ms (95% CI, 251.5–425.6) vs 121.7 ms (95%

CI, 21.20–222.3) seen in untreated fish. This also corresponds to the maximum HRV attained by the treated fish during the study. The increase in HRV may be attributed to the presence of sinus arrest as indicated by the blue brackets in Figure 4.1C. The HRV decreased during the second week of treatment, although it still remained above the HRV for untreated fish. On day 12 ($p = 0.851$), the heart rate variation for Meth-treated fish was 181.2 ms (95% CI, 48.12–314.3) compared to 164.1 ms (95% CI, 20.32–307.8) seen in untreated fish. Results from the second trial displayed a similar biphasic trend for HRV within treated fish (Supplemental Figure 4.1B). HRV exhibited a steady increase until Day 8 of treatment before subsequently decreasing through the end of the study.

In the first trial, Meth induced significant changes in the PR interval during the first week of treatment (Figure 4.2C). On day 1 ($p = 0.019$), the Meth-treated fish exhibited a PR interval of 56.00 ms (95% CI, 50.55–61.45), compared to the PR interval of untreated fish, which was 66.37 ms (95% CI, 60.08–72.66). For day 5 ($p = 0.007$), the PR intervals for Meth-treated fish and untreated fish were 57.55 ms (95% CI, 52.50–62.59) and 68.91 ms (95% CI, 63.09–74.74), respectively. There were no significant differences found during the second week of treatment. Interestingly, the differences in PR interval were not significantly evident during the second trial (Supplemental Figure 4.1C).

The QTc interval displayed a significant decrease during the first week for Meth-treated fish in both trials(Figure 4.2D and Supplemental Figure 4.1D). The most significant decrease occurred on day 5 ($p = 0.001$), with QTc interval being 226.8 ms (95% CI, 208.4–245.3) and 281.5 ms (95% CI, 260.2–302.8) for treated and untreated fish, respectively. The QTc interval stabilized during the second week, generally maintaining the significant decrease

for Meth-treated fish. On day 12 ($p = 0.017$), the QTc interval was 222.2 ms (95% CI, 200.6–243.8) and 262.7 ms (95% CI, 239.4–286.1) for treated and untreated fish, respectively.

4.3.2 Methamphetamine Treatment Leads to Increased Expression of cAMP and Ca^{2+} in a TAAR1-mediated, Dose-Dependent Manner. To help uncover the direct molecular mechanism in the induction of Meth-induced cardiotoxicity, zebrafish cardiomyocytes (n = 6 zebrafish) were isolated and treated with Meth to determine Meth induced cAMP expression via the GloSensor cAMP assay, which is involved in regulating GPCR pathways. TAAR1-overexpressed HEK293 cells have also been produced to complement the assay as the positive control, and original HEK293 cells served as the negative control. Figure 4.3A depicts the proposed GPCR/cAMP pathway that enables Meth-induced cardiotoxicity. In previous studies, Meth has been discovered to bind to GPCRs such as TAAR1 to trigger the upregulation of cAMP in cardiomyocytes [93]. cAMP downstream signaling may be linked with the onset of cardiac pathology, such as fibrotic dysregulation via lysyl oxidase and arrhythmia via CaMKII. The results from the cAMP assay indicate that Meth led to a dose-dependent upregulation in cAMP expression within zebrafish cardiomyocytes (Figure 4.3B). Additionally, TAAR1-overexpressed HEK293 cells displayed a greater increase in cAMP expression than original HEK293 cells, indicating that TAAR1 mediated cAMP expression due to Meth exposure. In a similar fashion, Ca^{2+} was also upregulated due to Meth exposure within zebrafish cardiomyocytes (Figure 4.3C). TAAR1-overexpressed HEK293 cells displayed a greater increase in Ca^{2+} concentration than original HEK293 cells, indicating that TAAR1 also mediated Ca^{2+} dysregulation due to Meth exposure. These results are further corroborated by experiments involving EPPTB, a TAAR1 antagonist. As indicated in Figure 4.3D, 4.3E, EPPTB attenuated Meth-induced cAMP and Ca^{2+} upregulation in a dose-

dependent manner. This also suggests that Meth-induced cardiotoxicity involving cAMP and Ca^{2+} dysregulation may be attenuated by targeting TAAR1 and the GPCR pathway.

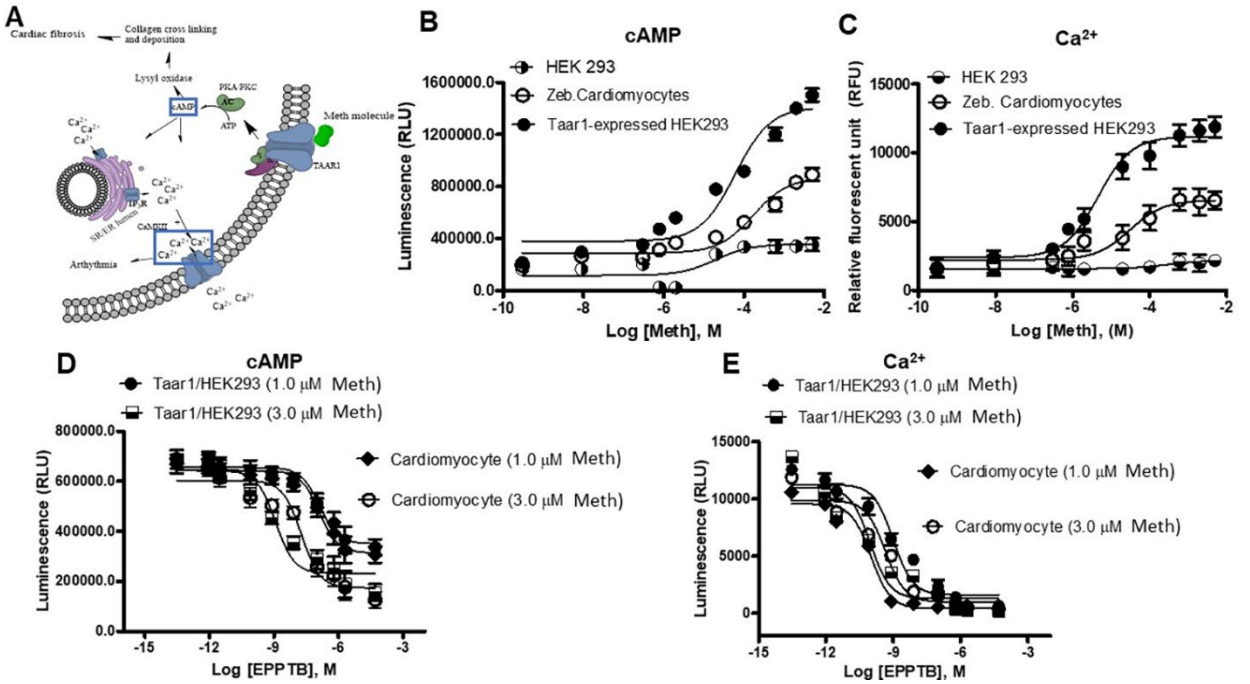

Figure 4.3. Zebrafish cardiomyocytes exhibit a TAAR1-mediated Increase in cAMP Expression and Ca^{2+} Concentration due to Meth Treatment. (A) Proposed mechanism of the pathologic effects of Meth on cardiomyocytes, including the upregulation of cardiac fibrosis via lysyl oxidase and the increased frequency of arrhythmia via the calmodulin CaMKII. cAMP, the upstream factor for both processes, and Ca^{2+}, the ion modulated by CaMKII, are both highlighted to indicate that they were investigated in this study. (B) Detection of cAMP expression after Meth treatment from zebrafish cardiomyocytes, HEK293, and TAAR1-overexpressed HEK293 cells via the GloSensor cAMP assay. TAAR1-overexpressed HEK293 cells served as the positive control for this assay. HEK293 cells served as the negative control. Results display that Meth induced dose-dependent cAMP expression in zebrafish cardiomyocytes. cAMP expression from TAAR1-overexpressed HEK293 cells exhibited a greater dose-dependent increase, demonstrating TAAR1-mediated cAMP expression due to Meth treatment. (C) Detection of Ca^{2+} after Meth treatment from zebrafish cardiomyocytes, HEK293, and TAAR1-overexpressed HEK293 cells. Results display that Meth increased Ca^{2+} concentration within zebrafish cardiomyocytes in a dose-dependent manner. Ca^{2+} expression from TAAR1-overexpressed HEK293 cells exhibited a greater dose-dependent increase, demonstrating that TAAR1 mediates Ca^{2+} concentration due to Meth treatment. (D-E) Results from the dose-response experiment with EPPTB, an inhibitor of TAAR1, in the presence of Meth, further corroborating previous results of TAAR1-mediated increases of cAMP expression (D) and Ca^{2+} concentration (E).

4.3.3 Methamphetamine Treatment Produce Excessive Fibrosis in Zebrafish Cardiac Tissue.

To determine if Meth induces fibrotic dysregulation, which was delineated above as one of the potential cardiotoxic factors contributing to arrhythmias, Masson's Trichrome staining

for collagen and collagen type I immunological staining were conducted on cardiac tissue obtained from both untreated and Meth-treated fish (n = 6 per group). Images obtained from Masson's Trichrome staining (Figure 4.4A, 4.4B) revealed a higher presence of collagen deposits in Meth-treated cardiac tissue, as highlighted in the dotted boxes. Immunological staining (Figure 4.4C, 4.4D) further revealed a higher presence of collagen type I with Meth-treated tissue. Collagen fluorescent assay of purified protein samples revealed that the collagen content increases from Meth treatment in a dose-dependent manner, displaying the highest difference at the highest concentration of Meth (Figure 4.4E). An expression profile of genes associated with fibrosis was also conducted, and the results determined that Meth-treated tissue displayed significantly higher expression ($p<0.005$) in lysyl oxidase (*LOX*) and lysyl hydroxylase (*PLOD*) (Figure 4.4F). This result signifies that the lysyl oxidase family of proteins was upregulated in response to Meth treatment. While the other genes involved in the profibrotic response (*COL1A1*, *COL3A1*, *MMP1*, and *TMP1*) did not display significance, their expressions have also shown marginal increases in Meth-treated cardiac tissue over its untreated counterpart. Overall, these results display an uptick in the fibrotic response due to Meth treatment, further outlining Meth-associated cardiotoxicity in relation to the GPCR/cAMP pathway.

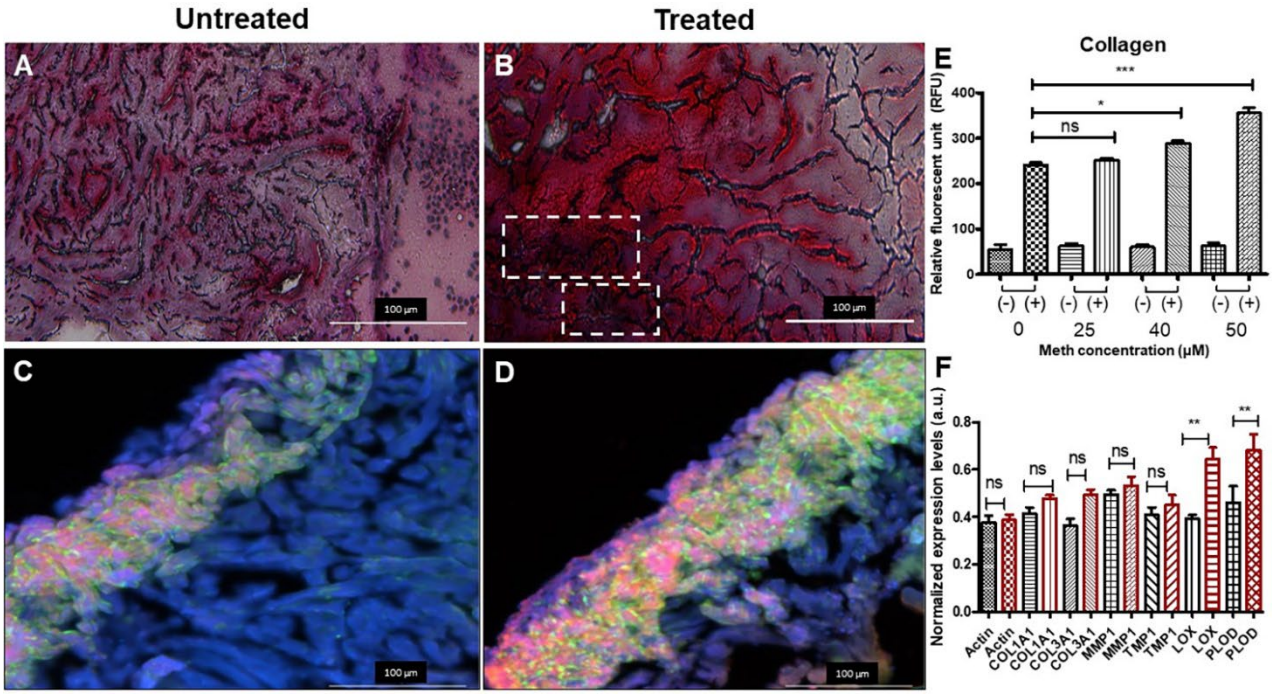

Figure 4.4. Meth results in increased fibrotic response in zebrafish cardiac tissue. (A-B) Masson's Trichrome Staining of cardiac tissue obtained from untreated zebrafish (n = 6) and Meth-treated zebrafish (n = 6). Myocardial tissue is stained in red, and collagen is stained in blue. Areas of collagen deposits are labeled by white dashed boxes in Meth-treated cardiac tissue. (C-D) Collagen type I immunological staining of untreated and treated cardiac tissue. Presence of lighter colors (*i.e.*, pink, yellow, green) indicates the presence of collagen. Meth-treated tissue displays higher amounts of collagen I. (E) Collagen fluorescent assay conducted on protein samples treated at various concentrations of Meth. Positive symbol (+) signifies collagenase I treatment and negative symbol signifies no treatment. Results indicate that collagen content increases due to Meth treatment in a dose-dependent manner. (F) Expression analysis of genes associated with fibrosis, including the family of lysyl oxidases. (*COL1A1* = collagen I; *COL3A1* = collagen III; *MMP1* = matrix metalloproteinase I; *TMP1* = thymidylate kinase; *LOX* = lysyl oxidase; *PLOD* = lysyl hydroxylase) Meth-treated tissue exhibited significantly higher expression of lysyl oxidase and lysyl hydroxylase, associated with the GPCR pathway. Expression of other genes displayed marginal increases in treated tissue, indicating higher instance of fibrosis. * denotes $p<0.05$. ** denotes $p<0.005$. *** denotes $p<0.0005$.

4.4 Discussion.

The methamphetamine epidemic continues to fester worldwide, and cardiovascular diseases remain leading causes of death for methamphetamine abusers. Utilizing animal models to study cardiovascular associated mechanisms could be critical in devising treatments for Meth associated diseases. The zebrafish is an excellent model for drug screening studies due to high fecundity, low maintenance, and similar genetic homology to that in humans. As the

zebrafish model is constantly evolving, studies have continued to delineate the applicability of the zebrafish in human medical research. During the initial conception of this study, we sought to 1. Establish the zebrafish model as an adequate model of drug screening for cardiotoxic effects, and 2. Characterize the electrophysiological abnormalities due to meth administration in a controlled environment. Utilizing our custom-designed zebrafish ECG acquisition system in our lab, we were able to acquire ECG from zebrafish during the two-week treatment period with Meth. Based on our results, we determined several significant ECG changes occurring between the Meth-treated and untreated fish. The progressive decrease in heart rate for treated zebrafish, while contradictory to the results seen in human clinical studies, was actually consistent with the results seen in previous animal model studies, including those performed on rats, monkeys, and zebrafish embryos [74, 94, 95]. Those previous studies suggested that the decrease in heart rate due to Meth administration may be attributed to the baroreceptor reflex, a homeostatic response to the increase in blood pressure [96]. Schindler *et al*. documented a consistent blood pressure increase with the dosage of Meth administered in squirrel monkeys [94]. However, they noted that heart rate modulation from Meth administration may be biphasic, as lower Meth concentrations induces tachycardia, while higher Meth concentrations induces bradycardia. This suggests that there is a critical Meth concentration where it achieves a maximum catecholaminergic effect without triggering a significant baroreceptor reflex. The decrease in PR interval due to Meth treatment suggests quicker atrial conduction, which is consistent with the mechanism of Meth to induce ventricular tachycardia [97]. The heart rate variability exhibited a peak at the end of the first week before decreasing during the second week.

HRV is used in cardiac physiology as a measure of healthy function and as a potential parameter for determining cardiovascular diseases such as sudden cardiac death[98]. More importantly, HRV may also provide insight into the brain-heart axis and how the autonomic nervous system impacts cardiac function, critical to the analysis of stimulant drugs such as Meth [99]. The initial increase in HRV may likely be due to the presence of sinus arrest in Meth-treated fish. As shown in Figure 4.1C, ECG acquired from Meth-treated fish displayed episodes of sinus arrest, where an instance of cardiac conduction normally present in regular sinus rhythm is absent. The HRV increase may also be attributed to the baroreceptor reflex, as the reflex would naturally adjust the heart rate in order to maintain stability in blood pressure and cardiac output. Most notably, the decrease in HRV during the second week of treatment is most likely associated with cardiac tissue damage and inflammation, consistent with the symptoms seen in Meth-induced cardiomyopathy [100, 101]. This is corroborated with research indicating that persistent hypertension induced a decrease in HRV, presenting the long-term pathophysiological effects of Meth [102]. Additionally, previous case studies involving Meth and amphetamine abusers indicated that the presence of elevated cardiac biomarkers such as troponin I and creatine kinase-MB, further suggesting that common symptoms of Meth use may be associated with cardiac damage [103-105]. Overall, the HRV results from this study suggest the biphasic nature behind the mechanism of Meth, where the cardiovascular system may initially respond to the effects of the drug before sustaining damage after a period of persistent exposure.

Additionally, the QTc interval, associated with ventricular contraction and proper heart function, decreased for Meth-treated fish, displaying the most pronounced differences in the second week of treatment. Initial observation suggested that the decrease in QTc interval

seemed to be associated with the decrease in heart rate (or increase in RR interval, as depicted in Figure 4.1D. The QT/HR relation has been widely documented, leading to the creation of the corrected QT interval to account for the effect of heart rate changes on the QT interval [106]. Nevertheless, the results obtained from this study remained contrary to the results seen in previous case studies, where Meth abusers tended to exhibit prolonged QTc intervals in response to Meth intake [76, 107]. However, these case studies utilized data from humans who were already predisposed to Meth for varying periods of time, usually to the point of drug dependence. Therefore, QTc prolongation could potentially be a symptom seen in the later stages of Meth-induced cardiotoxicity. Previous clinical trial research has associated the development of QTc prolongation with ventricular tachycardia and cardiomyopathy, which are common symptoms of Meth abuse [100, 108, 109]. QTc shortening seen in this study may also suggest that calcium channels are downregulated by Meth, as decreased calcium influx also reduces action potential duration. This is corroborated by ion channel expression analysis from rats suggesting that Meth reduces calcium channel expression [110]. Potassium channel expression may also play a role in analyzing the effect of Meth on modulating the QT intervals. Numerous anticonvulsants and antiarrhythmics have been known to shorten QTc by upregulating potassium channel function. Moreover, Meth has been shown to induce upregulation of potassium channels in the brain in relation to its neuropathic effects, suggesting that Meth has the potential to modulate potassium channels in other pathologies [111]. However, more research will be needed to elucidate the direct effects of Meth on ion channels *in vivo*, as patch clamp results from rat cardiomyocytes regarding the effect of Meth on calcium channels remain

controversial [107, 112]. In general, ion channel analysis in cardiovascular pathology remains scarce.

We surmise that Meth might pose an antagonizing interaction with tricaine, the anesthetic agent used to acquire ECG. Tricaine usage was also mandatory for this study due to regulatory purpose. However, both Meth and tricaine have opposing mechanisms, as Meth is a stimulant while tricaine is an established anesthetic, known for preventing action potential firing by blocking voltage-gated sodium channels [113]. The data revealed that Meth-treated zebrafish exhibited significant decreases in PR interval on certain days in the early stage of treatment due to the excitatory properties of Meth. However, a closer inspection of the data indicated that the increase in PR interval for untreated fish was responsible for the significant change instead. Indeed, tricaine may induce a decrease in myocardial contractility, which results in a decrease in heart rate and increase in PR interval during zebrafish sedation [114, 115]. Additionally, zebrafish subjected to repeated tricaine treatment exhibited increased susceptibility to anesthetic effects [116]. Results from the first trial revealed a decrease in heart rate for untreated fish during the treatment period (day 8). However, the heart rate remained stable during the second trial, suggesting that the susceptibility to anesthetic effects may be varied between individual organisms. Meth may also induce arrhythmic instances, which could confound HRV measurements [117]. In the first trial of this study, insignificant but noticeable increases in HRV were evident in days 10 and 12 for untreated fish. However, this was not seen in the second trial. Meth studies involving other animal models have also suggested the confounding effect of anesthetics. Research concerning the hemodynamic response to Meth reported differing results, as a study conducted on anesthetized cats documented a decrease in blood pressure due to Meth

administration, while a study conducted on conscious monkeys indicated an increase in blood pressure [94, 118]. It is unclear if the difference in results was due to the presence of anesthesia or an underlying combinatorial effect of Meth and the anesthetic agent. Research has also suggested that Meth confers a depressor effect in addition to the commonly known pressor effect, and the depressor effect may dominate for animals under anesthesia. Vaupel *et al*. reported a significant decrease in blood pressure after the onset of Meth administration in anesthetized rhesus monkeys, suggesting the presence of the depressor effect [119]. In addition, tricaine has been shown to induce augmented effects with other agents. Muntean *et al*. treated zebrafish larva with dopamine and verapamil under both tricaine-anesthetized and methylcellulose-embedded conditions, and their results indicate that the effects of the agents on myocardial calcium signaling and heart rate were greater in anesthetized fish than embedded fish [120]. This suggests that tricaine has the potential to induce drug-drug interactions with other agents to influence underlying electrophysiology. Therefore, future improvements should be implemented to reduce the effect of tricaine for zebrafish cardiotoxic studies, as tricaine could introduce confounding circumstances, especially when testing psychostimulants on zebrafish. Future studies should also seek to explain the effect of these chemical entities on ion channel function through analysis of sodium and calcium transients for zebrafish. These future experiments would determine the mechanism of methamphetamine in inducing cardiotoxicity as well as bolster the use of zebrafish as a suitable model for cardiotoxic studies.

GPCRs and one of their prominent secondary messengers, cAMP, have been attributed to modulate numerous neurological dysregulations due to Meth exposure [81, 121]. For example, studies have discovered that TAAR1 was significantly involved in the modulation

of the physiological and addictive response to Meth [84]. As a result, subsequent research has targeted TAAR1 for developing genetic and pharmacological treatments for the methamphetamine epidemic [44, 85]. Due to ubiquitous nature of TAAR and GPCRs, this signaling pathway is also located in other physiological systems. Fehler *et al*. determined the presence of TAAR receptors within the aorta and their role in drug-associated vasoconstriction, which leads to cardiovascular conditions such as high blood pressure [122]. Interestingly, this process does not appear to be mediated by the neuronal system [123]. Recent research has indicated that GPCRs may also play a role in producing detrimental cardiac effects of Meth, including arrhythmia, fibrosis, cardiomyopathy, and tissue remodeling [124, 125]. As depicted in Figure 4.3A, cAMP interfaces with numerous factors within the GPCR pathway that may induce such cardiovascular effects [126]. cAMP upregulation is known to lead to fibrosis via increased lysyl oxidase production, as lysyl oxidase plays a major role in collagen and ECM crosslinking [127]. cAMP is also involved in the modulation of CaMKII, principal in the maintenance of myocardial calcium ion homeostasis [128]. CaMKII dysregulation has been attributed to the development of cardiac pathologies, such as the regulation of cardiac extraction-contraction coupling and the activation of inflammatory and hypertrophic pathways [129]. Using the GloSensor cAMP assay, we demonstrated that the upregulation of cAMP occurred in a dose-dependent manner within zebrafish cardiomyocytes. This upregulation was inhibited by EPPTB, an antagonist of TAAR1 and cAMP. We also demonstrated that Ca^{2+} was upregulated by Meth in a TAAR1-dependent fashion. Collagenic assays on untreated and Meth-treated zebrafish further indicated that Meth induced an increased fibrotic response in cardiac tissue, consistent with the concept that Meth-associated fibrosis led to the dysregulation in cardiac

electrophysiology. The significant upregulation in the family of lysyl oxidase proteins further suggests that TAAR1 and GPCRs modulate this response. Overall, the results from this study indicate that Meth upregulated cAMP in zebrafish cardiomyocytes, causing dysregulation in Ca^{2+} homeostasis and fibrotic response, suggesting that cAMP and GPCRs play a role in Meth-induced cardiotoxicity.

Additional research should be conducted to further understand the role of heart-brain axis due to Meth exposure, such as the link between neurotransmitter response and cAMP/GPCR expression to cardiovascular abnormalities, as well as an investigation on ion channel function in the heart after Meth administration The zebrafish model has already been utilized in numerous Meth studies, mostly related to behavioral studies due to the ability of Meth to disrupt dopamine release and reuptake, thus increasing dopamine expression [130]. Therefore, it would be intriguing to understand the role of dopamine in Meth-induced cardiotoxicity, as it would explain whether Meth-induced cardiotoxicity is caused by dopamine or through a direct effect from Meth. One consequence of dopamine response is the change in ion channel expression. For example, studies have shown the modulation of L-type calcium channels by Meth, but it is not fully understood whether Meth alters calcium channel function directly or via dopamine [112, 131, 132]. As mentioned earlier, ion channel modulation may also be integral in understanding the cardiac electrical remodeling induced by Meth. Meth has been determined to alter the expression and functionality of potassium and calcium within cardiomyocytes, which were correlated to Meth-associated arrhythmic events [107, 112]. These effects were not attributed to neuronal functions, indicating that separate mechanisms may also be in play for Meth-associated alterations in the neuronal and cardiovascular system.

The goal of this study is to provide elucidation into the effect of Meth on cardiac physiology and electrophysiology in a standardized, controlled setting. The generated results suggest that Meth induces a predominant depressor effect on cardiac electrophysiology most likely due to the baroreceptor reflex and cardiac damage. This was manifested as a progressive decrease in heart rate and eventual decrease in HRV. This effect persisted through the end of the two-week treatment, which may be a sign of cardiac damage as seen in Meth-induced cardiotoxicity. Molecular analysis suggested that the Meth exposure via cAMP upregulation leads to the development of fibrosis and arrhythmia.

4.5 Conclusion.

The objective of this study is to provide a detailed analysis of the effects of methamphetamine (Meth) on cardiac physiology and electrophysiology within a standardized, controlled environment. Leveraging the technology developed and presented in Chapter 5, the study's findings suggest that Meth exerts a significant depressive effect on cardiac electrophysiology, likely mediated by the baroreceptor reflex and resulting cardiac damage. This depressive effect is evidenced by a progressive decline in heart rate and a subsequent reduction in heart rate variability (HRV). Notably, these effects persisted throughout the two-week treatment period, which may indicate underlying cardiac damage consistent with Meth-induced cardiotoxicity.

Molecular analysis further revealed that Meth exposure leads to upregulation of cyclic AMP (cAMP) and dysregulation of calcium (Ca2+) signaling, which are associated with the development of fibrosis and arrhythmia, respectively. These findings provide critical insights into the mechanisms by which Meth impacts cardiac function, contributing to the broader understanding of Meth-induced cardiovascular pathology.

CHAPTER 5

Development of Zebrafish ECG System for Extended Measurement for Drug Screening and Genetic Functional Analysis

5.1 Introduction.

Cardiovascular diseases (CVDs) are the leading cause of death worldwide. According to the 2020 AHA Annual Report, almost 860,000 people died of CVDs in the U.S. in 2017, and the overall financial burden from CVDs totaled $351.2 billion in 2014–2015, emphasizing the urgency to explicate the etiologies of CVDs [6]. One such CVD is the sick sinus syndrome (SSS), a collection of progressive disorders marked by the heart's inability to maintain a consistent rhythm of heart muscle contraction and relaxation [133]). The sick sinus syndrome is characterized by age-associated dysfunction of the sinoatrial node (SAN), with varying symptoms such as syncope, heart palpitations, and insomnia [134]. The SSS has multiple manifestations on electrocardiogram (ECG) data, including sinus bradycardia, sinus arrest (SA), and sinoatrial block. The pathophysiology of SSS is not fully understood, but scientists have determined that it can be caused by numerous factors ranging from pharmacological medications and sleep disturbances to fibrosis and ion-channel dysfunction [135]. Previous research has emphasized SSS-associated genetic pathways as potential avenues to a more permanent treatment for SSS [136-138].

The zebrafish serves as an ideal model for cardiovascular studies because of its similar homology to humans in both morphology, physiology, and genetics [139, 140]. Despite having only two discernible chambers in the zebrafish heart compared to four in human hearts, the zebrafish heart possesses a similar contractile structure with an analogous conduction system [141, 142]. Therefore, the zebrafish model is appropriate in the study of

SSS and the correlation of related genetic pathways to the electrophysical phenotype via ECG. Currently, several research groups have developed systems to assess zebrafish ECG. Regarding sensor design, conventional needle electrodes are commonly used. Lin et al (2018)[143] designed and tested the needle electrode with different materials, including tungsten filament, stainless steel, and silver wire to investigate the recorded data quality. Along with a portable ECG kit, the authors aimed to provide a standard platform for research and teaching laboratories. The needle system was also deployed in other studies [143-146] to conduct biological and/or drug-induced research. Although the system demonstrated promising results, the needles had to be gently inserted through the dermis of zebrafish in order to collect favorable signals. The sharpness of the needles could cause injury to the fish's heart, thus possibly changing signal morphology [145]. Moreover, it requires an intensive effort to precisely position the electrode on the tiny heart in order to achieve clear ECG acquisition. Therefore, several alternative probe systems have been developed, including the micro-electrode array (MEA) and the 3D-printed sensors. Our team and other research groups have demonstrated the use of MEA for acquisition and provided data with a favorable signal-to-noise ratio (SNR) and high spatial and temporal resolution [86, 147, 148]. For instance, we presented a MEA array covering the fish's heart, which enabled site-specific ECG signals [86, 147, 149] developed a MEA printed on a flexible printed circuit board (FPCB) based on a polymide film for multiple electroencephalogram (EEG) acquisition for epilepsy studies. Although the MEA allowed multiple signal recordings, only one fish can be assessed at a time due to the limited number of electrode channels. To address this shortcoming, our group recently demonstrated a prolonged system for acquiring ECG from multiple fish simultaneously [150]. The MEA was replaced with two electrodes made of 125-

μm thick polymide with sputtered-Au electrodes embedded at the bottom of the housing for data acquisition. However, noise generated from a pump used for water circulation precluded high-SNR ECG signals. Furthermore, bulky and expensive acquisition tools were used to collect and transfer data through a cable to a computer. In the market, commercially available systems, such as the iWORX (Dover, NH), can provide improved system mobility with a compact amplifier. However, several challenges have not been resolved, such as i) the commercial systems only record for a short period of time (3–5 min), which is inadequate for experiments that need longer recording such as acute drug interactions; ii) the ECG acquisition requires anesthetized animals, rendering those systems stressful to the fish and inadequate to provide intrinsic cardiac electrophysiological data; iii) manual one-by-one measurement limits the capability of conducting studies necessitating a large number of fish; and iv) ECG data processing is carried out offline with exorbitant effort. Last but not least, no high throughput systems integrated with microelectronic systems have been reported for characterizing mutant phenotypes. Therefore, developing high throughput systems capable of prolonged ECG acquisition is an essential step for finding associations between arrhythmic phenotypes and mutant genotypes, identifying multiple arrhythmic phenotypes that are linked to a single mutant genotype, as well as elucidating cardiac drug efficacy using the zebrafish model.

In this work, the novel Zebra II system is introduced, which is capable of prolonged ECG acquisition from multiple fish simultaneously. An in-house electronic system was developed, leveraging the Internet of Thing (IoT) capability with wireless data transmission and data processing on a mobile application. The IoT capability enhanced the mobility and versatility of the system as well as supported distanced collaborations to conduct research on zebrafish

models. The system was validated through numerous experiments, displaying its potential with 1) simultaneous ECG acquisition from 4 fish; 2) continuous ECG acquisition for up to 1 h compared to several minutes (min) of currently available systems; 3) reduction in confounding effects from anesthesia with the use of 50% lower Tricaine concentration. The system featured a robust capacity in prolonged ECG acquisition from different experiments including sodium-induced SA, temperature-induced heart rate variation, and drug-induced arrhythmia for *Tg(SCN5A-D1275N)* mutant and wildtype fish in standardized experimental conditions. The implementation of multiple electrode channels for prolonged ECG acquisition also enables the implementation of randomized controlled trials, with two fish per experimental group in identical experimental conditions. Finally, the developed ECG system holds promise and solves current drawbacks in order to greatly accelerate arrhythmic phenotype analysis and drug screening applications in zebrafish.

5.2 Materials and Methods.

5.2.1 Mutant Tg(SCN5A-D1275N) and zebrafish husbandry. Mutant *Tg(SCN5A-D1275N)*, a transgenic zebrafish arrhythmia model bearing the pathogenic cardiac sodium channel mutation *SCN5A-D1275N*, was used to characterize and validate system performance, study sinus node dysfunction, and perform drug high throughput screening assays. Correlation between clinical phenotype and the mutant line has been reported for bradycardia, conduction-system abnormalities, episodes of SA [138].

Adult wild/mutant-type zebrafish with the age of 13–20 months (body lengths approximately 3–3.5 cm) were used in this study. Zebrafish were kept in a circulating system that was continuously filtered and aerated to maintain the water quality required for a

healthy aquatic environment. The fish room was generally maintained between 26 and 28.5°C, and the lighting conditions were regulated within a 14:10 h light: dark cycle.

All animal protocols in this study were reviewed and approved by the Institutional Animal Care and Use Committee (IACUC) protocol (#AUP-18-115 at University of California, Irvine). All drug administration experiments (section 1 Introduction, 2 Materials and Methods supplementary document), chemicals, reagents, and materials were performed in accordance with relevant guidelines and regulations.

5.2.2 Design and validations of the Zebra II system. The Zebra II system is composed of a perfusion system, an in-house electronic system, apparatuses, and sensors (Figure 5.1A). The perfusion system comprised four syringes, four valves and tubing. The four syringes contained Tricaine solution with low concentration, which continuously fed to the fish through the tubing system. Tricaine (MS-222) was used as an anesthetic to reduce the fish's aggressiveness and activity while maintaining their consciousness. The four valves were used to adjust the solution's flow rate within a range of 5.5–6 ml/min, while housing apparatuses and sensors were improved from the previous work [150]. Specifically, multiple side-fitted housings were made of polydimethylsiloxane (PDMS), which provided comfort to the fish and minimized unwanted movements. Moreover, the top and bottom of the apparatus were designed to allow the fish to lay comfortably on electrodes within the curved bottom. The top was fitted with an additional part on the wall to keep the fish from escaping the apparatus. The zebrafish ECG system was placed within a home-made incubator (Figure 5.1). Temperature within the chamber ranged from 20 °C to 32 °C, as measured by a thermometer and controlled by a thermostat with an accuracy of ±1 °C.With the thermo box, a specific temperature was set by the thermostat control, and the light bulb was turned on

so that the box's temperature can be maintained at the setup temperature and vice versa. The electronic system and the mobile application are described in Figure 5.1B-D and Supplemental Figure 5.1. The overall system electronic specifications are shown in Sup. Supplemental Table 5.1.

The Zebra II wirelessly transmitted ECG signals to a smartphone, and the data were displayed on a mobile application as shown in Figure 5.1D. To test the reproducibility, ECG signals were acquired from 8 wild type (WT) fish for 7 trials, and the variations in terms of signal to noise ratios (SNR), heart rate, QTc interval, and QRS interval were monitored. These results are further illustrated in Supplemental Figure 5.2. Furthermore, a robust and scalable real-time stream processing system leveraging the Google Cloud infrastructure was designed and implemented to facilitate remote monitoring and high-throughput ECG analysis. The processing system is illustrated in Supplemental Figure 5.3. The system was constructed to provide a collaborative platform for different research groups regardless of their geographical locations. With the capabilities of acquiring ECG from multiple fish simultaneously for up to 1 h, the proposed design can save time and efforts by nearly 40–50 fold compared with conventional approaches [138, 143, 144].

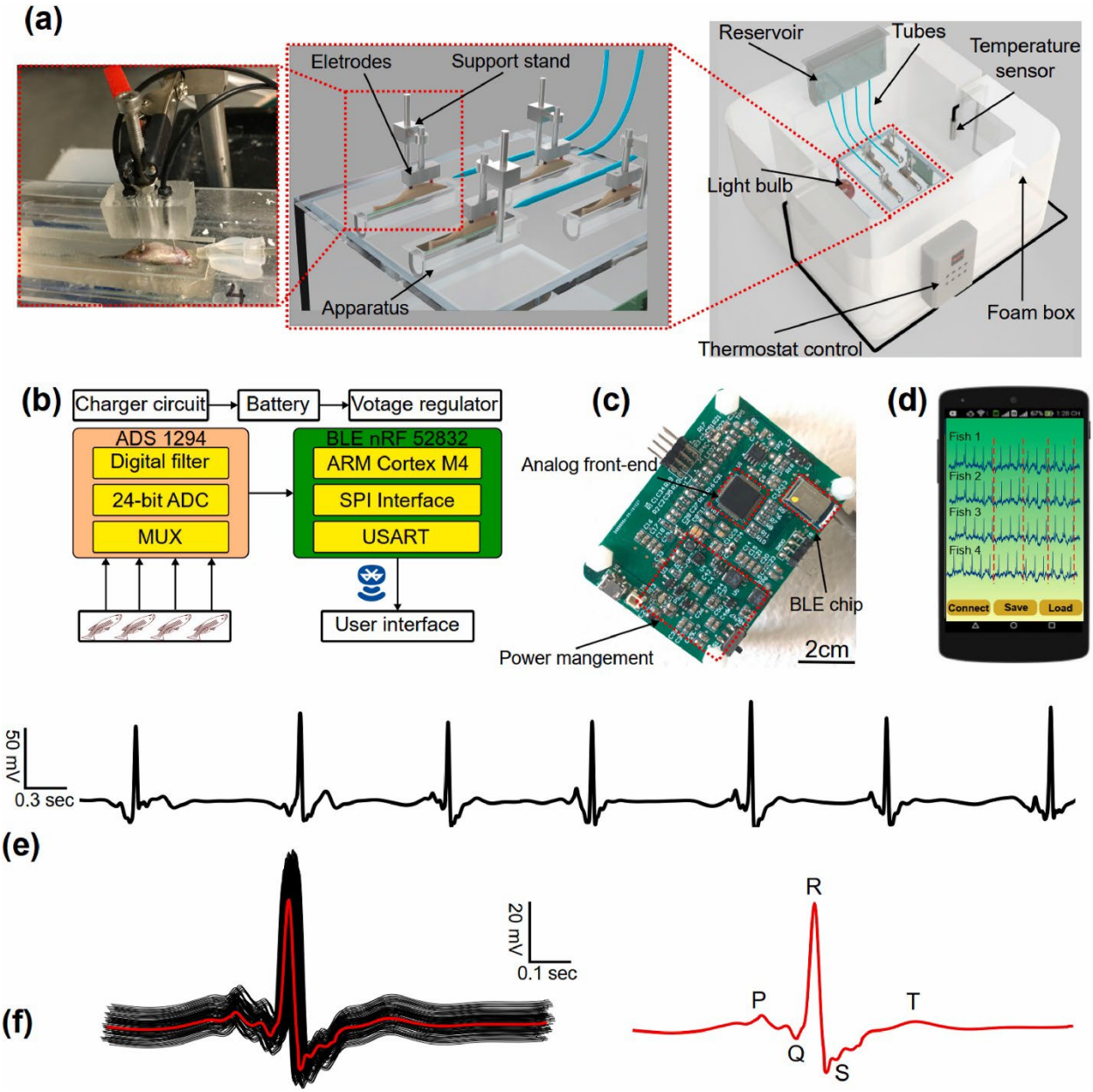

Figure 5.1. The prolonged ECG system for multiple adult zebrafish acquisition. (a) the prolonged ECG system design: the reservoir for containing Tricaine solution, the tube system for feeding the solution to the fish, the electrodes and support stand for acquiring ECG signals. (b) System-level block diagram showing analog front-end chip, signal transduction, wireless transmission from the ECG to user interface. (c) In-house electronic board having system-on-chip for wireless transmission, power management connecting to the electrode for ECG acquisition. Scale bar: 2 cm. (d) User interface of the mobile application receiving ECG data from multiple fish. (e) Representative ECG data collected by the system. (f) ECG data segments superimposed, and its average ECG segment in red with clear ECG waves (P wave, QRS complex and T wave).

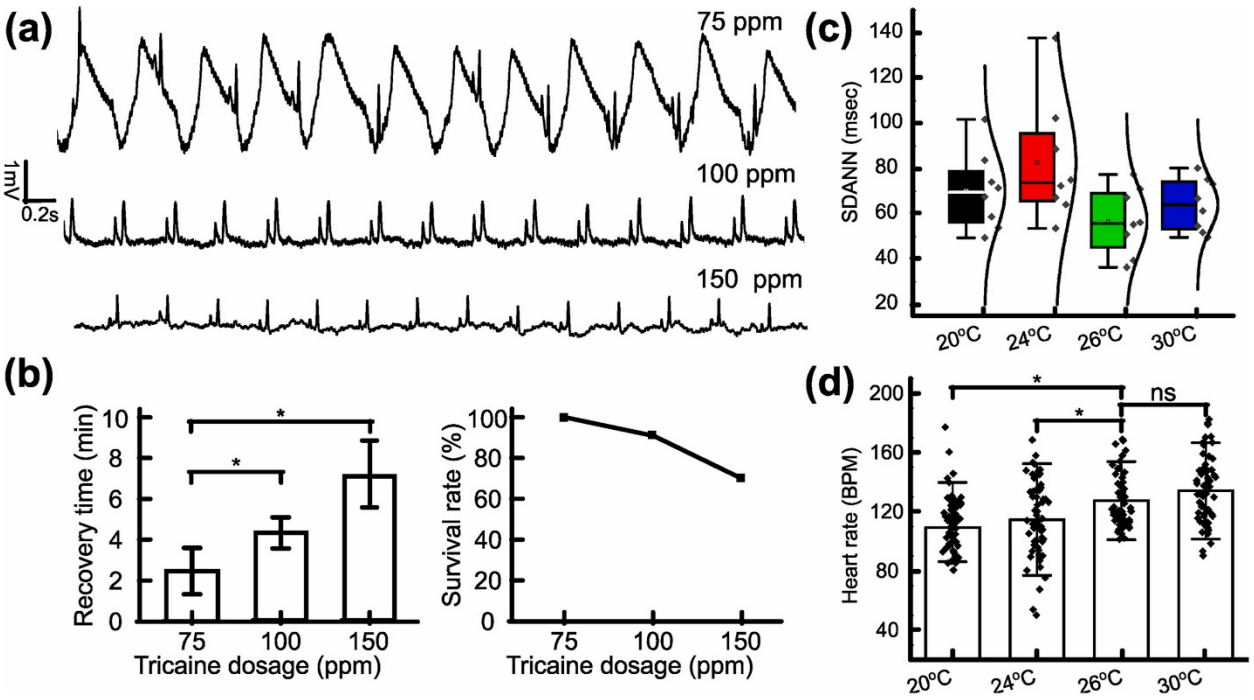

Figure 5.2. Investigation of Tricaine and Temperature to Reduce Cardiac Rhythm Side Effects. (a) Representative ECG data recorded from fish treated with different Tricaine concentrations. (b) Bar chart comparing recovery time needed after treatment for each Tricaine concentration. Line graph describing the survival rate of zebrafish treated by different Tricaine concentrations. (c) SDANN in WT fish with different temperatures. (d) HR in WT fish with different temperatures (N = 64, standard deviation (SD) of HR at 20 °C, 24 °C, 26 °C, 30 °C: 17.8 BPM, 25.2 BPM, 17.6 BPM and 21.7 BPM, respectively). *p < 0.05; **p < 0.01 (one-way analysis of variance). *ns* indicates not significant.

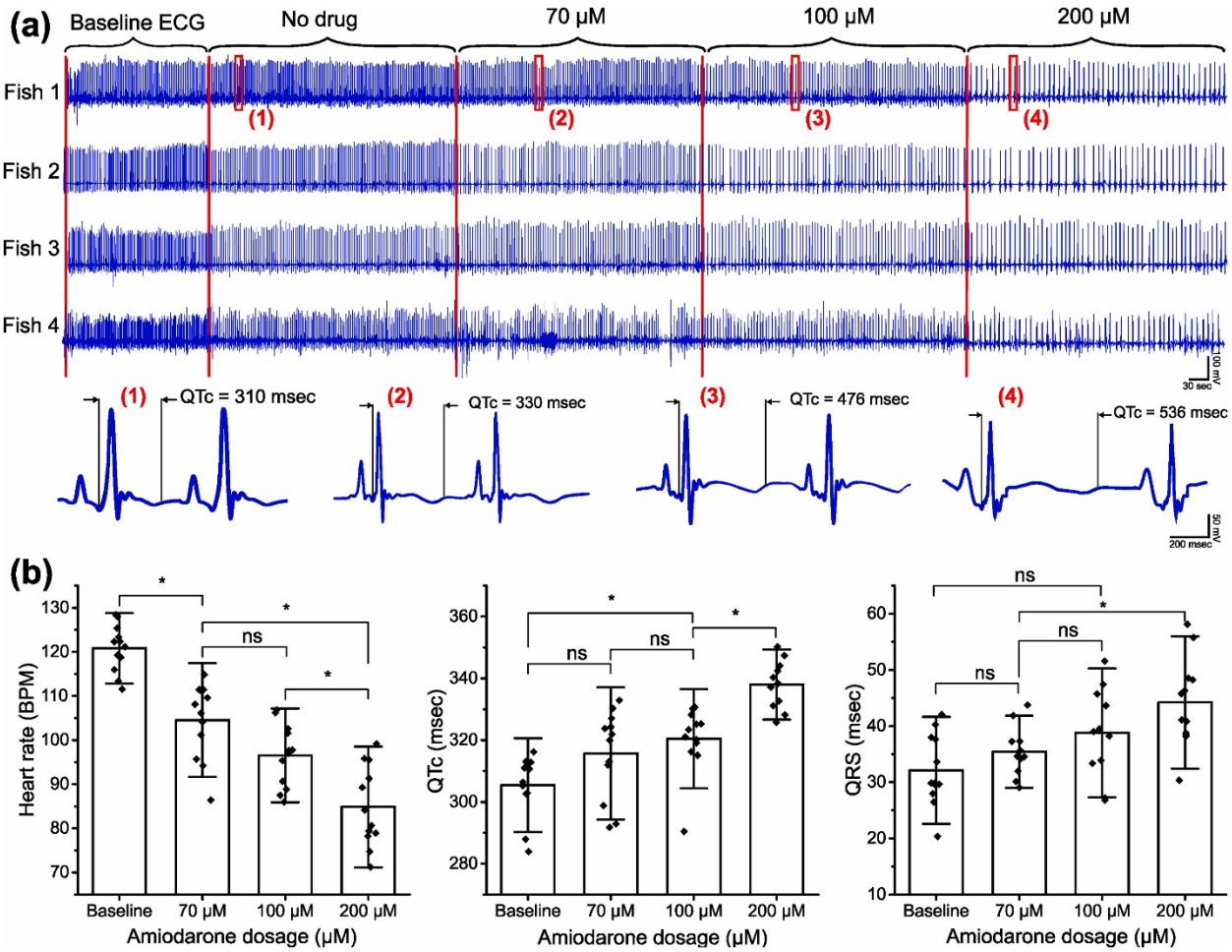

Figure 5.3. Demonstration of the Prolonged System Showing ECG Changes in Response to Rifferent Amiodarone Concentrations. (a) Representative ECG data obtained by the developed system and its change in ECG parameters due to different Amiodarone concentrations. (b) Bar chart describing the discrepancy of HR, QTc interval and QRS interval in ECG data with different Amiodarone concentrations (n = 8 fish). Quantification of heart rate decreased in response to Amiodarone (120.8 ± 5.3 BPM without treatment, 84.9 ± 9.1 BPM with 200 μM Amiodarone) while the QTc and QRS interval tend to increase (337.9 ± 7.5 msec with no drug and 44.2 ± 7.9 msec with 200 μM Amiodarone). *p < 0.05 (one-way analysis of variance with Turkey test). *ns* indicates not significant.

Experiments were conducted to validate the performance of the developed system. First, zebrafish ECG signals were acquired simultaneously using the Zebra II and the commercial system developed by iWORX (Dover, NH) to assess the data quality from fish under Amiodarone treatment. Then, the optimal Tricaine concentration and temperature were determined for ECG acquisition (n = 64).

To further investigate this mutant line as a candidate for cardiac studies, we assessed the relationship between *SCN5A* and Meth [151])– a controlled substance. Several groups have studied its connection of using addictive drugs with sudden death. For instance, Nagasawa et al., screened several variations in the long QT syndrome-associated genes *KCNQ1 (LQT1)* and *KCNH2 (LQT2)*, showing the increased risk of severe cardiac arrhythmia for addictive drug abusers [152]). However, they did not test for *SCN5A* variants, which was explored in the current study. Additionally, rescuing arrhythmic phenotypes induced by high sodium intake could provide insights into the nature of those arrhythmic phenotypes, as Meth has been previously demonstrated to increase HR after administration [100]. Specifically, we treated two groups of zebrafish (labelled as "control" – WT fish and "mutant" – *Tg(SCN5A-D1275N)*) in 0.9‰ NaCl for 30 min before immersing the fish in 50 μM Meth for 30 min. As shown in Figure 5.5, the HR, SDNN and QTc interval were compared between the two groups in the following three treatments: without drug treatment, with NaCl treatment, and with NaCl + Meth treatment (n = 12 WT fish and n = 8 Tg(*SCN5A-D1275N* fish)).

5.2.3 Signal Processing and Statistics. The recorded ECG data were analyzed, and several parameters were extracted, including heart rate (HR), QT, and QTc intervals[153]. The standard deviation of normal sinus beats (SDNN) was calculated based on the short-term, beat-to-beat variance of HR in each 5 min segment of the data, and the standard deviation of the average normal-to-normal (SDANN) intervals was calculated based on the variance of average HR from each 5 min segment. SDNN was used for short-term data analysis based on each 5 min segment, and SDANN was used for long-term data analysis for the whole 40 min segment[154].

Statistical analysis was performed using the following tests with OriginLab 2019. Multiple comparisons were tested with one-way ANOVA, and significant results ($P < 0.05$) were analyzed with pairwise comparisons using Student's t-test applying significance levels adjusted with the Bonferroni method. Significant P-values are indicated with asterisks (*) with $*P < 0.05$, $**P < 0.01$ and $***P < 0.001$. Correlation analysis was performed using Pearson's correlation.

5.3 Results and Discussion.

5.3.1 Multiple Zebrafish ECG Acquisition with Zebra II. The ECG data collected from Zebra II are shown in Figure 5.1E. The data were pre-processed using the Wavelet technique [153] to reduce various types of noise. Figure 5.1 F illustrates the ECG segments superimposed during the measurement, with each line representing one cardiac cycle. The full set of ECG waves symbolized with the P-wave, QRS-complex, and T-wave was present in the mean of ECG segments as highlighted in red, showing waveform reproducibility and stability during the recording period. Moreover, prior to the acquisition of ECG data, the impedance of the electrodes on zebrafish skin was verified (Supplemental Figure 5.4). The low standard deviation error indicated that ECG acquisition from the electrodes will remain stable for the duration of the measurement, ensuring that any variations in ECG acquisition were not caused by faulty electrodes. The relative standard deviation (RSD) of such parameters is presented in Supplemental Table 2.

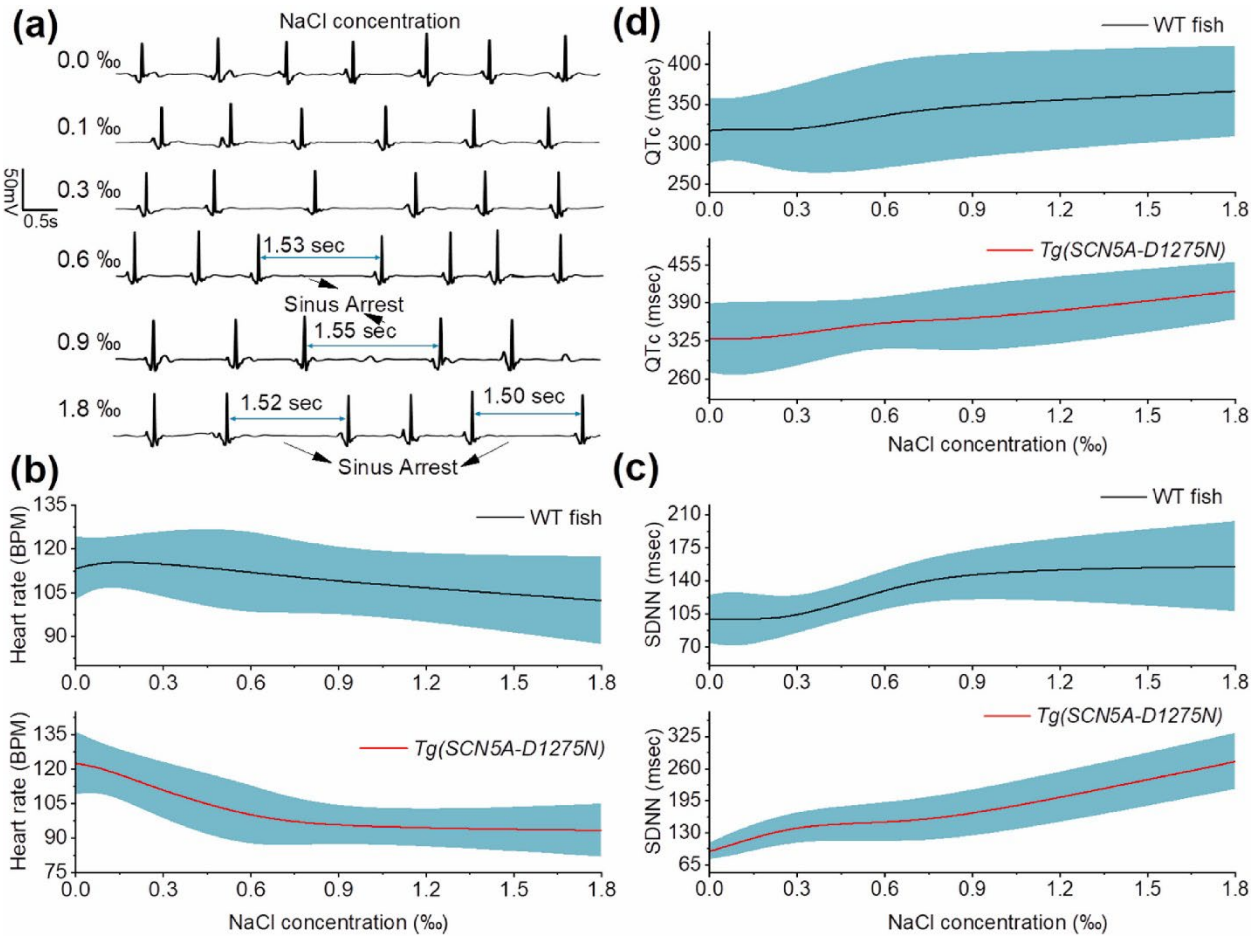

Figure 5.4. Evaluation of sodium sensitivity in the development of sinus arrest in *Tg*(*SCN5A-D1275N*). (a) Representative ECG data before and after NaCl treatment with different concentrations. SA appears more frequently in response to the increase of NaCl concentration. (b) The average HR of WT fish (n = 12), showing the slight decrease from 113.4 ± 10.8 BPM without treatment to 102.1 ± 15.0 BPM; the averaged HR of *Tg(SCN5A-D1275N)* mutant fish (n = 8), showing significant reduction from 122.6 ± 13.7 BPM without treatment to 93.3 ± 11.5 BPM after NaCl treatment. (c) SDNN of WT fish (n = 12) and mutant fish (n = 8), displaying similar variations in HR. (d) QTc values shows slight increase in both wild-type and mutant fish after NaCl treatment.

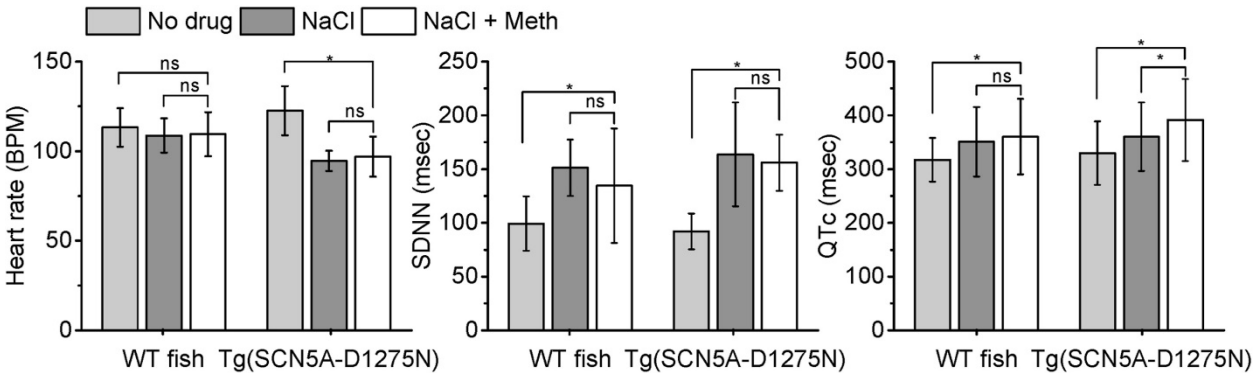

Figure 5.5. Investigation of methamphetamine (Meth)'s efficacy to rescue arrhythmic phenotypes after treatment with NaCl. The experiment analyzed and compared HR, QTc and SDNN among three treatments (*e.g.*, no drug treatment, NaCl and, NaCl + Meth). The experiment was conducted in both WT fish and mutant fish *Tg*(*SCN5A-D1275N*). The average HR and SDNN for mutant fish treated with NaCl + Meth did not show significant difference from average HR and SDNN treated with NaCl only. *p < 0.05 (one-way analysis of variance with Turkey test). *ns* indicates not significant.

The acquired ECG data were then compared in both frequency domain and time domain (Supplemental Figure 5.5a & 5.5b). Specifically, the correlation coefficients were 98.78% and 96.54% in time domain and frequency domain, respectively. Moreover, the HR and QRS interval were also compared (Supplemental Figure 5.5c and 5.5d). As shown in the data, the Zebra II's performance was comparable to that of the commercial iWORX system. Then, another experiment was performed on 36 wildtype (WT) zebrafish divided into the following 2 groups: 1) control (n = 20) and 2) Amiodarone treated (n = 16) fish. As shown in Supplemental Figure 5.6, HR, QRS duration and QTC interval were analyzed. With the control group, no significant difference (p-value > 0.05) between two systems in terms of QRS and QTc value was observed. Similarly, the HR value and QTc value showed no significant difference in the treated group. Furthermore, the Bland Altman analysis in Supplemental Figure 5.6b, 5.6d and 5.6f showed the agreement level between two systems, with most of HR values and QTc values located within the limit of agreement (LOA) region.

Electrode placement contributed significantly to the intensity of ECG data. With the use of the low Tricaine concentration to enable longer ECG acquisition, the fish tended to exhibit unexpected strong movement, thus leading to electrode dislocation. In the future, a mechanism may be utilized to automatically detect the impedance of electrode-tissue interface, which can be used to indicate the contact between electrode and fish's chest. In terms of the current electronic system, the low-noise and high-resolution ADS chip provided favorable ECG data with additional data processing feature. However, scaling up to 8, 16 or even 24 channels to include more fish may be challenging at this point. For instance, it would require multiple ADS chips cascaded together, which would increase its computational power. However, wireless data transmission using BLE will no longer be compatible with this scenario due to the limit of bandwidth [155]. Another challenge was presented in terms of time delay. Since the recorded ECG data were wirelessly transmitted to the mobile app via BLE, the connection between the fish system and mobile phone needs to be established first. A set of connection parameters (*e.g.*, connection interval, slave latency, and connection supervision timeout) was sent by the smartphone (BLE master device) to the fish system (BLE slave device), which takes about 2 s based on the observation during the experiment. Thus, establishing the initial connection contributed to the delay in wireless data transmission between the Zebra II and the phone. Additionally, with the sampling rate of 250 Hz, the operation time for ADC and BLE communication between the system (a slave device) and a phone was 4 msec. In regard to the cloud system, the time from acquiring ECG data to displaying the data on the cloud with Grafana was approximately 2 s. As a result, the total delay from the initial ECG acquisition to the presence of data on the cloud was 6 s. Thus, the entire operation can be considered as pseudo-real time.

5.3.2 Investigation of Side Effects of Tricaine and Variable Temperature Cardiac Rhythm.

Tricaine (MS-222) and temperature have been shown to affect cardiac physiology of adult zebrafish and the HR of the treated subjects [114, 143]. At low temperatures (*e.g.*, 18 - 20 °C), myocyte activity is reduced as a natural adaptive mechanism to aid survival during colder climates or seasons, which leads to a reduction in HR. At higher temperatures, increased HR facilitates greater cardiac output to support a higher metabolic activity/demand for oxygen consistent with normal physiological function [156]. Therefore, with an optimal environment temperature, the prolonged ECG system introduced in this work will help lower the Tricaine concentration used in experiments, which can reduce the confounding effects of Tricaine in order to obtain intrinsic ECG data.

As shown in Figure 5.2a, the ECG data from 8 fish per concentration group (75, 100, and 150 ppm) of Tricaine were obtained. The ECG data showed gill motion noise, manifested as low frequency, cyclic perturbations in the data. The noise interfered with the identification of ECG waves such as P waves, T waves and QRS complexes from fish treated with 75 ppm Tricaine, while the noise appeared to be more subdued in data obtained from fish treated with 100 ppm and 150 ppm. As a result, ECG data acquired from fish treated with 100 ppm and 150 ppm displayed clear ECG waves. After 40 min measurement, the recovery time and the survival rate after treatment were collected (Figure 5.2b). It was found that fish treated with higher Tricaine concentrations necessitated longer recovery times. Specifically, fish treated with 150 ppm Tricaine took an average of 7 min to recover compared to the 3 min and 4.2 min for fish treated with 75 and 100 ppm, respectively. Furthermore, the survival rate of fish treated with 150 ppm Tricaine was about 75%, while other concentrations yielded survival rates above 90%. It reflected the effect of extremely high Tricaine

concentration similar to that used for euthanasia (*i.e.*, 168 ppm) [157]). Given the recovery time, the survival rate, and the acquired ECG data, the Tricaine concentration of 100 ppm was most optimal for ECG acquisition. Additionally, the variation of HR was also assessed in each 5-min segment during the 40-min measurement (Supplemental Figure 7). No significant difference was observed between the 5–min to 10–min, 10-min to 15–min, 15-min to 20–min, and 20-min to 25–min segments for ECG data from fish treated with either 75 ppm or 100 ppm Tricaine. The only difference occurred in the last 10 min of the 40-min measurement when the HR displayed more fluctuation with 75 ppm Tricaine (115.67 ± 25.29 BPM) than that with 100 ppm (115. 93 ± 11.28 BPM).

After determining the optimal Tricaine concentration, the effect of temperature on acquired ECG was investigated. As shown in Figure 5.2C, SDANN at 26 °C had the lowest value with the range of 36 ms (msec) to 75 msec, while the SDANN at 24 °C is highest with the range of 50 msec–139 msec. Moreover, the data distribution from HR collected every 5 min at 26 °C was the most condensed (Figure 5.2d). Thus, the HR obtained at 26 °C was the most stable compared to the values obtained at other temperatures.

5.3.3 Response Analysis to Drug Treatment in Real Time with the Zebra II System. One of the key novelties of the Zebra II system is the capacity to test drugs with different concentrations on individual fish with a continuously prolonged assay. First, the effect of Amiodarone with different concentrations on zebrafish ECG was analyzed. Three doses of Amiodarone were consecutively filled in the reservoir to feed to the fish during ECG acquisition, and each dose lasted around 5 min. As shown in Figure 5.3a, the changes in response to different dosages in all four fish were apparent. Zooming in on the data acquired from fish 1 at timepoints denoted from (1) to (4) corresponding to different Amiodarone concentrations revealed that

the QTc interval displayed considerable changes. The QTc interval was 310 msec without drug treatment. Noticeable increases in QTc interval were observed after Amiodarone treatment. Specifically, the interval was 330 msec at 70 μM of Amiodarone, 476 msec at 100 μM, and 536 msec at 200 μM. Figure 5.3b depicts the overall changes in terms of QTc interval, QRS interval, and HR in response to different Amiodarone concentrations. As Amiodarone concentration increased over the duration of the experiment, QTc interval and QRS interval increased, while the average HR decreased.

In drug response studies, conducting real time or pseudo-real time measurements with the same fish is most ideal due to biological variability among subjects. The perfusion system is equipped with multiple chambers for multiple drug doses in order to provide seamless transitions of multiple drug treatments, decreasing potential noise and perturbations. The developed system was able to demonstrate that a longer acquisition enables the treatment of multiple drugs, as indicated by the successful demonstration of dose-response Amiodarone-associated ECG changes described earlier in this section, as well as sodium-associated ECG changes described later in section 5.4.4. The utility of the perfusion system can also be expanded to include the testing of multiple drugs simultaneously to assess ECG changes due to drug-drug interactions, a developing field of study. The chambers in the perfusion system can also contain multiple drugs for the precise modulation of zebrafish drug intake in order to accurately determine the effects of each tested drug as well as the onset of potential drug-drug interactions. While the subsequent ECG analysis of *Tg(SCN5A-D1275N)* indicates that Methamphetamine (Meth) did not improve SA frequency and HR, it demonstrated the assessment of effects of multiple drugs, as seen from the prolongation of the QTc interval after treatment of 50 μM of Meth (Figure 5.5). In both groups, the QTc

interval was longer (by 350 msec for WT and 385 msec for *Tg(SCN5A-D1275N)*) after Meth treatment. Thus, the robust performance of the system allowed incorporation of multiple drugs with different effects (*e.g.,* antagonistic effects) in a single continuously prolonged assay to study the effect of drug-drug interactions on ECG changes, which was previously heavily performed on the short time course of other existing systems. Various ECG changes due to drug treatment were detected in prolonged ECG acquisition) to provide intuitive insights into drug-drug interaction effects, demonstrating the potential of the developed system to evaluate drug efficacy. As shown in Figure 5.4d for the sodium sensitivity experiment, the average SDNN was 125 msec for WT fish but was 255 msec for *Tg*(*SCN5A-D1275N*), consistent with reduced conduction velocities due to sodium ion channel dysfunction[158].

5.3.4 Evaluation of High Sodium Intake in the Development of Sinus Arrest (SA) in Tg(SCN5A-D1275N). No previous research studies investigated the role of high sodium intake on the development of SA for zebrafish with increased susceptibility to arrhythmia due to genetic causes. Here, the developed system demonstrated the role of excess sodium ions in inducing ECG changes in the *Tg(SCN5A-D1275N)* mutant, successfully characterizing the onset of arrhythmic phenotypes such as SA. Figure 5.4a illustrates the ECG data obtained from *Tg(SCN5A-D1275N)* fish with different NaCl concentrations. Zebrafish started displaying a reduction in HR when treated with a low NaCl concentration of 0.1‰. More significant reductions were detected when the fish were treated with higher concentrations. According to the SA criteria (e*.g.*, RR interval is greater than 1.5 s) determined in our previous work [138], SA appeared more frequently after treatment with 0.6‰ NaCl and above (Table 5.1). The result confirmed a strong association between high sodium intake

and arrhythmic phenotypes, previously reported in hypertensive populations [159]. High sodium intake is associated with alterations in various proteins responsible for transmembrane ion homeostasis and myocardial contractility. Recent studies provided important evidence that high sodium intake promotes structural and functional impairment of the heart, especially in populations bearing mutant phenotypes of the major cardiac sodium channels such as $Na_v1.5$ and its corresponding gene *SCN5A*. However, there was a current lack of a functional prolonged ECG acquisition system to characterize arrhythmic phenotypes from $Na_v1.5$ sodium channel mutants, including the functional response of $Na_v1.5$ to initiate action potentials based on high sodium intake. SA induced by high sodium intake was observed in this study and may be associated with a rise in intracellular sodium concentration within cardiomyocytes due to the gain-of-function of *Tg(SCN5A-D1275N)* for sodium ions traveling into the cardiomyocyte. Detection of SA by the developed system implied that the *Tg(SCN5A-D1275N)* fish is susceptible to arrhythmic phenotypes after high sodium intake due to hastening epicardial repolarization and causing idiopathic ventricular conduction. These pathological changes were manifested as ECG changes and ventricular arrhythmias. ECG data acquired by the developed system were consistent with clinical reports, indicating that Brugada syndrome in human and animals resulted in ventricular conduction abnormalities due to high sodium intake [160, 161]. High sodium intake can cause destabilized closed-state inactivation gating of $Na_v1.5$ that may attenuate the ventricular conduction delay as shown in the ECG data (Table 5.1).

Fish	WT				Tg(SCN5A-D1275N)			
Drug	Average HR (BPM)	Percentage of fish with SA (No. of cycles)	SA frequency epm	QTc (msec)	Average HR (BPM)	Percentage of fish with SA (No. of cycles)	SA frequency epm	QTc (msec)
0% NaCl	113.3 ±10.8	8.3 (1)	0.08	317.2 ± 40.7	122.6 ± 13.7	12.5 (1)	0.125	329.8 ± 59.1
0.1 % NaCl	115.9 ±7.5	8.3 (1)	0.08	319.7 ± 36.3	120.4 ± 9.9	12.5(1)	0.125	327.2 ± 64.8
0.3% NaCl	114.9 ±11.5	8.3 (1)	0.08	316.1 ± 56.6	110.3 ± 12.6	37.5(7)	0.875	335.7 ± 55.8
0.6% NaCl	112.1 ±15.2	16.6 (2)	0.16	337.2 ± 68.2	98.9 ± 14.4	75(8)	1	359.9 ± 37.1
0.9% NaCl	108.7 ±9.5	25 (3)	0.25	350.7 ± 64.7	94.6 ± 5.7	75(15)	1.875	360.1 ± 64.0
1.8% NaCl	102.4 ±15	50 (7)	0.42	366.1 ± 56.4	93.3 ± 11.5	87.5(17)	2.125	410.5 ± 49.5
0.9% NaCl + 50 uM Meth	109.4 ±12.3	25 (3)	0.25	360.2 ± 70.3	96.95 ± 21.2	75(15)	1.875	391.3 ± 76.1

Table 5.1. Comparison of WT and *Tg*(*SCN5A-D1275N*) fish with NaCl treatment.

As shown in Figure 5.4b, mutant fish exhibited a significant decrease in HR after treatment of 0.6‰ NaCl. In contrast, NaCl treatment did not show a profound effect to the WT fish, as evidenced by the smaller decrease in HR after NaCl treatment. It was worth noting that these WT fish were at 1.5 years old, which could attribute to an increase of SA [138], and the slight reduction of HR in the experiment (Supplemental Figure 5.8). In terms of HRV, *Tg(SCN5A-D1275N)* fish showed a remarkable increase at high NaCl concentrations (0.9‰ and 1.8‰) compared with other concentrations. These results provided evidence that the *Tg*(*SCN5A-D1275N*) triggered more SA under NaCl treatment (Table 5.1). Moreover, the SDNN and QTc interval in response to NaCl treatment were also measured, exhibiting similar trends for both WT and mutant fish. (Figure 5.4c and Supplemental Figure 5.9).

Notably, the results indicated that high sodium intake induced more drastic ECG changes in *Tg(SCN5A-D1275N)* fish. NaCl treatments at 0.6‰, 0.9‰, and 1.8‰ resulted in SA with durations of 1.53 s, 1.55 s and 1.52 s, respectively. Additionally, slower HR and prolonged QTc intervals were observed only in mutant fish. These results provided a significant

association between the increased frequency of SA, slower HR, and prolonged QTc with increased sodium intake in mutants. According to previous reports [162, 163], $Na_v1.5$ can disrupt the heart's electrical activity and lead to a dramatic decrease of HR. The slow-conducting *Tg(SCN5A-D1275N)* mutant has been demonstrated previously by voltage-clamp measurement [164, 165], which corroborated with the results in this study. The average QTc intervals were as high as 385 msec, indicating that the QTc intervals in mutant fish were generally more prolonged than wild type animals. Overall, high sodium intake led to various arrhythmic phenotypes, including slow HR, prolonged QTc, and increased SA frequency in *Tg(SCN5A-D1275N)* fish (Figure 5.4d).

5.3.5 Rescue of Arrhythmic Phenotypes Induced by High Sodium Intake in Tg(SCN5A-D1275N) Fish. The average HR of mutant fish after the NaCl + Meth treatment (96.96 ± 7.61 BPM) was slightly higher than that of mutant fish solely treated with NaCl (94.59 ± 5.69 BPM) (Figure 5.5); however, the difference was not significant ($P > 0.05$). Similarly, the SDNN value did not show any significant difference between mutant fish treated with NaCl + Meth and those solely treated with NaCl (Figure 5.5). Meth was administered to the fish to determine if their cardiac systems could respond to the drug's mechanism of inducing ECG changes (*i.e.,* increased HR, QTc prolongation). However, the obtained data indicated that Meth treatment did not affect the HR and SDNN in both groups (Table 5.1), implying that NaCl administration resulted in some irreversible arrhythmic phenotypes (*i.e.,* slow HR) that could not be easily rescued with other agents that increase HR. In contrast, a significant increase in QTc interval was detected in the mutant fish after Meth treatment (391.3 ± 76.1 msec vs. 360.1 ± 64.0 msec), indicating the additive effect of Meth to QTc interval prolongation (Table 1). Considering that no significant increase in QTc interval was seen in

WT fish, the data indicated the mutant fish were more susceptible to agents causing QTc prolongation. Therefore, these results suggested different susceptibilities for arrhythmic phenotypes in the mutant *Tg*(*SCN5A-D1275N)*.

The ECG data obtained from this study provided new evidence that high sodium intake increased the susceptibility of *Tg*(*SCN5A-D1275N*) fish to arrhythmic phenotypes. Results from mutant fish indicated the pathological slowing of HR, prolonged QTc interval, and higher frequency of SA. Although the developed system cannot provide other cardiac indices, such as ejection fraction and cardiac output, the system's ability to detect arrhythmic phenotypes in real time is valuable for many applications such as drug screening and phenotype assessment.

5.4 Conclusion.

The novelties of the developed Zebra II lie in the extended measurement for multi-step experiments (up to 1 h), high throughput screening with multiple zebrafish, controlled setting with minimal confounding effects, and automated cloud-based analytics. The system was successfully demonstrated to investigate the arrhythmic mutant line *Tg(SCN5A-D1275N),* revealing the effect of high sodium intake on the development of sinus arrest (SA), slow HR, and prolonged QTc. In the future, the Zebra II can be used for a host of cardiac disease studies, including phenotypic screening for genetic engineering studies and new drug screening applications.

CHAPTER 6

Zebra II as a Novel System to Record Electrophysiological Signals in Zebrafish

6.1 Introduction.

Cardiovascular diseases (CVDs) are the leading cause of death worldwide. According to the 2024 AHA Update Report, around 2552 people die every day of CVDs in the U.S., and the average direct and indirect cost of CVD was estimated at $378.0 billion in 2017-2018[7]. Atrial fibrillation (AF) is one of the most common cardiac arrhythmias in the U.S.[166] and is associated with an unfavorable prognosis, increasing the risk of stroke and death in both CVDs and non-cardiovascular disease scenarios, leading to an increased risk of adverse outcomes[167]. This type of arrhythmia is distinguished by its rapid and irregular electrical activity in the atria, which usually results in a fast and irregular ventricular rhythm[168]. Further, given the recent events of COVID-19, there has been an increased number of studies and evidence that show an increased appearance of arrhythmia in relation to COVID-19, mostly to sinus bradycardia[169]. On the opposite side of AF, sinus bradycardia presents a decreased and slower heart rhythm, with a heart rate lower than 60 beats per minute (bpm). This diagnosis requires an electrocardiogram (ECG) showing a normal sinus rhythm at a rate lower than 60 bpm.

The zebrafish, *Danio rerio*, has proven to be an ideal model for cardiovascular and drug development studies because of its homology to humans in both morphology, physiology, and genetics[139, 170]. Despite only having two discernible chambers compared to the four-chambered heart in humans, the zebrafish possesses a similar contractile structure with an analogous conduction system[141, 142]. Hence, the zebrafish model is suitable for

researching cardiac arrhythmias and exploring the association between related genetic pathways and electrophysiological characteristics through ECG analysis. Regarding the sensor design for ECG recording in zebrafish, conventional needle electrodes are commonly used[114]. Other studies presented alternatives for conventional needles by designing a different type of needle made of different materials[143], these incorporated materials such as tungsten filament, stainless steel, and silver wire to assess the quality of the recorded data. Together with the portable ECG kit, they sought to establish a universal platform for both research and educational labs.

The needle system was also deployed in other studies[143-146] for carrying out research on biological and/or drug-induced effects, in which it showed encouraging outcomes. However, to obtain optimal signals, it was necessary to carefully insert the needles through the zebrafish's dermis. This invasive procedure can cause injury to the fish's heart due to the sharpness of the needles, thus possibly changing signal morphology[145]. Furthermore, accurately placing the electrode on the small heart without causing harm to ensure clear ECG capture presents a significant learning curve. Consequently, various substitute probe systems have been introduced, such as microelectrode arrays (MEA) and 3D-printed sensors. Both our team and other researchers have successfully utilized MEA for data acquisition, achieving data that offer a good signal-to-noise ratio (SNR) along with high spatial and temporal resolution[86, 147, 148]. For example, we introduced an MEA that envelops the heart of the fish, allowing the capture of site-specific ECG signals[86, 147]. In contrast, another team developed a different kind of MEA based on a flexible printed circuit board (FPCB) crafted from polyimide film aimed at recording multiple electroencephalograms (EEGs) for epilepsy research[149]. While MEAs enable the recording

of numerous signals, they are limited by the capacity to assess only one fish at a time due to the restricted number of electrode channels. In response to this limitation, we have recently showcased an advanced system capable of simultaneous ECG recordings from multiple fish[150]. This system employs two electrodes, each 125 μm in thickness and made of polyimide, with gold-sputtered electrodes positioned at the bottom of their housing to facilitate data acquisition. However, the inclusion of a water circulation pump introduced noise, affecting the signal-to-noise ratio (SNR) quality of the ECG signals. Additionally, the use of bulky and costly data collection tools, which required a wired connection to a computer, was necessitated. On the market, systems like iWORX offer improved portability through a compact amplifier, yet they face unresolved issues: (i) their recording time is too short (3–5 min) for experiments needing longer durations, such as those involving acute drug effects; (ii) the requirement for anesthetizing the animals, which can stress them and skew innate cardiac electrophysiological data; (iii) manual, sequential measurements hinder research with large numbers of fish; and (iv) the need for offline, labor-intensive ECG data processing. Importantly, no high-throughput systems incorporating microelectronics for analyzing mutant phenotypes have yet emerged. Therefore, the creation of high-throughput systems that enable extended ECG recording is crucial for uncovering links between arrhythmic phenotypes and mutant genotypes, identifying multiple arrhythmic phenotypes associated with single mutant genotypes, and testing the effectiveness of cardiac drugs using the zebrafish model. Consequently, we introduced, in 2022, the groundbreaking prototype of the Zebra II system. This novel system is equipped to perform extended ECG recordings from several fish at once. To achieve this, an in-house electronic system was crafted, utilizing the Internet of Things (IoT) technology for wireless data transmission and enabling data

analysis through a mobile application. The inclusion of IoT technology not only bolstered the system's flexibility and portability but also facilitated remote collaborations for research on zebrafish models. In a prior study, we validated the system's efficacy through extensive testing, showcasing its ability to 1) acquire ECG data simultaneously from four fish; 2) perform continuous ECG recordings for up to 1 h, which significantly exceeds the capacity of existing systems that only capture a few minutes; 3) minimize the confounding effects of anesthesia by employing a 50% reduced concentration of Tricaine. Furthermore, the system demonstrated a strong capability for lengthy ECG recordings across various experiments, such as those involving sodium-induced sinoatrial (SA) block, temperature-induced heart rate changes, and drug-induced arrhythmias in both *Tg(SCN5A-D1275N)* mutant and wildtype fish under controlled experimental conditions. The system's adoption of multiple electrode channels for extended ECG recording further enables the execution of randomized controlled trials, allowing for two fish per experimental group to be studied under identical conditions[2]. In this paper, we introduce the upgraded version of the system, featuring a 4-point electrode. This enhancement enables users to capture ECG readings from various locations on the fish, significantly reducing the chance of obtaining low-quality ECG signals. Moreover, this iteration builds upon and refines the majority of the functionalities outlined in previous research[19]. This evolved ECG system shows great promise in addressing existing limitations, thereby substantially facilitating the analysis of arrhythmic phenotypes and the screening of drugs in zebrafish. The innovative addition of the 4-point electrode was rigorously tested through a brief study on drug-induced arrhythmia in wild-type zebrafish, further validating its effectiveness.

6.2 Methods.

6.2.1 Fish Husbandry. Zebrafish were kept at 28–29°C in tanks connected to a system of recirculating water with a 14 h/10 h day-night cycle. Divide the 40 fish into four groups, each consisting of 10 fish, and house them in separate tanks.

6.2.2 Fish Preparation and Amiodarone Treatment**.** Separate 40 fish in four groups of 10 into four separate tanks. Then prepare four Amiodarone doses of 70 μM, 100μ and 200 μM. Each fish should be submerged into an Amiodarone solution for 5 minutes, after the time has passed, it should be immediately transferred to Tricaine to be anesthetized prior of ECG collection.

6.2.3 Electrode Positioning and ECG Collection. Position the electrode array in a rhombus shape over the fish's chest area to capture ECG signals from four different points simultaneously (Figure 6.2A, 6.2B). Make sure to adjust each electrode carefully so every pin makes contact with the fish's skin. Rotate each electrode, lowering the pin until it makes contact with the fish's underside. If the pin is too high, turn the corresponding thumbscrew clockwise to lower it until it touches the fish. Perform the adjustment described before for the electrodes in all chambers. Close the chambers' lid once all electrode arrays are correctly positioned over the fish in the operational chambers.Mark each chamber for recording by selecting it on the touchscreen, then initiate the recording by clicking the **Record** button on-screen. Click the **Stop** button after 2 min and then click on **Save** button from the prompt windows that pop ups on-screen after stopping. Save the information either on a disk or to the cloud, depending on specific research needs.

6.2.4 Troubleshooting the Four-Electrode Array Positioning System. Press the **Stop** button on the device interface to halt the recording process and identify the channel or channels

with inconsistent signals. Lift the front lid for access to the electrode chambers. Identify which chamber(s) and specific electrodes are causing issues.

1.1. Turn the top thumbscrew clockwise to adjust the electrode's proximity to the fish. This action will lower the electrode closer to the fish.

1.2. Repeat step 6.2.3 as needed. If merely moving closer does not solve the issue, rotate the electrode to a different spot on the fish until a satisfactory signal is achieved.

6.2.5 Extracting and Analyzing Data**.** Once data has been saved to either the disk or the cloud, retrieve it for analysis or send it directly to a cloud server for further processing. Navigate to the saved data by clicking the **Browse** button on the screen and select the data sets to use. Select the **Extract** button on the options on-screen and attach a USB drive to the back part of the device to extract the data.Follow the device prompts to save the selected data sets onto the external drive for subsequent retrieval and analysis.

6.3 Results.

The ability to simultaneously record ECG signals from multiple fish significantly distinguishes this device, offering a considerable advantage in reducing the time required for drug or cardiac research on zebrafish or other similar species (Figure 6.1). Recording accurate ECG signals can be challenging due to the anatomical variations among fish, especially when it comes to electrode placement. Traditionally, obtaining a clear ECG signal involves positioning the active electrode over the heart to circumvent capturing mechanical beats or motion artifacts, with the reference electrode placed towards the lower abdomen. However, pinpointing the heart's precise location can be difficult due to its depth within the tissue or the fish's uneven surface. Sometimes, electrodes must be maneuvered with

micromanipulators for accurate placement, which may require multiple attempts before capturing a quality signal.

To overcome these challenges, the system introduces an innovative approach by using a configuration of four electrodes instead of conventional single-working electrodes. Each electrode operates independently, allowing adjustments in three dimensions-up and down (heave), tilting forward and backward (pitch), and rotating around the vertical axis (roll). This flexibility proves particularly useful when working with fish of various shapes, as it enables precise electrode positioning to either capture the optimal ECG signal or explore how ECG readings vary with different contact points on the fish.

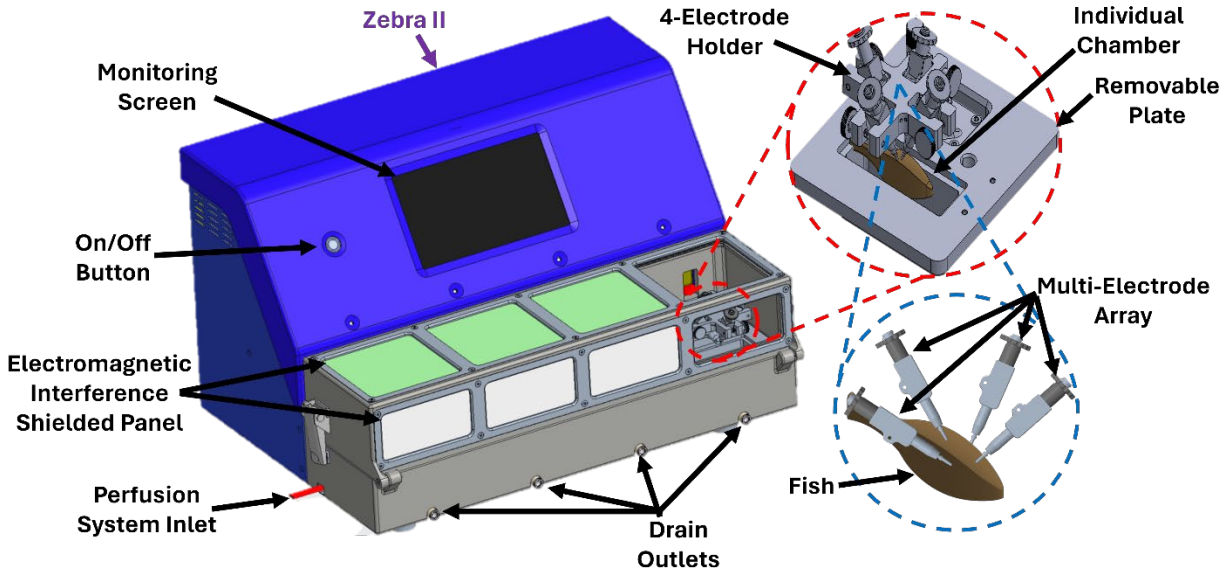

Figure 6.1. Zebra II System. Isometric view of Zebra II device (SolidWorks model) with labeled components.

This feature not only enhances the efficiency of cardiac and drug studies but also broadens the possibilities for ECG and even ECG recording techniques. Given that these methods have yet to be standardized and are often customized to accommodate the specific conditions of the experimental subject, this device opens new avenues for research, offering more adaptable and reliable data collection methods (Figure 6.2).

One of the distinctive features of this system is its ability to evaluate up to four different drugs concurrently on four separate fish or to investigate the effects of up to four different doses of a single drug across four distinct fish. The experimental setup can range from a brief acute exposure to longer sessions spanning 1 h, involving variable drug dosages or changes in environmental conditions such as temperature and anesthesia. In this study, we conducted a brief experiment to demonstrate the method's efficacy, particularly highlighting the functionality of the four-electrode array. We tested three varying doses of Amiodarone, a class-III anti-arrhythmic drug known for inducting bradycardia and prolonging the QT interval in zebrafish, over a 5 min exposure period, similar to a previous study[20] using the first prototype of this device.

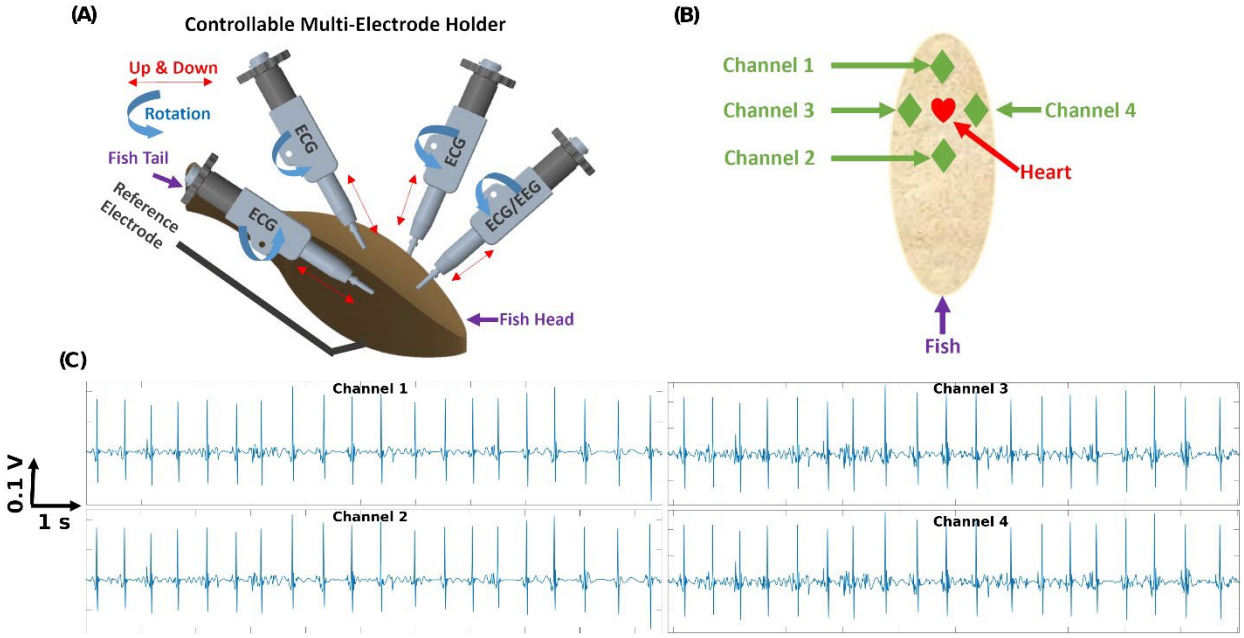

Figure 6.2. Electrode Positioning on Zebrafish. (**A**) The 4-point electrode holder degrees of freedom (conceptual image). (**B**) Electrode positioning on fish's chest. (**C**) ECG signal from the 4-point electrode holder (Channels 1-4).

Consistent with prior research, the fish showed both a prolonged QTc interval and a reduction in heart rate compared to the untreated control group. Despite the brief exposure

time, which is shorter than in many comparable studies that extend to 1 h, we were able to observe significant alterations in the ECG signals and cardiac parameters (Figure 6.3).

How Amiodarone treatment elicited observable modifications in the ECG, which escalated with an increase in dosage, is illustrated in Figure 6.3A, 6.3B. Notably, the QTc interval extended with each successive dosage increase relative to the control group, which exhibited a QTc interval of 330 ms. Following the treated groups, the QTcs intervals were measured at 365 ms for 70 µM of Amiodarone, 480 ms for 100 µM, and 546 ms for 200 µM. Correspondingly, a noteworthy decrease in heart rate was observed in reaction to the varied Amiodarone dosages and the prolonged QTcs intervals. Heart rate dropped significantly from an average of 120 ±5 BPM in the control group to 105 ±10 BPM at 70 µM of Amiodarone, 90 ± 5 BPM at 100 µM, and 84 ±5 BPM at 200 µM (Figure 6.3C, 6.3D).

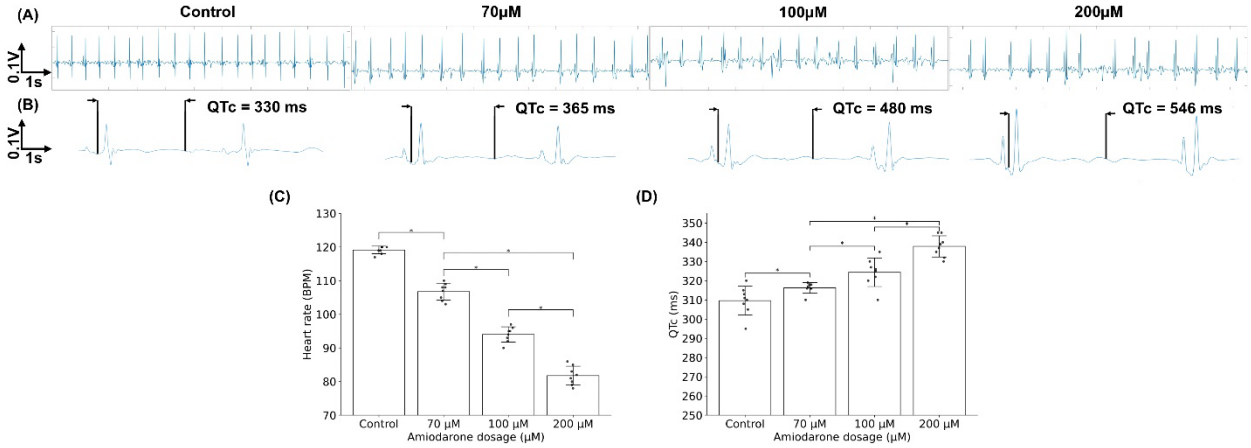

Figure 6.3. Effects of Acute Amiodarone Exposure (ECG Signals). (**A**) Representative ECG data obtained from the system and its change in ECG parameters due to different Amiodarone concentrations. (**B**) Change in ECG due to Amiodarone exposure. (**C**) Bar chart describing the discrepancy of HR. (**D**) Bar chart describing the discrepancy QTc interval in ECG data with different Amiodarone concentrations. *p<0.05 (one-way analysis of variance with Tukey test). Error bars show standard deviation. This figure has been modified from[2].

Based on these findings, we can confidently state that the newly proposed technique demonstrates comparable quality to previous studies employing a two-electrode approach (one working and one reference electrode). We successfully gathered data from four

working electrodes, selecting the optimal one for analysis to then report the anticipated cardiac parameters. The criteria for selection align with those of earlier methods, emphasizing the need to distinctly visualize PQRST complex and low baseline noise in the ECG signal. This enables the calculation of QT and QTc intervals and facilitates the identification of clear differences. Also, the methodology underwent further validation through testing by three additional researchers from our group, who had not participated in the development of the current device. They first implemented the preliminary methodology suggested by the designers and subsequently suggested modifications based on their feedback, leading to the refinement of the approach now presented. This iterative process of enhancement has been crucial for improving the device, leveraging insights from external researchers to make it more-user-friendly and effective for future applications.

This brief study on drug response underscores the device's proficiency not only in concurrently recording ECGs from four distinct fish under different conditions but also in capturing multiple (four) ECG signals per fish. This multifactored capability significantly reduces the time and effort required for electrode placement and minimizes the likelihood of human error by providing a selection of signals. This choice allows for either the selection of the most accurate signal or the ability to aggregate data from multiple signals based on the study's goal. However, it's important to clarify that employing the four-electrode setup does not automatically ensure that all four signals will be clean and of high quality. The primary aim of introducing this innovative feature is to mitigate human errors and save time by enabling four concurrent recordings instead of sequential ones, which is more time-efficient and less stressful for the fish, given their limited tolerance for time out of water and under anesthesia.

6.4 Discussion.

The current steps were modified and improved according to this new device version from a previous study made by our team[2]. Here, a labeled computer-aided design (CAD) of the device is also included.

As highlighted in the protocol's troubleshooting guide, the device necessitates the user to execute certain critical steps with diligence and precision, as these steps crucially affect the ECG signal's quality. Consistent with findings from our prior study[20], the positioning of the electrodes plays a significant role in acquiring high-quality and clear ECG readings from zebrafish samples. Due to this method expanding the number of working electrodes from one to four and introducing additional degrees of freedom, it demands supplementary troubleshooting steps and refined electrode placement over the fish's ventral area for optimal results.

The advantages and novel features of the device lie in extended measurement for multi-step experiments, limited to hour-long studies, high throughput screening with multiple zebrafish (four simultaneous studies), highly controllable experiment setup, additional electrophysiology recordings per sample (up to four) and automated cloud-based analytics and data storing. From this, we would like to emphasize that the major issue being addressed is the time needed to perform drug screening and cardiac studies in zebrafish, as traditional methods require a one-by-one screening and multiple trials to gather enough information[171]. This also offers a new way of using multi-channel arrays to record ECG in a simpler way compared to those that use microelectrode arrays (MEA) or flexible printed circuit boards (FPCB)[149] which required extra steps in the fabrication of the mentioned

electrodes plus the procedure needed to attach them to the fish compared to the proposed method that also relies on surface contact but in a less invasive way.

The limitations of the system are not different from those presented in traditional methods[2, 150] but are less intensive as a multi-channel array is used to decrease the number of recording trials needed for the study. These limitations rely on the electrode positioning as it is recommended to follow the proposed positioning presented in Figure 6.2B. It also needs to be clear that the user cannot expect to have perfect recordings during the first trial on the four channels as the anatomical differences of fish and the pre-processing of the sample (des-scaling, open-chest procedures, etc.) will directly affect the quality and success of the tests.

CHAPTER 7

Electrocardiogram Assessment in Doxorubicin Induced Cardiomyopathy in Adult Zebrafish

7.1 Introduction.

Doxorubicin (DOX), also known as Adriamycin, is a chemotherapeutic drug approved by the US Food and Drug Administration (FDA) since the 1960s for its anti-cancer properties[172, 173]. It remains a widely used and potent chemotherapeutic agent, effective against a wide range of tumors in both adult and pediatric patients[174-179]. Its efficacy places it among the top chemotherapy drugs for treating solid tumors. Despite its benefits, the clinical use of DOX is limited due to its dose-dependent toxicities, particularly cardiotoxicity, which can manifest as a wide range of symptoms from asymptomatic electrocardiographic changes to severe conditions like pericarditis and decompensated cardiomyopathy[172, 173]. DOX works by hindering DNA synthesis through its insertion between DNA base pairs, leading to DNA uncoiling, thus, stopping the proliferation of cancer cells[29]. It can be used alone or in combination with other chemotherapy drugs and treatments to manage symptoms. However, its administration may lead to several side effects, including fatigue, hair loss, nausea, vomiting, and mouth sores, along with cardiotoxicity in both acute and long-term treatments.

Consequently, animal models of Doxorubicin-Induced Cardiomyopathy (DIC) have been developed for comprehensive research aimed at elucidating the cardiotoxic impacts of DOX. In addition to the pre-existing rodent models, the Zebrafish (Danio rerio) DIC model stands out for its exceptional utility. Owing to its comparative heart rate, contractility, and action potential that closely mirrors human physiology, alongside a greater efficiency in screening

compared to rodent counterparts, the zebrafish has emerged as a preferable model for cardiovascular research and pharmacological studies[29].

Previous research has demonstrated effective techniques for inducing Doxorubicin-Induced Cardiomyopathy (DIC) in zebrafish through intraperitoneal (IP) injection. A notable advancement over traditional IP injection methods, the proposed alternative approach offers a simpler, more reliable means of drug delivery, achieving greater consistency across different investigators in the field[180, 181]. While these methods have been validated for their high survival rates in both acute and chronic models, they lack comprehensive cardiac analysis. Therefore, this current manuscript introduces the first electrocardiogram (ECG) evaluation of the acute DIC model in zebrafish. We compare the three recommended methodologies utilizing a specialized ECG-assessment device, the Zebra II system, developed within our team.

7.2 Methodology.

7.2.1 Dox Preparation. Doxorubicin is light-sensitive in both powder and solution versions. Store in opaque containers and keep them away from light exposure. Perform all the following steps from this section inside a fume hood and use the appropriate Personal Protective Equipment (PPE). DOX solution must be store inside a fridge.

1.1. Dissolve DOX powder into deionized water (DI) and prepare a stock solution of 5 mg/ml.

1.2. Store DOX solution into an opaque container at 4°C for short term (less than one month) or -20°C for long term storage.

7.2.2 Zebrafish Selection and Sorting. Separate 60 WT zebrafish from the main system. Then anesthetize each fish with a tricaine solution of 0.16 mg/ml for 2 minutes. After fully

anesthetized, position the anesthetized fish with its ventral side up and remove scales using a tweezer and a stereo microscope. (Optional). Follow up with placing the fish over a dry paper towel and gently remove any excess water on both sides of the fish. Then, put the fish inside a previously weighted petri dish inside a precision balance and weight. After finding out the weight, make sure to separate the weighted fish into groups within a 10% difference of body weight as these are considered to be the same size to simplify the experiment. Place back into the system, the recently created fish groups for DOX injection.

7.2.3 Pre-Injection Preparation. Fast the fish 24 hours before performing the DOX injection. Then prepare the dose, 50 µg/g of DOX according to the body weight (BW) of the fish groups using the following formula:

$$Injection\ Volume\ (ml) = \frac{Fish\ BW\ (g) x\ Fish\ Dose\ (50 \frac{\mu g}{g})}{Stock\ Solution\ (5 \frac{mg}{ml})}$$

Add 1x Hank's Balanced Salt Solution (HBSS) to a separate reservoir for later use. Place the new DOX solutions into covered testing tubes at 4°C before use. Equip a 10 µL micro-syringe with a 34 G beveled needle. It is important to flush the needle using the 1x HBSS to eliminate bubbles and any other blockage from the syringe before filling it with DOX solution. Then fill the syringe with the calculated volume from 3.2 with DOX solution.

7.2.4 IP DOX Injection Procedure. Re-anesthetized the fish before the injection. Perform one of the following methods to each of the groups using DOX and HBSS:

1.3. Classic IP Injection

1.3.1. Place the fish with its ventral side facing up below a stereo microscope.

1.3.2. Insert the needle at a 45° angle to the fish body between the pelvic fins and penetrate approximately 1 -2 mm (Figure 7.1A).

1.3.3. Release DOX solution slowly. Once all the solution has been injected, wait for 5-10 seconds before pulling the needle out.

1.3.4. If injection was done correctly, a small red colored section will be visible in the fish's lower belly (Figure 7.1G).

1.4. Alternative IP Injection #1

1.4.1. Place the fish on its side over the sponge below a stereo microscope (Figure 7.1B)

1.4.2. Position the tip of the syringe below the lateral line above the pelvic fin, with the bevel facing up. Make sure that it is pointing at 7'oclock at a 45° angle.

1.4.3. Insert the needle 3-4 mm and slowly release the DOX solution. Once all the solution has been injected, wait for 5-10 seconds before pulling the needle out.

1.4.4. If injection was done correctly, a small red colored section will be visible in the fish's lower belly (Figure 7.1H).

1.5. Alternative IP Injection #2

1.5.1. Place the fish with its ventral side facing up below a stereo microscope.

1.5.2. Insert the needle at a 0° angle to the fish body at the between the pectoral fins,

1.5.3. below the heart and penetrate until reaching the same area as the previous methods (Figure 7.1C).

NOTE: it is important to keep the needle at 0° as any alteration might end up in damaging other internal organs that might lead to early death.

1.5.4. Release DOX solution slowly. Once all the solution has been injected, wait for 5-10 seconds before pulling the needle out.

1.5.5. If injection was done correctly, a small red colored section will be visible in the

fish's lower belly (Figure 7.1I).

1.6. Rinse syringe with HBSS solution prepared at step 3.3 between injections.

1.7. Repeat step 4 using HBSS solution from step 3.3 instead of DOX solution. Make sure to use the same volumes per fish group.

7.2.5 Post-Injection Fish Management. Return the fish to each group tank after injection. Keep the tanks connected to the same water system, isolated from other fish not related to the experiment to avoid cross-contamination. Fast the fish for the following 24 hours post injection. Monitor the fish daily and remove any dead fish from the system as soon as possible.

7.2.6 ECG Data Collection. Position the electrode array in a rhombus shape over the fish's chest area to capture ECG signals from four different points simultaneously (Figure 6.2A, 6.2B). Make sure to adjust each electrode carefully so every pin makes contact with the fish's skin. Rotate each electrode, lowering the pin until it makes contact with the fish's underside. If the pin is too high, turn the corresponding thumbscrew clockwise to lower it until it touches the fish. Perform the adjustment described before for the electrodes in all chambers. Close the chambers' lid once all electrode arrays are correctly positioned over the fish in the operational chambers. Mark each chamber for recording by selecting it on the touchscreen, then initiate the recording by clicking the **Record** button on-screen. Click the **Stop** button after 2 min and then click on **Save** button from the prompt windows that pop ups on-screen after stopping. Save the information either on a disk or to the cloud, depending on specific research needs.

7.2.7 Troubleshooting the Four-Electrode Array Positioning System. Press the **Stop** button on the device interface to halt the recording process and identify the channel or channels

with inconsistent signals. Lift the front lid for access to the electrode chambers. Identify which chamber(s) and specific electrodes are causing issues.

1.3. Turn the top thumbscrew clockwise to adjust the electrode's proximity to the fish. This action will lower the electrode closer to the fish.

1.4. Repeat step 7.2.6 as needed. If merely moving closer does not solve the issue, rotate the electrode to a different spot on the fish until a satisfactory signal is achieved.

7.2.8 Extracting and Analyzing Data**.** Once data has been saved to either the disk or the cloud, retrieve it for analysis or send it directly to a cloud server for further processing. Navigate to the saved data by clicking the **Browse** button on the screen and select the data sets to use. Select the **Extract** button on the options on-screen and attach a USB drive to the back part of the device to extract the data.Follow the device prompts to save the selected data sets onto the external drive for subsequent retrieval and analysis.

7.3 Results.

Utilizing our in-house ECG assessment device, Zebra II, we recorded ECG signals from zebrafish for a week following their treatment with an IP injection of DOX. Our experimental protocol was aligned with the IP injection methods outlined by Ma et al. (2018)[180] and Moossavi et al. (2024)[181] at the Mayo Clinic. The standard IP injection technique involves inserting the needle into the lower abdomen of an adult zebrafish, penetrating 1-2 mm deep until it reaches the internal organs, whereupon the chemical is released. Although this approach has not significantly increased mortality rates compared to other drug screening studies, the survival rate has decreased, indicating the necessity for an alternative method. The precision required for the injection, given the short penetration distance, demands skilled researchers to maintain or improve reproducibility. Despite the fact that this

technique does not typically result in a higher mortality rate in comparison to other drug screening methods, the use of DOX has shown to notably increase mortality due to its cardiotoxic properties. Furthermore, the success of experiments and reliable screening heavily depend on the precise delivery of the drug, underscoring the ongoing need for accurate injection techniques. The suggested improvements to the IP injection techniques aim to enhance the ease and efficacy of drug delivery by modifying the needle's entry point, thereby allowing more maneuverability within the fish for better injection outcomes. The first revised method involves administering the injection laterally, 2-4 mm from the traditional site, at an angle of 45° (as illustrated in Figure 7.1B). This approach provides easier access to the internal organs for releasing the DOX solution, similar to the classic method, where correct injection is indicated by red pigmentation on the fish's lower abdomen. In contrast, the second alternative method advises inserting the needle just below the heart, amid the pectoral fins, positing a more straightforward penetration. This area presents an opening beneath the exterior tissue and the silver lining of the fish, allowing the needle to be inserted directly towards the lower internal organs, consistent with the prior methods. Testing two angles of insertion revealed that an angle of 0° caused minimal to no damage to other organs, such as the intestines (see Figure 7.1C). Although this latter technique enables the longest path for drug administration, its difficulty can vary depending on the executing researcher, and there remains a risk of harming other organs during the procedure.

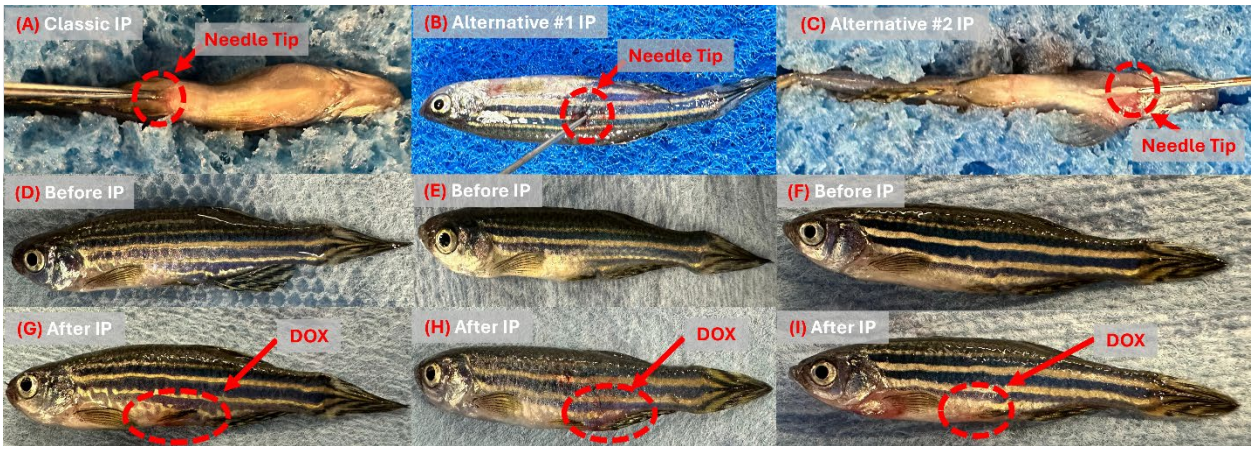

Figure 7.1. Three Different IP Methodologies for Zebrafish DIC Model. **(A)** Classic IP injection. **(B)** Alternate Method #1 IP Injection. **(C)** Alternative Method #2 IP injection. **(D)** Zebrafish before Classical IP Injection. **(E)** Zebrafish before Alternative Method #1 IP Injection. **(F)** Zebrafish before Alternative #2 IP Injection. **(G)** Zebrafish after Classical IP Injection. **(H)** Zebrafish after Alternative Method #1 Injection. **(I)** Zebrafish after Alternative Method #2 IP Injection.

The impact of DOX on fish mortality has been observed, with acute exposure to DOX (50 μg/g) significantly increasing the risk of mortality beyond that already associated with IP injection methods, in contrast to chronic exposure at a lower dose (20 μg/g). When employing these methods alongside acute exposure, it was found that between 70%-90% of the specimens succumbed within the first week, indicating that cardiac assessments should be promptly conducted post-injection. Accordingly, we organized six sets of 10 fish, each subjected to one of the methods at the acute exposure level, with subsequent ECG evaluations aimed at elucidating the causes of early mortality under these specific conditions. Initial observations noted a spike in mortality rates between the fifth and seventh days, with the counts in groups for alternative methods #1 and #2 falling to three and five fish remaining from the initial ten, respectively, as depicted in Figure 7.2. Although previous studies reported lower mortality rates with the alternative approaches, challenges were noted due to variations in fish size and scale. For alternative method #1, it was discovered that descaling the injection site beforehand facilitated the procedure, as the thickness of the

scales could hinder needle penetration or cause the needle to misalign if not quickly managed. Such misplacements could damage the fish or inadvertently redirect the needle away from the target injection site. Contrastingly, alternative method #2 was found to vary in difficulty based on the executing researcher's experience and the physical characteristics of the fish, particularly size and gender. In this method, male zebrafish proved easier to inject than females, whose rounder shape and larger abdomens increased the challenge of avoiding other organs in route to the lower internal organs. Additionally, the proximity of organs in smaller fish posed an increased challenge compared to larger fish.

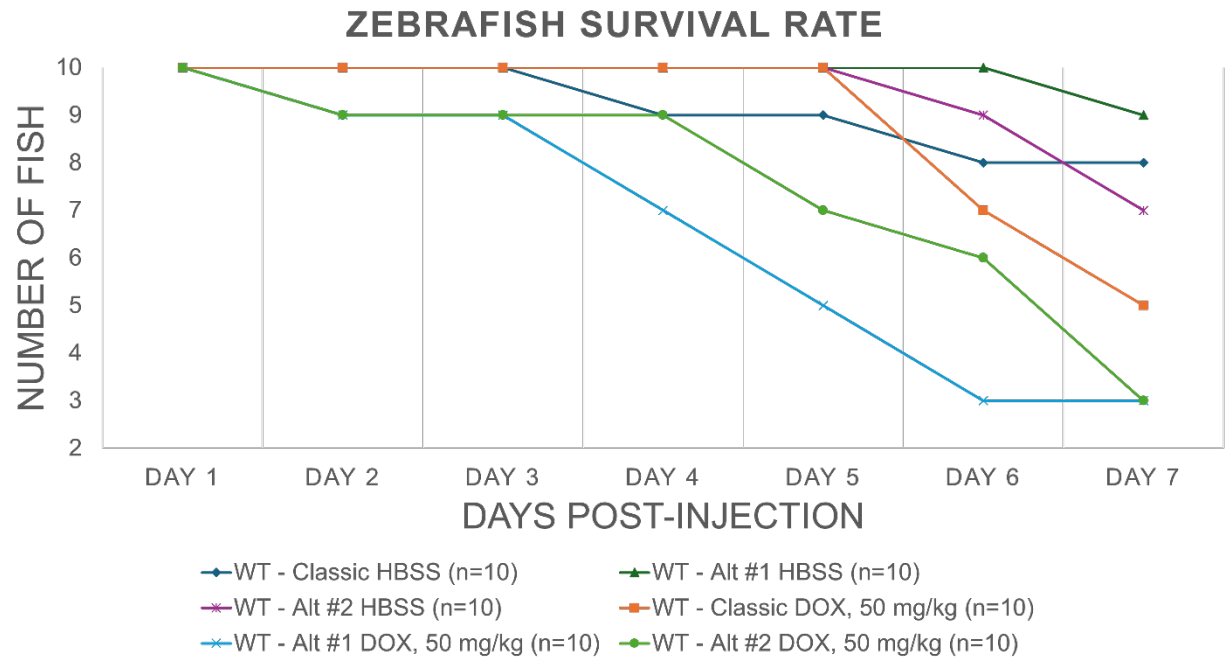

Figure 7.2. Zebrafish Survival Rate. Survival rate decreased for the acute DOX treated zebrafish towards days 5-7 where 50%-70% of the fish did not survive.

In addition to the physical challenges associated with DOX IP injections that may contribute to increased mortality in fish, a notable decrease in heart rate (HR) was observed during the first seven days post-injection, as illustrated in Figure 3A. The experiment recorded an approximate 20%-25% reduction in HR, with the control groups maintaining an average of 100 beats per minute (BPM), compared to 78 BPM for the classic IP injection method, 76

BPM for the alternative #1 IP method, and 77 BPM for the alternative #2 method. Concurrently, fish subjected to these injection methods exhibited an elevated heart rate variability (HRV) throughout the seven-day period, in contrast to the control groups, which displayed consistent HRVs. The observed decrease in HR, coupled with the increase in HRV, suggests a significant impact on cardiac function (Figure 3B).

Moreover, the ECG data revealed an increase in the average R-R interval for the groups receiving treatment when compared to those that did not, with figures showing an average R-R interval of 802 ms for the classic IP method, 810 ms for the alternative #1 method, and 798 ms for the alternative #2 method, as detailed in Figure 3C. This alteration is further illustrated in Figure 4, which depicts the evolution of the ECG from day one to day seven post-injection. Initially, the heart rates for the classic and alternative method #2 appear similar, as shown in Figures 4A and 4C, whereas the alternative method #1 displays a ~10% increase in heart rate. However, after seven days, all three methods exhibit a marked decrease in heart rate. Additionally, the occurrence of arrhythmias with the alternative method #2 is highlighted in Figure 4F.

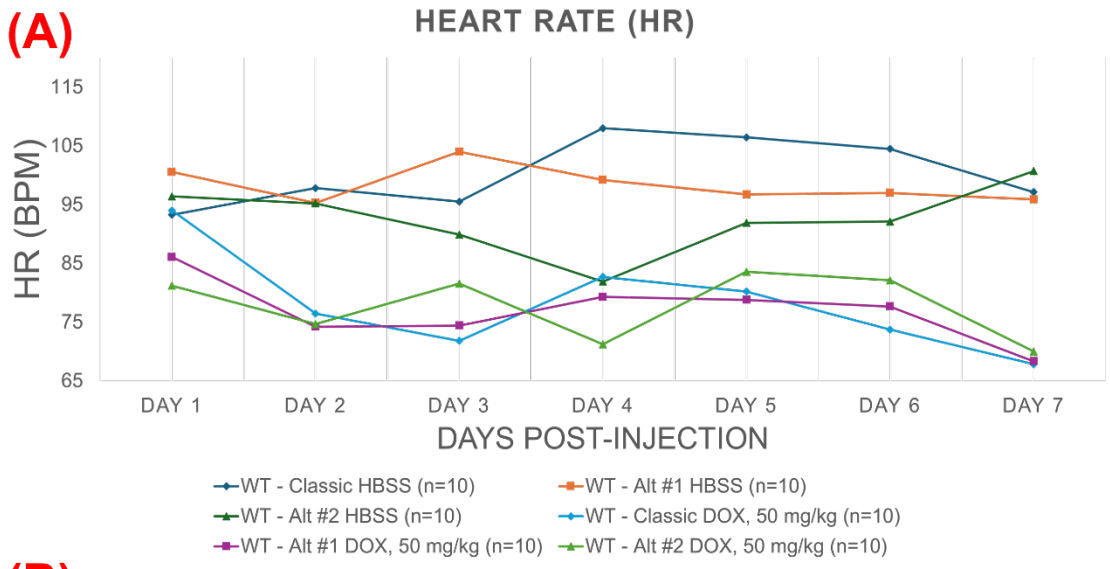
(A)
HEART RATE (HR)
HR (BPM)
115
105
95
85
75
65
DAY 1
DAY 2
DAY 3
DAY 4
DAY 5
DAY 6
DAY 7
DAYS POST-INJECTION
WT - Classic HBSS (n=10)
WT - Alt #1 HBSS (n=10)
WT - Alt #2 HBSS (n=10)
WT - Classic DOX, 50 mg/kg (n=10)
WT - Alt #1 DOX, 50 mg/kg (n=10)
WT - Alt #2 DOX, 50 mg/kg (n=10)

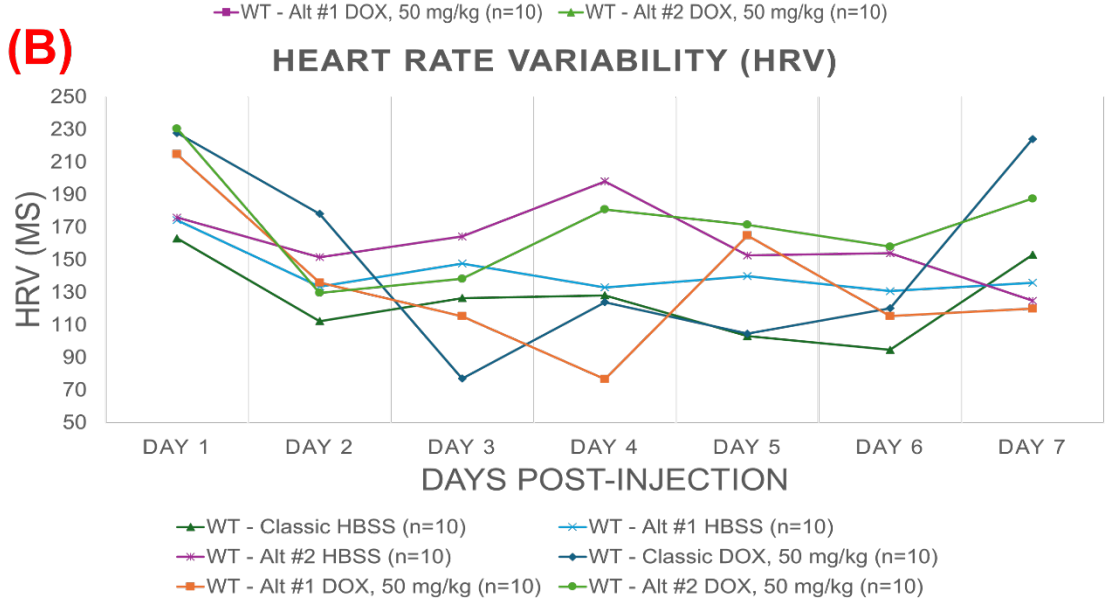
(B)
HEART RATE VARIABILITY (HRV)
HRV (MS)
250
230
210
190
170
150
130
110
90
70
50
DAY 1
DAY 2
DAY 3
DAY 4
DAY 5
DAY 6
DAY 7
DAYS POST-INJECTION
WT - Classic HBSS (n=10)
WT - Alt #1 HBSS (n=10)
WT - Alt #2 HBSS (n=10)
WT - Classic DOX, 50 mg/kg (n=10)
WT - Alt #1 DOX, 50 mg/kg (n=10)
WT - Alt #2 DOX, 50 mg/kg (n=10)

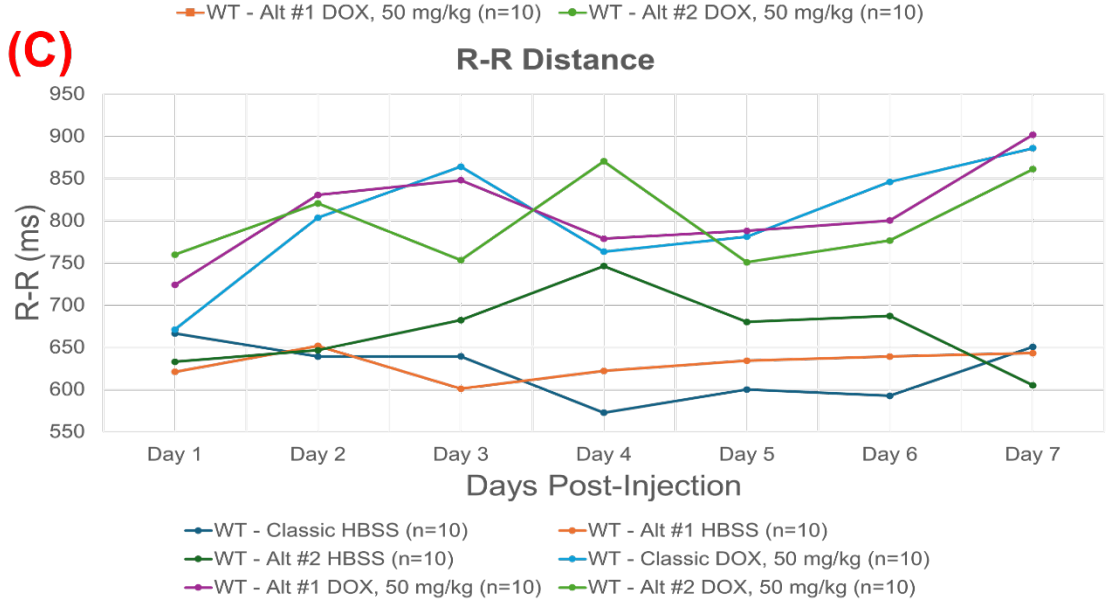
(C)
R-R Distance
R-R (ms)
950
900
850
800
750
700
650
600
550
Day 1
Day 2
Day 3
Day 4
Day 5
Day 6
Day 7
Days Post-Injection
WT - Classic HBSS (n=10)
WT - Alt #1 HBSS (n=10)
WT - Alt #2 HBSS (n=10)
WT - Classic DOX, 50 mg/kg (n=10)
WT - Alt #1 DOX, 50 mg/kg (n=10)
WT - Alt #2 DOX, 50 mg/kg (n=10)

Figure 7.3. Heart Rate, Heart Rate Variability and R-R Distances. **(A)**Heart rate. A decrease in heart rate is shown during the seven days post injection for those treated groups compared to the controlled groups. **(B)** Heart rate variability. Higher heart rate variability is shown for acute DOX treated zebrafish, even though the average HRV for each group seems similar, daily HRV differs for each group significantly. **(C)** ECG morphology interpretation. R-R distance between treated groups is close and higher than control groups, demonstrating a successful DOX IP injection and possible arrhythmia presence.

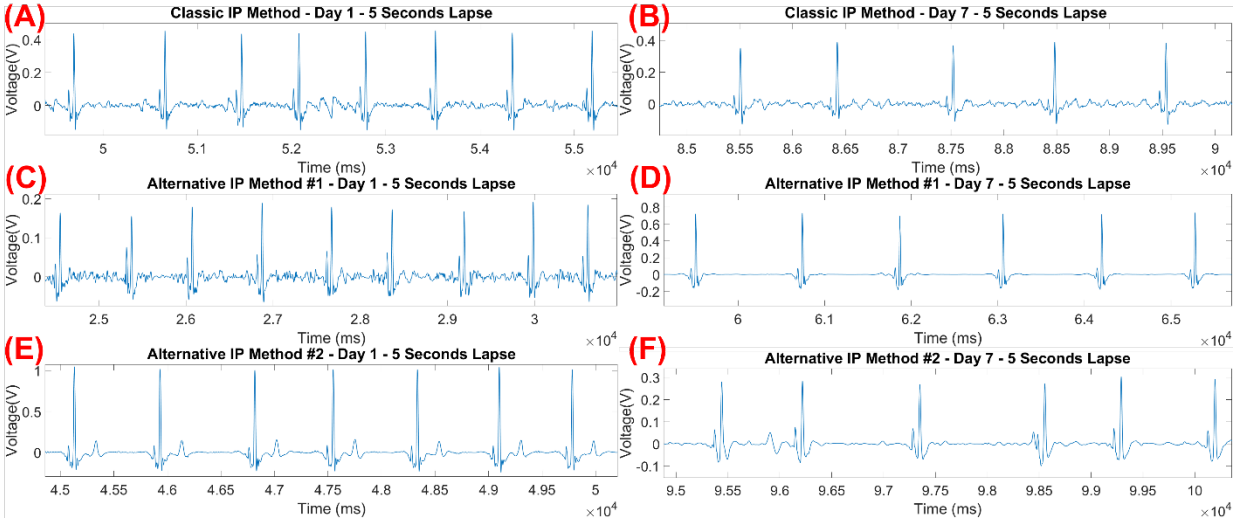

Figure 7.4. ECG Change in Treated Fish from Day 1 to Day 7. **(A)** 5 second lapse for Day 1 for Classical IP Method. **(B)** 5 second lapse for Day 7 for Classical IP Method. **(C)** 5 second lapse for Day 1 for Alternative IP Method #1. **(D)** 5 second lapse for Day 7 for Alternative IP Method #1. **(E)** 5 second lapse for Day 1 for Alternative IP Method #2. **(F)** 5 second lapse for Day 7 for Alternative IP Method #2.

7.4 Discussion.

The current study follows up on the previous work made by Ma et al.[180] and Moossavi et al.[181]. In their work, they proposed two alternative methodologies that could replace the classical IP injection methodologies used for creating DIC models in adult zebrafish. The objective for these new methods is to decrease the mortality of presented by the classical IP method when using highly toxic chemical compounds like DOX in order to be able to conduct acute and chronic exposure studies using different cardiac diagnostic tools like ECG, and Echocardiograms (ECHO). They have presented that zebrafish undergoing these methodologies can survive up to seven days for those exposed to acute doses and over seven

days for those exposed to chronic studies. Given that acute exposure has demonstrated a high mortality rate in a short period of time for all the previously mentioned methodologies, we decided to replicate the DIC model in zebrafish described and perform ECG assessment to try to characterize the cardiac damage cause by acute DOX exposure and why this is leading an early death in adult zebrafish. We also implemented the use of our ECG assessment methodology using our in-house designed device [2] in order to get the best signals as possible. We later compared the ECG signals collected from the three treated groups against each other and control groups, trying to identify any significant changes in ECG morphology and other cardiac parameters that might explain the early death of fish.

Since this is the first time we are replicating this methodologies for creating DIC zebrafish models in lab, there were some limitations in terms of experience while performing the IP injections as there were a couple of outliers for the first few fish (less than 3 fish) that showed an abnormal behavior due to possible physical damage during the injection. These have been separated from the analyzed data, which have showed a clearer result within the study. Also, it was detected that removing the scales beforehand from the ventral and lateral sides of the fish aides the researcher who is performing the injection to have a easier and better performance as scales can sometimes make the needle penetration harder or even cause a minor displacement that will end up releasing the drug in the incorrect place. Following the same path, the alternative IP method #2, shows an easier delivery compared to alternative method #1 and the classical method once it is mastered as it is very easy to miss or to damage other internal organs if not made with care.

Even though ECG was collected and analyzed, it is recommended to perform other studies in parallel to try to characterize other cardiac affections that can't be clearly identified with electrical signals. The use of ECHO and molecular studies are recommended, as well as using a bigger batch of fish to have a better statistical significance and reduce the probability of failure or outliers. On the same spot, probably adding different aged fish can create a more complete study as DOX might or might not affect the fish differently according to their age. These studies and suggestions will eventually complement the knowledge we have regarding the cardiac affections of DOX and later better understand the drug to regulate its use and better treat its side effects as it is one of the most important drugs used for chemotherapy in both adults and pediatric patients[175].

CHAPTER 8

Deep Learning-Based Framework for Cardiac Function Assessment in Embryonic Zebrafish from Heart Beating Videos

8.1 Introduction.

Despite extensive research and medical expenditures, cardiovascular disease continues to be the leading cause of mortality and morbidity in the modern world [5]. Among animal models used in cardiovascular research, zebrafish (*Dario rerio*) has been proven to be the premier model for studies of developmental genetics and functional genetics owing to their conserved genome, small size, low-cost for maintenance, short generation time, and optical transparency, just to name a few [182]. In addition, zebrafish cardiac physiology shows similar phenotypes to humans [183] and the time-lapse videos of the heart development can be easily acquired [184]. All these make zebrafish an ideal choice to investigate cardiac development, congenital heart disease as well as therapeutic potentials.

Dilated cardiomyopathy (DCM) is a hereditary, progressive disease, which eventually leads to heart failure [185]. Thus, it is essential to evaluate the early cardiac functions associated with DCM. Dozens of pathogenic genes have been found in the genetic studies of cardiomyopathy, and the incidence rate of DCM is about 1/250 [186]. Titin truncated variants (TTNtv) are the most common genetic factor in DCM, accounting for 25% of DCM cases [187]. Therefore, we have recently restated the allelic heterogeneity in zebrafish segments and established a stable mutation system to systematically and accurately assess cardiac functions in mutant zebrafish. In order to study the mechanobiology of induced defects of these disease models, heart functions need to be reliably evaluated [188]. This effort requires a thorough knowledge of blood flow patterns as well as hemodynamics.

Furthermore, in studies on cardiogenesis for screening distinct roles of different genes in mediating heart development and cardiac functions, investigating cardiomyocyte sizes and numbers resulting in measures of the ventricular chamber volume was usually utilized [189]. To this end, a systematic and simple approach for quantifying cardiac functions in zebrafish embryos would provide important insights into the development of phenotypes and disease. The standard quantitative indices are Ejection Fraction (EF) and Fraction Shortening (FS), which are different measures of the heart's muscular contractility.

The embryonic zebrafish (up to ~ three days post-fertilization - dpf) are transparent with decent internal organs visibility, including the heart and the vascular system. Thus, bright field microscopic videos can quantify cardiac mechanism and morphology at this stage [55]. Usually, two-dimensional (2D) videos for cardiovascular analysis are recorded. Then, continuous changes in ventricular wall position throughout the cardiac cycle would be tracked by first identifying a linear region of interest for the ventricle's borders [55]. Structural analysis of the zebrafish heart is based on taking 2D images at specific time points to measure chamber dimensions. However, in conventional approaches, researchers have to label the ventricle manually, find the End Systolic (ES) and End Diastolic (ED) frames, and then derive the desired parameters, such as EF and heart rate (HR). To date, most of the reported work only dealt with simple detection of heart rate, such as via edge tracing [56]. Nasrat et al. presented a semi-automatic quantification of FS in video recordings of zebrafish embryo hearts [190]. Their software provides automated visual information about the ES and ED stages of the heart by displaying corresponding-colored lines into a motion-mode display. However, the ventricle diameters in frames of ES and ED stages are marked manually, and then the FS is calculated. This will be extremely tedious, time-consuming, and

inconsistent when segmentation is done manually for a large number of frames. Akerberg et al. proposed a Convolutional Neural Network (CNN) framework that automatically segments the chambers from the videos and calculates the EF [191]. Nevertheless, particular transgenic animals expressing the myocardial-specific fluorescent reporter and hi-end fluorescence microscopes were used, which cannot be widely applicable for the research community, especially those without access to transgenic lines or fluorescence microscopes. Additionally, Huang et al. showed that transgenic expression of fluorescence protein could cause dilated cardiomyopathy [192], as high levels of expression of some foreign proteins affect the myocardium. Further, more importantly, as reported by Akerberg and colleagues, frames from only four videos have been used, which can result in overfitting in cases where the features of the video like the position of the fish, lighting, or the focus of the lens on the ventricle are different comparing to the training set. Zebrafish in the videos can have different sizes, and the focus on the heart can be different in each video. In manual segmentation, the ventricle could occasionally be partially masked. Therefore, in order to have a framework with the ability to estimate these masked spots accurately, the dataset should include a variety of videos with different settings. However, their work has raised the optimism of applying machine learning to this problem.

U-net, a symmetric convolutional neural network architecture, could be an ideal option since it is created explicitly for biomedical image segmentation [193]. A similar architecture has been employed by Decourt et al. to segment the human left ventricle from magnetic resonance imaging (MRI) images [194]. The main idea of the U-net is to complement a traditional contracting network by successive layers, where pooling operations are replaced by up-sampling operators. Besides, a subsequent convolutional layer can then be trained to

assemble a precise output based on this information [193]. The training of the network uses the original image as an input and the mask of the corresponding image as the output, and the objective is to minimize the error of the estimation and the mask.

In this work, our *Zebrafish Automatic Cardiovascular Assessment Framework* (ZACAF) was developed to analyze heart beating videos of zebrafish embryos simultaneously and quantify specific cardiac functions, namely FS and EF. A deep learning model has been trained using 50 videos of wildtype and mutant zebrafish. Additionally, several image processing techniques have been applied to the videos to investigate the effectiveness, and then the best one was chosen to preprocess the data before training. We then evaluated the performance of our framework with the wildtype as well as the established TTNtv mutant fish having a condition of DCM [190]. Finally, in-depth discussion and future directions are presented.

8.2 Methods.

8.2.1 Experimental Animals. Zebrafish (*Danio rerio*; WIK strain) were maintained under a 14 h light/10 h dark cycle at 28.5 °C. All animal study procedures were performed in accordance with the Guide for the Care and Use of Laboratory Animals published by the U.S. National Institutes of Health (NIH Publication No. 85-23, revised 1996). Animal study protocols were approved by the Mayo Clinic Institutional Animal Care and Use Committee (IACUC #A00002783-17-R20).

8.2.2 Video Imaging of Beating Zebrafish Hearts at the Embryonic Stage. Zebrafish in the embryonic stages were anesthetized using 0.02% buffered tricaine methane sulfonate (MS222 or Tricaine) (*Ferndale,* Washington, US) for 2 min and then placed lateral side up with the heart facing the lower-left corner. The specimens were held

in a chamber with 3% methylcellulose (*Thermo Fisher Scientific*, Massachusetts, US). The videos were recorded using a Zeiss Axioplan 2 microscope (Carl Zeiss, Oberkochen, Germany) with a 10X lens and differential interference contrast (DIC) capacity. The used Zeiss' Axiocam 702 mono Digital Camera 426560-9010-000 records videos with 60 fps; however, using the Zeiss computer software, videos get stored in 5 fps, 10 fps, and 20 fps. Video clips were processed using ImageJ for manual quantification of cardiac functional indices, including heart rate and fraction shortening, as detailed in the following sections.

8.2.3 Cardiac Function Assessment. Fraction Shortening (FS), one of the measures of ventricular contractility, can be calculated from ventricular diameters (Short-axis) at end-diastole (ED) and end-systole (ES) (Dd and Ds, respectively) as follows [55]:

$$FS = \frac{(D_d - D_s)}{D_d} \quad (1)$$

By assuming a prolate spherical shape for the ventricle, the following volume formula can be used:

$$Volume = \frac{1}{6} \times \pi \times D_L \times D_{S^2} \quad (2)$$

where D_L And D_S are long and short-axis diameters of ventricle from 2D static images as shown in Figure 8.1.

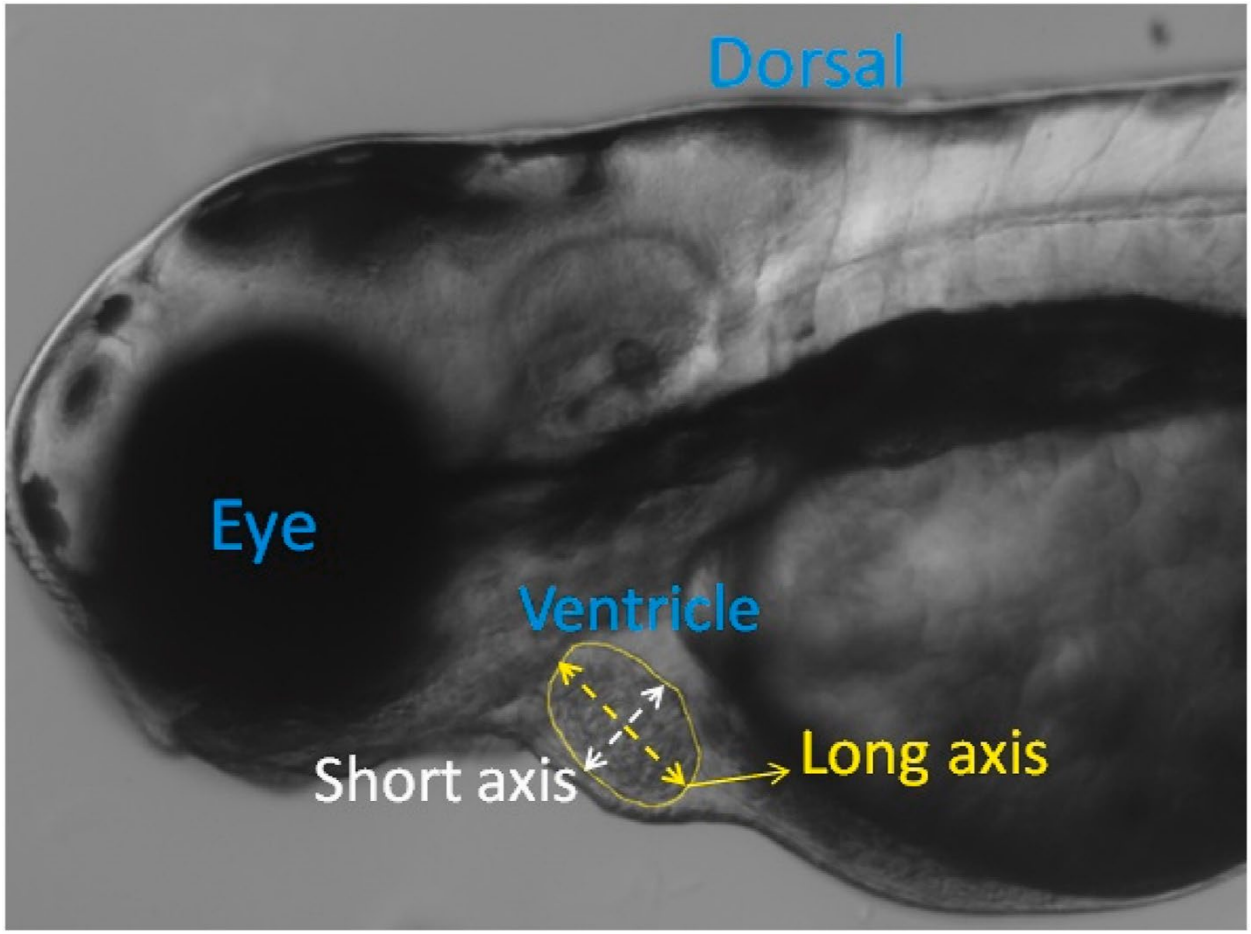

Figure 8.1. A Frame in a Video Recorded from a 3-dpf Zebrafish with Segmentation for Ventricle Border and Long and Short Axes.

One extremely important index in quantifying the heart mechanisms is ejection fraction (EF). It is defined as the fraction of blood ejected from the ventricle with each heartbeat and can be calculated using the following formula:

$$EF\% = \frac{(EDV - ESV)}{EDV} \times 100\% \quad (3)$$

where EDV and ESV are volumes at ED (EDV) and ES (ESV), respectively. Since measurement of the ventricular volume is not possible with 2-D videos, researchers usually use the area as an estimation. Finally, heart rate (HR) could be determined by measuring the time between two identical successive points (*i.e.*, ED or ES) in the recorded images [55]. EF ranges between 50% and 70% for healthy zebrafish, and it is one of the crucial indications to

diagnose heart failure. EF reflects the function of the systolic ventricular pump. The stronger the myocardial contractility, the higher the stroke volume and EF will be. Therefore, in patients with heart failure, the left ventricular ejection fraction (EF) is significantly reduced. 8.2.4 Automated Quantification of Cardiovascular Parameters Using Image Processing. For automatic quantification of important cardiovascular parameters like EF or FS from the microscopic videos, the zebrafish's ventricle needs to be segmented. Several image processing methods have been employed as an effort to identify the edges of the ventricle in the videos, including edge detection, background subtraction, color filtering, and histogram-based segmentation. The Canny algorithm is used in edge detection, which has a multi-stage algorithm to detect a wide range of edges in images [195]. In background subtraction, continuous frames from a video would be subtracted from each other to find the moving objects. Considering that most of the fish body is static and the only pixels moving in the video belong to blood cells and the heart; thus, the static pixels can be removed. Lastly, the idea behind color filtering and histogram-based segmentation is to identify the ventricle due to its distinct color or gray intensity. In manual histogram thresholding, after plotting the image's grayscale histogram, those peaks and valleys in the histogram are used to locate the clusters in the image [196]. Otsu's algorithm performs automatic image thresholding by finding a single intensity threshold that separates pixels into two foreground and background classes [197]. Finally, contrast limited AHE (CLAHE) is a variant of adaptive histogram equalization, which over-amplifies the contrast on small regions in the image[198]. Here, the above-mentioned methods have been implemented not only to compare with the approach using deep learning described in the next section but also to use for preprocessing. All these are shown in Figure 8.2a-d panels.

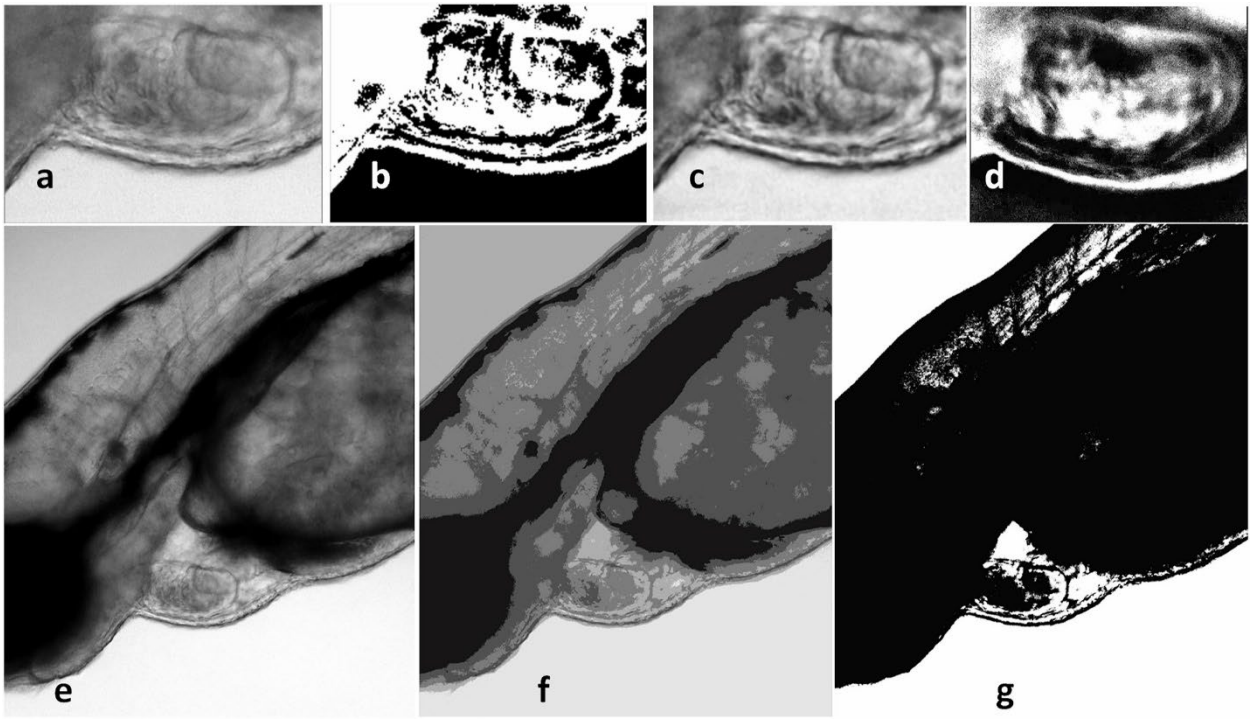

Figure 8.2. Ventricle Segmentation using Different Methods**.** Panel **a-d**: A frame from the video of a 3 dpf zebrafish with 40X zoom undergoing different HBS algorithms. **a**. Original frame. **b**. Manual histogram thresholding. **c**. CLAHE. **d.** Otsu thresholding. Panel **e-g**: A frame from the video of a 3 dpf zebrafish with 10X zoom undergoing GMM and K-means approaches. **e**. Original frame **f**. GMM. **g**. K-means.

Those methods, namely edge detection, color filtering, and background subtraction, are not robust with different videos since ventricle edges might have multiple shades of gray. Therefore, we also attempted to use machine learning approaches to compare. First, unsupervised learning segmentation methods like K-means and Gaussian mixture model (GMM) were applied to the videos. As shown in Figure 8.2e, f, and g, although these methods improve the visibility of the ventricle borders, the heart's automatic segmentation is not possible. Moreover, much of the unnecessary information (pixels) in the image, particularly in the image generated using K-means, are still remaining.

8.2.5 U-Net-Based Deep Learning Approach. Figure 8.3 illustrates the architecture of the proposed U-net model with details. The network consists of a contracting path and an expansive path, which gives it a U-shaped architecture. The contracting path is a typical

convolutional network that consists of repeated convolutions, each followed by a rectified linear unit (ReLU) and a max-pooling operation. Dropouts have been used to prevent overfitting. The architecture has been optimized to obtain the best result. For training, NVidia's T4 GPU from Google Collaboratory was employed. The most commonly used loss functions for semantic image segmentation were deployed to evaluate the model, namely Binary Cross-Entropy and Dice loss function. Cross-entropy can be defined as a measure of the difference between two probability distributions for a given random variable or set of events. It is extensively used for classification problems, and since segmentation is the classification at a pixel level, cross-entropy has been widely used. Binary Cross-Entropy is defined as:

$$Loss_{BCE}(y, \hat{y}) = -(ylog(\hat{y}) + (1 - y)\log(1 - \hat{y})) \quad (4)$$

where y is the true value and $\hat{y}$ is the predicted outcome.

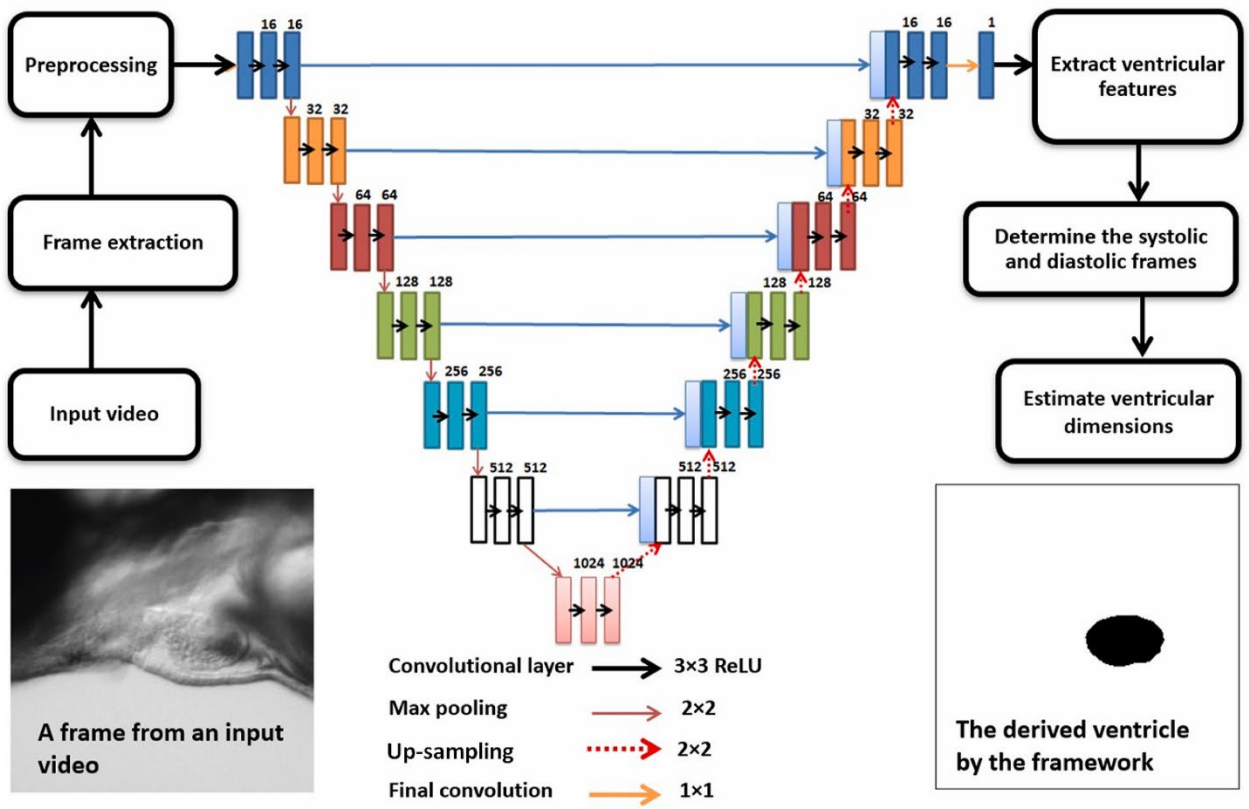

Figure 8.3. The Process Flow and the U-net Architecture**.** Each rectangle represents a layer and the number above it shows the number of the neurons inside. A trained model can estimate a mask of the ventricle from all the extracted frame of the input video. When all the frames have a predicted mask, by determination of ES and ED frames, important cardiac indices like EF, FS, and stroke volume can be automatically calculated and saved in a desired format.

The Dice coefficient is a commonly used metric in computer vision problems for calculating the similarity between two images. In 2016, it was also adapted as a loss function, namely Dice Loss [199].

$$Loss_{Dice}(y, \hat{y}) = 1 - \frac{2y\hat{y}+1}{y+\hat{y}+1} \quad (4)$$

The U-net model has been trained with both models, and the performance has been assessed using validation and test sets. Further, the calculation of EF has also been evaluated using both aforementioned loss functions.

8.2.5.1 Dataset. A training dataset was created employing the raw microscopic videos of zebrafish containing 800 pixel-wise annotated images. 50 videos of the lateral view from 50 different 3-dpf zebrafish were analyzed for creating the dataset. 10 of these videos are from the TTNtv mutant line. From each video, 10 to 30 frames were extracted. A total number of 850 frames were extracted for the training set. Each training set has a frame from the video, and a mask manually created showing only the ventricle with ImageJ software. After making the masks, all image and mask sets have been organized into folders. Each set has two folders inside, one for the extracted original frame and the other for its corresponding mask. Finally, all sets were shuffled to avoid overfitting. The validation set with the 10% of the data's size has been split from the dataset before training.

8.2.5.2 Preprocesssing. In the preprocessing stage, a region of interest is defined, knowing all recordings have the same positioning for the zebrafish. Although this cropping improves the accuracy by removing unnecessary information, it can be avoided to make the framework robust to different video types. Additionally, a sharpening filter accomplished by performing a convolution between a custom weighed kernel and an image is used to make edges more visible. After training, the U-net architecture was able to predict the ventricle segment. The model has been trained several times by applying the mentioned image processing methods to the training images. The method with the best results was CLAHE thresholding which was added to the preprocessing section.

8.2.5.3 Quantification of the Diameters of the Predicted Ventricle. The ventricle's diameters are measured for all extracted frames automatically with the contour tool from OpenCV (an open-source computer vision library). The maximum and minimum measured areas of the ventricle in different frames show the ES and ED stages, respectively. Using the measurement

of ES and ED frames, we can calculate the ejection fraction (EF), fractional shortening (FS), and stroke volume (SV). Also, the time between two ES (or ED) frames could be used to derive heart rate (HR). The predicted ventricle is assumed to be an ellipsoid. For quantification of EF, the ventricle area can be used (Eq 3 above) by counting the pixels inside the predicted shape. Since the frames are 2D, we are estimating the ventricle volume to its area. For FS, measurements of the short axis in ES and ED frames are needed. As the ventricle is not a perfect ellipsoid, estimation of the short and long axes can be carried out in two different ways. In the first method, an ellipsoid could be fitted in the predicted shape, and then the axis of the fitted ellipsoid would be measured. The second way is to find the longest line as the long axis of the estimated ellipsoid, which could be found in the geometrical shape; then, the short axis of the ellipsoid is the short axis of the ventricle. In this framework, the 2-D area of the ventricle directly measured from the mask has been used for EF since it is more accurate.

8.2.5.4 Graphical User Interface (GUI). This framework was developed in Python, and thus, for researchers who are not familiar with programming, working with it can be challenging. To address this, a Graphical User Interface (GUI) has been designed to provide a user-friendly interface to facilitate researchers' process. Moreover, after training the U-net, the trained model can be saved, which means the most computationally heavy part could be done only once. The GUI saves the output files in the CSV format, along with information about EF, FS, diameter readings of the area, short and long axis, and frame numbers. Therefore, each video's data can be easily accessed at anytime and anywhere with the expandable cloud feature. Our ZACAF provides an end-to-end interface to researchers to automatically calculate, classify, and record various cardiac function indices reliably. ZACAF

can work with multiple videos simultaneously and output the results in the fraction of the time compared to that of manual segmentation. The deep learning model in the ZACAF can easily be updated and optimized with a new model and data.

8.5.6 Quantitative Comparison of Approaches. In this framework, our objective is to predict the geometrical shape identifying the ventricle with high accuracy in terms of its position, size, and shape with the ground truth. Since the manually created masks are considered as the ground truth, we would expect the predicted shape and the manual mask to be identical or close to them. In semantic image segmentation, the most commonly-used metrics include pixel-wise accuracy, Dice coefficient, and Intersection over Union (IoU).

8.5.6.1 Pixel-Wise Accuracy. In this work, since the mask indicating the ventricle is either white or black, there are only two classes so that we can use the binary case of pixel accuracy. The accuracy is defined as the percent of pixels classified correctly as

$$pixel - wise\ Accuracy = \frac{pixels\ classified\ correctly}{All\ Pixels} \quad (6)$$

On average, in a wildtype mask frame, around 3000 black pixels are identifying the ventricle, and the rest are with for background. Considering the resized frame is 256 × 256, there are 65536 pixels in each mask. It appears that black pixels are minority since they are 0.045% of all pixels in one mask. However, the correct identification of white pixels is as essential because they ensure the position and the shape of the ventricle are also correct.

8.5.6.2 Dice Coefficient. The dice coefficient is an extensively used indicator to elaborate the similarity of two objects. It ranges from 0 to 1 in which 1 means perfectly matched or completely overlapped. For a binary case, the coefficient is calculated as

$$Dice = \frac{2|A \cap B|}{|A|+|B|} \quad (7)$$

where A is the predicted image and B is the ground truth (manually created mask).

8.5.6.3 Intersection Over Union. It is also known as the Jaccard Index, which is simply the area of overlap between the predicted segmentation and the ground truth divided by the area of union between the predicted segmentation and the ground truth. This metric ranges from 0 to 1, with 0 signifying no overlap and 1 signifying perfectly overlapping segmentation. For the binary case, it can be calculated as:

$$J = \frac{|A \cap B|}{|A \cap B|} \quad (8)$$

In this work, all three of the mentioned metrics have been used to show the framework's performance.

8.3 Results.

8.3.1 Assessment of the Accuracy of the Framework with the Defined Metrics. The model's performance can be seen in Figure 8.4. The model has been trained with two loss functions discussed in section 8.2.6, and the best results with parameter tuning are illustrated. The metrics mentioned above resulted in 99.1% for pixel-wise accuracy, 95.04% for Dice coefficient, and lastly 91.24% and for the IoU. All mentioned metrics are evaluating the best performing model that had a Dice loss function with an Adam optimizer and a 0.001 learning rate along with decay steps of 240 and a decay rate of 0.95. The validation split was 10% which means 80 sets. Following the training, we visually assessed the framework's ability to correctly segment ventricular chambers and also the periodic pulsating movement of it within series of frames of a test video. This process was used in parameter tuning for the deep learning model.

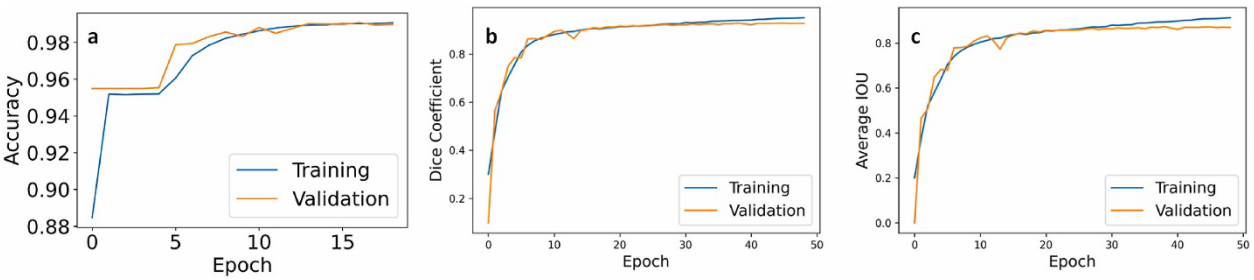

Figure 8.4. The Proposed Model's Performance Plotted with the Metrics Commonly used in Semantic Image Segmentation**. a.** Pixel-wise accuracy **b.** Dice coefficient **c.** IoU metric. This plot shows the performance of the framework with the training and validation sets during the process of training of the deep learning model.

8.3.2 Assessment of the Performance of the Framework for EF. The framework was evaluated by comparing the results obtained by manual assessment of EF from an experienced biologist with those using the software since one of the primary purposes of this framework is EF calculation. In this calculation, finding the area in all frames of a video is important because we want to find the ED and ES areas. Hence, assessment should involve the series of frames in a test video rather than having random images in a validation set. For this reason, we assess the performance of ZACAF with EF calculation. First, 8 videos of wildtype zebrafish embryos and another 8 from TTNtv mutant embryos were used as the framework's input. These videos are the test set and have not been used in training. Second, manual processing and estimation were performed for each video to derive EF by an expert to use as the ground truth. The program saves the predicted ventricle masks for each and every frame of a video, and the ED and ES frames are simply the frames with a maximum and minimum area of the segmented ventricle, respectively. After automatically finding ES and ED frames, the EF of the fish in the input video would be calculated and saved in a CSV file along with other indices calculated. The averages of absolute errors and standard deviations for the calculated EF of the 8 wild type test videos comparing to the expert's manual calculation were 6.13% and 3.68%, respectively.

As ED and ES frames are the most important parameters to quantify cardiovascular indices, we plotted the correlation of the automated and manual measurements (Figure 8.5a and b). Moreover, Bland–Altman analysis was then used to assess the agreement in manual and automatic ventricle segmentation. The Bland–Altman plot demonstrates the difference which was measured at the same time plotted against the average of the EF with two methods. Larger differences would specify larger disagreement between the two calculations [200]. From 16 test videos, two different sets of ES and ED frames (meaning 4 frames from each video) have been manually and automatically segmented. As it can be seen in Figure 8.5c, the Bland-Altman has been plotted for all pairs of measurements in the same figure with blue and red points representing mutant and wildtype fish, respectively.

Figure 8.6 presents the comparison of manual and automatic segmentation of the ventricle in 6 continuous frames to cover an entire cardiac cycle for both wild type (**a)** and TTNtv (**b)**. In manual segmentation, measures were done using the freehand selection tool in the ImageJ software.

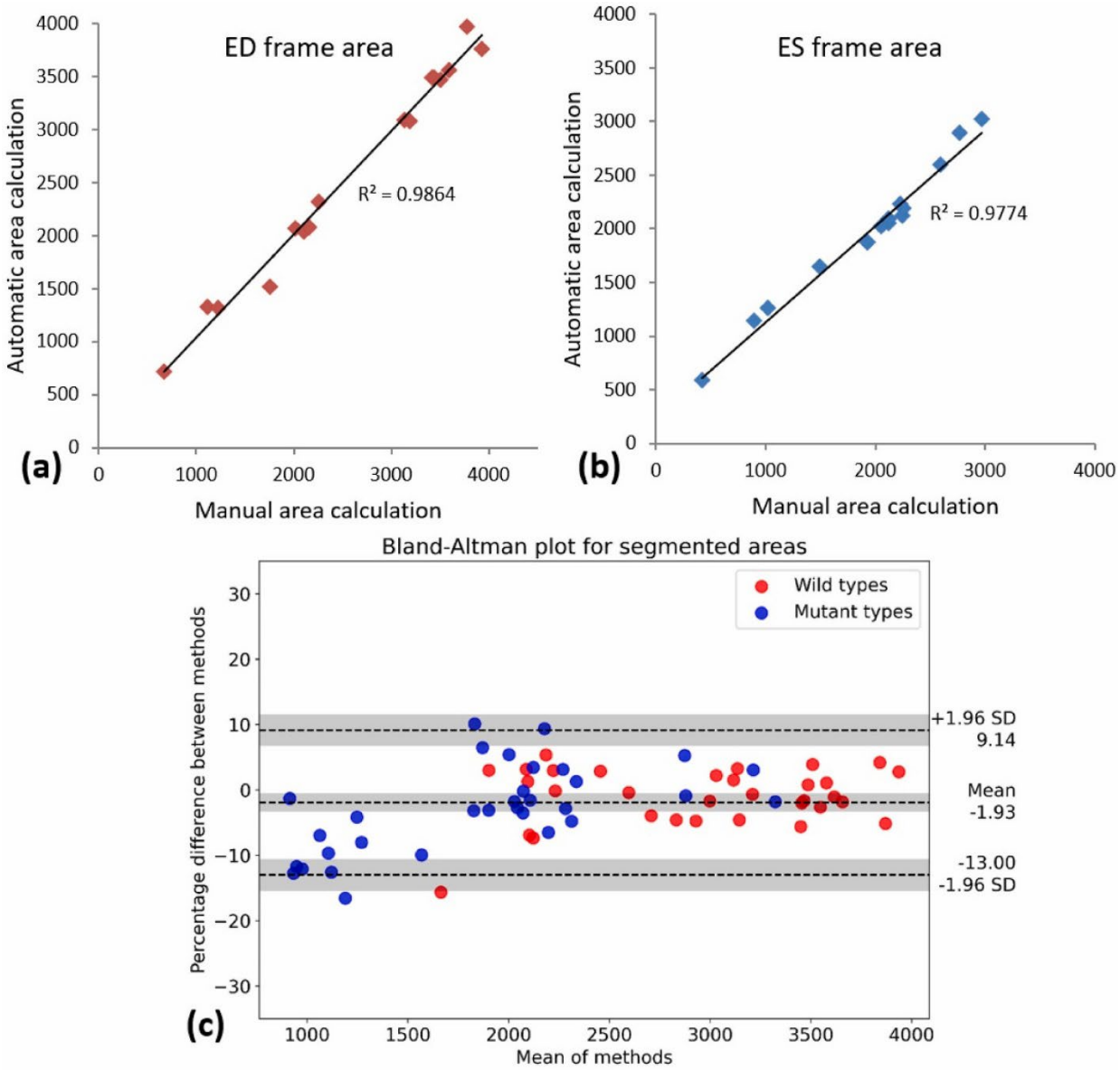

Figure 8.5. After finding and measurement of the ventricle area in ED and ES frames of 8 wild type and 8 TTNtv mutant fish with both manual and automated methods, the results are demonstrated in a correlation plot while the calculated EF for the wild and mutant types is plotted in Bland-Altman to demonstrate the agreement of measured values. Linear relation of the measurements with slopes close to 1 shows the accuracy of the ZACAF. (**a**) ED frame area. (**b**) ES frame area. (**c**) Bland-Altman plot for 64 sets of measurements of the segmented ventricle using manual and ZACAF methods. Both mutant and wild have 32 pairs each represented in the plot. Red and blue dots represent wild and mutant fishes respectively. The measurements are in pixels.

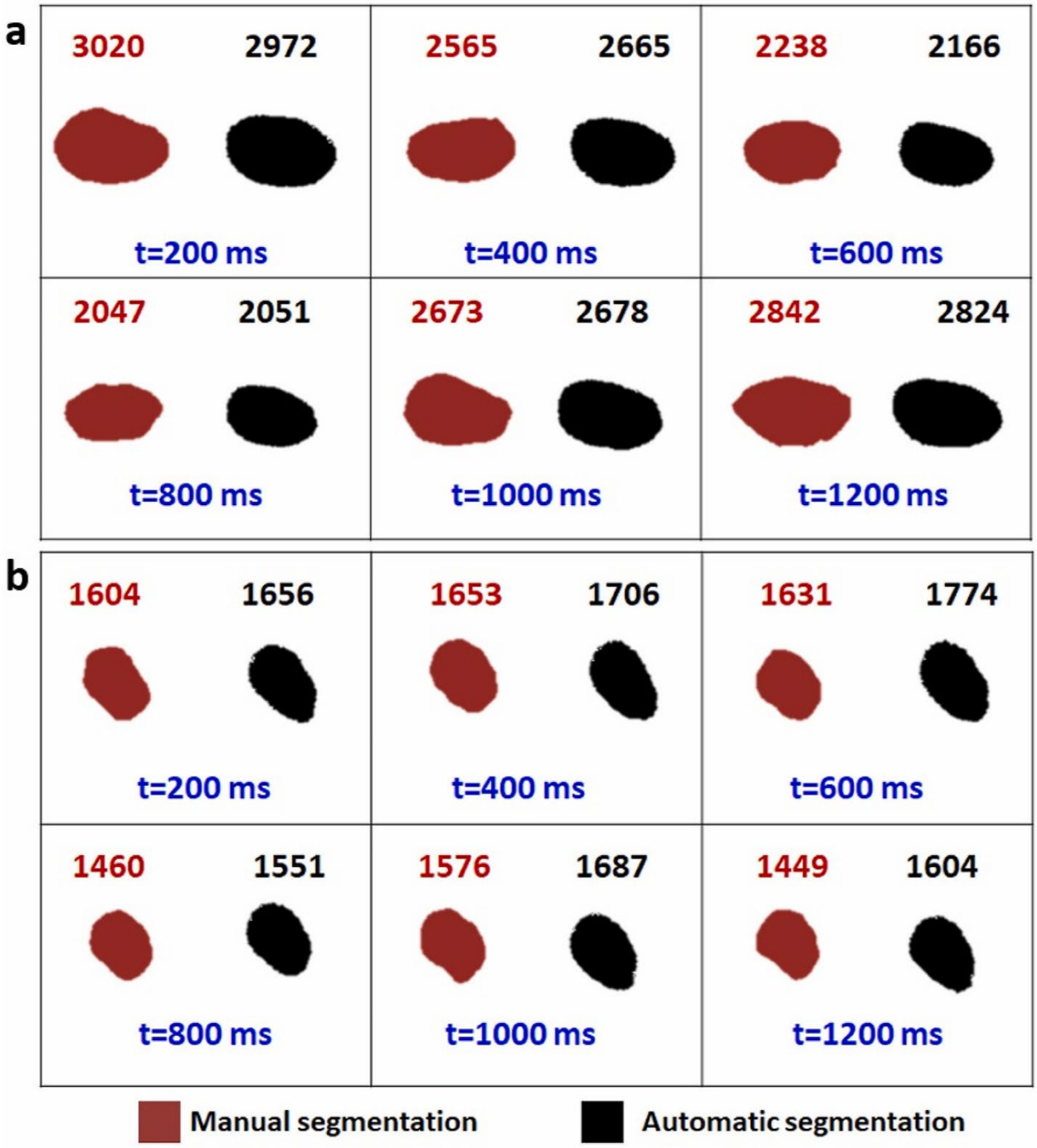

Figure 8.6. Validation of U-net Image Segmentation Framework. The sequential frames from a wild type zebrafish recorded video with fps of 5 are extracted. The respective ventricle mask of each frame is shown in each panel via manual and automatic segmentation. The area of each ventricle is measured and written above its own box. Considering the fps of the videos and the average heart rate of the zebrafish, 6 consecutive frames have been shown in this figure to ensure having at least one full cycle.

8.4 Discussion.

Conventional image processing methods such as background subtraction, HBS, and edge detection have been widely used for segmentation, showing excellent efficiency and efficacy. However, in this case, as can be seen in Figure 8.2, the ventricle's automatic segmentation is still not possible. Past work involving machine learning algorithms has shown promise with the proven semi-automatic feature, however requiring specific fluorescence videos. Here, our framework can help researchers quantify the cardiac functions and parameters of studied zebrafish with minimum manual engineering efforts. In EF derivation, counting the pixels is more relevant and accurate than finding the long axis, which can be complicated since the ventricle is not a perfect ellipse. Further, the tool that most researchers use in the ImageJ software is a freehand ruler, which could introduce inaccuracy, especially with the small size of heart chambers. Additionally, manual segmentation is not consistent. Segmentation of the ventricle in these videos is a challenging task, even with tedious manual processing. The small size, ambiguous edges, and partial obstruction of the heart in the videos can also add complications to manual detection. We have investigated this quantitatively. We asked two experts to segment and measure the ventricle area in single frames of 12 sample videos. They were instructed to do the measurement twice for each frame manually with a short break between each try. The results were 12 frames, each measured 4 times. The standard deviation for each frame measurement was calculated, and the average of standard deviations of the measurements in these 12 frames was about 150 pixels with 50 pixels standard deviation. This is approximately 8% of an average size ventricular area in our setting's scale. This shows the inconsistency in the manual segmentation. This could be especially significant with mutant embryos whose EF is usually

very small. In most cases of the TTNtv videos, the difference of the area in the ED and ES frames is between 100 and 300 pixels (considering the resolution of the videos used in this work). However, due to the nature of neural networks, ZACAF is consistent, which means that the measurement of a frame multiple times will always result in only one consistent measurement. It is noteworthy to mention since the ground truth is created using the same frames for segmentation of the ventricle, the frame rate is less important in comparing manual and automatic segmentation. The ES and ED frames are the most important frames when it comes to the quantification of parameters like HR, EF, and FS. While recording the videos, the camera shutter takes a sequence of images with a certain fps. The higher the video's fps, the higher chance for exact ES and ED stages being recorded. This fact cannot be proved using the metrics because the prediction is only being compared with the existing manually segmented ground truth, and if the low fps causes the loss of ED or ES frames, there is no way to show it with the metrics. From the segmentation point of view, there are two significant differences between the mutant and wildtype fish. The ventricle and the heart, in general, have abnormal shapes in several mutant types. In our case here, EF is much lower in the TTNtv model as the shape as well as the contractility are significantly affected. Thus, the ventricle area difference in ES and ED frames in TTNtv mutants is very low. Figure 8.7 provides examples to compare wild and TTNtv zebrafish. In some cases, the ventricle is barely contracting; thus, the area difference in ED and ES frames is lower than the segmentation error. In other words, the ventricle area hardly changes to the point that occasionally, the nominator of the formula of EF is lower than the estimation error. That is the primary source for the inaccuracies with the TTNtv mutants, and further improvements of preprocessing or optimization of the framework will not affect the result with the mutant

significantly. The videos used in this work have low resolution (data rate of 2500 kbps) in order to demonstrate the capability of our framework. Although this is beneficial for researchers to reduce required storage capacity, higher resolution would help resolve this issue, thus improving the robustness and accuracy for TTNtv mutant and wildtype fish in general.

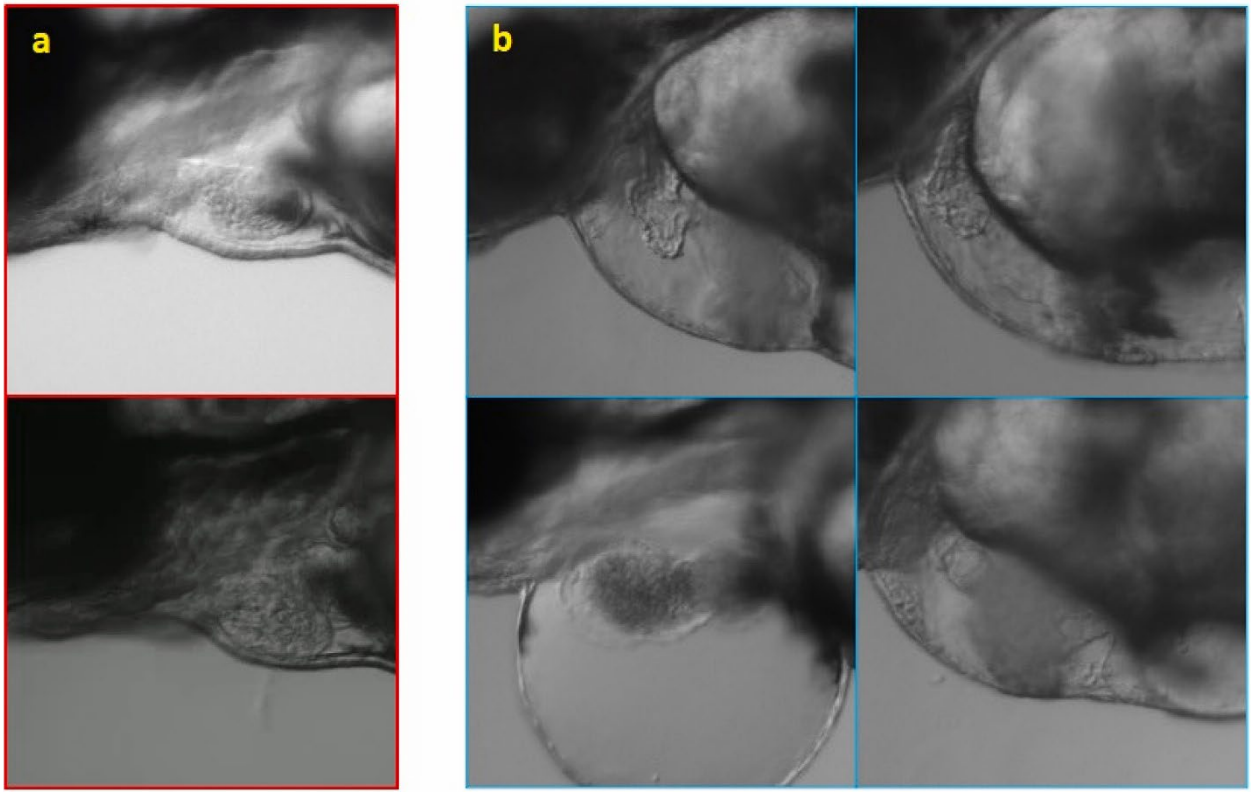

Figure 8.7. Comparison of the Shape and Size of Wildtype (a) and TTNtv mutant zebrafish (b). Besides the abnormal shape of the heart with the swollen ventricular wall, the smaller size of the ventricle is also found with TTNtv mutants. Further, the swollen chest can be also noticed.

The novelty of our supervised learning-based ZACAF lies in the automatic feature and the robustness in working with black and white videos at different configurations (*i.e.,* frame rate). The first novelty was demonstrated as creating a mask and training can be carried out only once then ZACAF can be run easily by a non-expert person. The second novelty possesses several broader impacts. First, the versatility to work with regular bright-field microscopic videos would make ZACAF widely accepted by the research community. Second,

the capability to work with monochrome low fps videos would help save storage space when thousands or more videos are used. The videos' resolution and frame rate have a direct connection with the size of them; thus, it is useful to find out the minimum required video quality. In our work, videos with a resolution of 640 × 404 pixels, a frame rate of 5 fps, and a data rate of 2500 kbps would have a file size of about 5 megabytes for a 20-s video. It is evident that improving the resolution will increase the accuracy and robustness of the framework. This also helps reduce the processing time and increase the accuracy and robustness, thus enabling big scale projects involving multiple research groups.

For future work, we plan to not only improve the deep learning model in our ZACAF but also include additional information in the output. For example, in some mutant cases, the ventricle has two borders: an outer layer and an inner layer (8.7b). The thickness of this wall in the mutant type could give researchers new insights, which is extremely difficult to perform manually. However, it is possible using a training dataset from videos with better resolution and increased magnification. Additionally, the shape of the ventricle can be used as a phenotype for the classification of different mutant types. It is straightforward to improve the accuracy of the deep learning model by adding more labeled data to its training dataset. The GUI can be improved in a way so the framework can process multiple videos simultaneously. We also plan to improve our framework for 3-D segmentation of the ventricle. Using the same state of the art with z-stack images of the heart sequentially recorded from the beating heart as the input allows for a 3-D segmentation of the ventricle over time. This is important because it would further avoid estimation and improve the overall accuracy significantly.

8.5 Conclusion.

In this work, a framework, namely ZACAF, has been developed to automatically segments the beating ventricle of zebrafish embryos from microscopic videos. The employed U-net deep learning algorithm was evaluated with wildtype and cardiomyopathy mutant fish (TTNtv) using three metrics, and favorable accuracy was achieved. Our framework would help enable and accelerate numerous biological studies in cardiology and developmental biology using the zebrafish model. Moreover, as the work is being improved, it could be utilized with other animal models and even humans, and with different imaging techniques such as ultrasound or MRI imaging. Ultimately, this automated system could be translated for use in processing and machine learning-based analysis of various physiological parameters to support studies and disease diagnosis and manufacturing and automation.

CHAPTER 9

Electrocardiogram and Video Assessment of Amiodarone Effects in the Development Heart of Zebrafish Embryos

9.1 Introduction.

Larval zebrafish have emerged as a valuable model organism in fields such as genetics, developmental biology, neuroscience, and social behavior due to their numerous advantageous characteristics. These include their small size, high reproductive rate, transparent bodies, rapid development post-fertilization, and a genetic similarity to humans of approximately 70% [28, 201-204]. The combination of their compact size and prolific breeding makes zebrafish particularly cost-effective for large-scale experiments, especially when tools and techniques are available to handle and study large numbers of larvae simultaneously. This economic efficiency, alongside their biological relevance, positions zebrafish as an ideal model for a wide range of experimental applications. The unique accessibility of internal organs in zebrafish, including the heart, blood, and blood vessels, makes this model organism particularly well-suited for studying the mechanisms underlying cardiovascular diseases using in vivo non-invasive imaging techniques [205-209]. In zebrafish, the heart is the first organ to form, beginning as a linear tube at approximately 24 hours post-fertilization (hpf). This tube undergoes a remodeling process, known as looping, that culminates in the development of two chambers: a single atrium and a single ventricle, which are separated by the atrio-ventricular valve to prevent blood backflow. Additionally, the outflow tract, known as the bulbous arteriosus, plays a critical role in directing blood flow [210, 211].

One of the unique advantages of zebrafish embryos is their ability to absorb oxygen directly from water through passive diffusion. This capability allows embryos with malformations in

the cardiac system that result in a lack of blood circulation to continue developing, growing, and surviving, thereby facilitating the investigation of such dysfunctions [212].

Among the critical parameters for assessing cardiac function in embryonic zebrafish, heart rate and heart rate variability (HRV) are of paramount importance. These parameters are particularly relevant as they are known to be affected by cardiotoxicity in humans. Consequently, embryonic zebrafish serve as valuable models for studying the cardiotoxic and neurotoxic effects of pharmacological compounds in drug discovery. Additionally, these parameters provide insights into the developmental aspects of the sympatho-vagal balance within the cardiovascular system [213].

Various methods have been developed to detect and quantify heart rate in zebrafish, including visual inspection, the use of specialized electrocardiographic devices, and image processing techniques [213-216]. While visual inspection is time-consuming and subject to operator bias, recording electrocardiographic signals offers the advantage of clearly distinguishing cardiac events in ECG traces. However, precise electrode positioning is essential when recording ECG traces from embryonic zebrafish to ensure reproducible and reliable signals [214, 215].

The widespread use of time-lapse imaging has also enabled the recording of dynamic processes, such as blood flow and heart contraction, in transgenic zebrafish lines [217]. In particular, the advent of fast recording tools, such as confocal scanners, has marked significant progress in image-based methods for evaluating embryonic cardiac function, further enhancing the utility of zebrafish as a model in cardiovascular research.

9.2 Methodology.

9.2.1 Embryo Preparation. Husbandry, system maintenance and spawning of adult zebrafish were conducted using the standard procedures[218, 219]. The zebrafish embryos use for this study were bred in house and raised at 29 °C in E3 Medium (5 mM NaCl, 0.17 mM KCl, 0.4 mM $CaCl_2$, and 0.16 mM $MgSO_4$.) [220]. At 24 hours post-fertilization (hpf), embryos were separated in four groups from which three were treated with 10 μM, 20μM & 30 μM [221, 222] respectively and the fourth group was left as control. ECG data was collected from larvae at 72 hpf. The larvae were sedated at 0.02% MS-222 (Tricaine) and place in a petri dish filled with 30% Danieau Solution (174 mM NaCl, 2.1 mM KCl, 1.2 mM $MgSO_4$ 7 H_2O, 1.8 mM $Ca(NO_3)_2$, and 15 mM HEPES (pH 7.2)).

9.2.2 Micropipette and Suction Electrode Preparation. A micropipette fabricated in house using 4 step pipette puller (PUL-1000) from World Precision Instruments (WPI). This was prefilled using a microfil with 300% Danieau Solution [220]. Once the micropipette was filled, this was assembled to a suction electrode (A-M Systems Inc) for recording. An additional reference electrode was attached to the side of the same suction electrode and place 5 mm away from the larvae. The silver wire electrical connection with the larva was made through the previously filled Danieau Solution from the micropipette.

9.2.3 ECG and Video Recording. All the experiments were performed inside a grounded Faraday Cage located over a vibration free table. The suction electrode was connected to a differential amplifier (Model 1700, A-M Systems Inc) located outside the cage through a actively shielded cable. The differential amplifier settings consisted on a notch filter to remove the 60 Hz coming from the powerline, and a high and low pass filters of 0.1 Hz & 500 Hz respectively with a gain amplification of 10, 000. The differential amplifier was connected

to a DAQ (USB-6001, National Instruments) that digitalized the data to be read by an in house written LabVIEW code. The suction electrode was attached to the chest of the larvae before starting the electrical recording by fixing the tip with slight suction force to avoid physically altering the blood flow which eventually altered cardiac activity that could reach to fatal results. A manual micromanipulator (M3301-M3-L, WPI) was used to precisely position the tip of the micropipette into the larvae's chest as seen in Figure 9.1.

The larvae were observed using a trinocular microscope (PTZMTIII-BS, WPI) and video recorded using a HDTV microscope camera (PRO-300HDS, WPI). Since LED light brings an increased electrical noise, a normal incandescent flashlight was used to illuminate the larvae under the microscope to ease the video recording task.

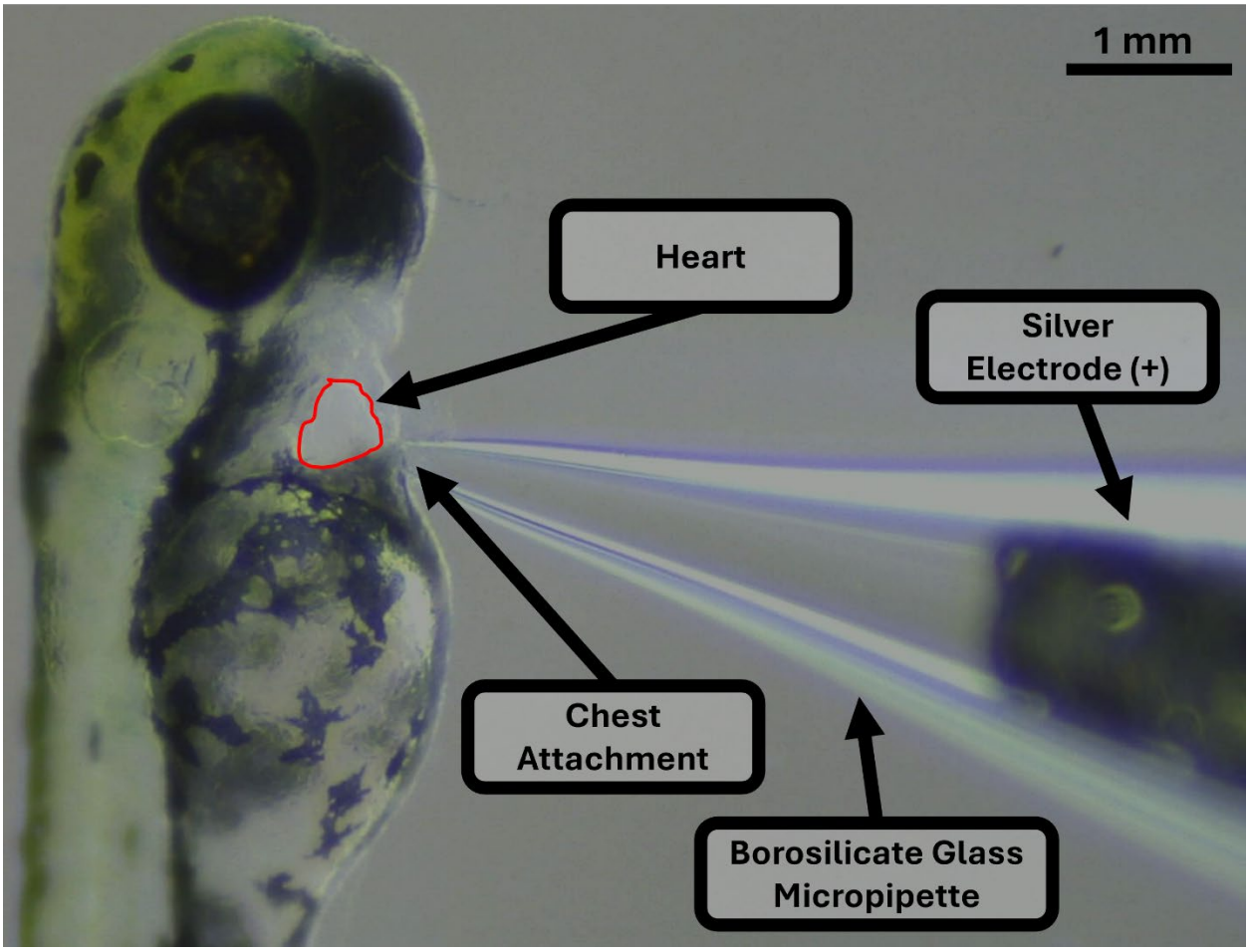

Figure 9.1. Suction Electrode Positioning in Embryonic Zebrafish. 72 hpf zebrafish larva with labeled components.

9.3 Results.

At first glance, recording ECG signals while simultaneously capturing video footage might seem straightforward. However, the low amplitude of ECG signals in zebrafish embryos, compared to those in adult zebrafish and mammals, necessitates additional precautions. To mitigate interference, initial ECG recordings of Amiodarone-exposed larvae were conducted without connecting the microscope camera and lights to any power source. Since the camera and lights must be housed within a Faraday cage, ensuring proper grounding and active shielding of cables was essential. Despite these precautions, achieving high-quality ECG recordings remained challenging due to the critical need for precise positioning. The

distance between the silver electrode and the larva's chest must be minimized, as illustrated in Figure 9.1. Even a slight increase in this distance can drastically reduce the signal-to-noise ratio (SNR), allowing environmental electrical noise to overpower the desired signal, rendering it impossible to filter out.

Figure 9.2 presents the ECG recordings from the control group and two Amiodarone-treated groups (10 μM and 30 μM). For the 20 μM Amiodarone-treated group, the SNR was too low, making it impossible to isolate the ECG signal from the noise.

Following the ECG recordings, video recordings were conducted separately to generate new datasets for training our machine learning algorithm, which is designed to calculate cardiac parameters such as ejection fraction, as demonstrated in our previous work [3]. Although the zebrafish embryos used in this study were similar in age to those in our prior research, the current videos differed in several technical aspects. The resolution was increased from 480 to 720 pixels, the frame rate was doubled from 15 to 30 frames per second (FPS), and the videos were recorded in color rather than grayscale, adding complexity to the processing. To train the neural network accurately, each video was segmented into individual frames, which were then manually labeled. The labeling process involved highlighting the heart's contour in each frame and marking the long and short axes, which are perpendicular to each other, to aid in volume estimation. An example of this labeling process is shown in Figure 9.3. At this stage, further analysis was limited due to the experiment's reproducibility issues. More samples need to be tested to generate reliable data for QTc, QT, HR, and QRS analysis, as current data do not yet meet the necessary standards for trustworthiness.

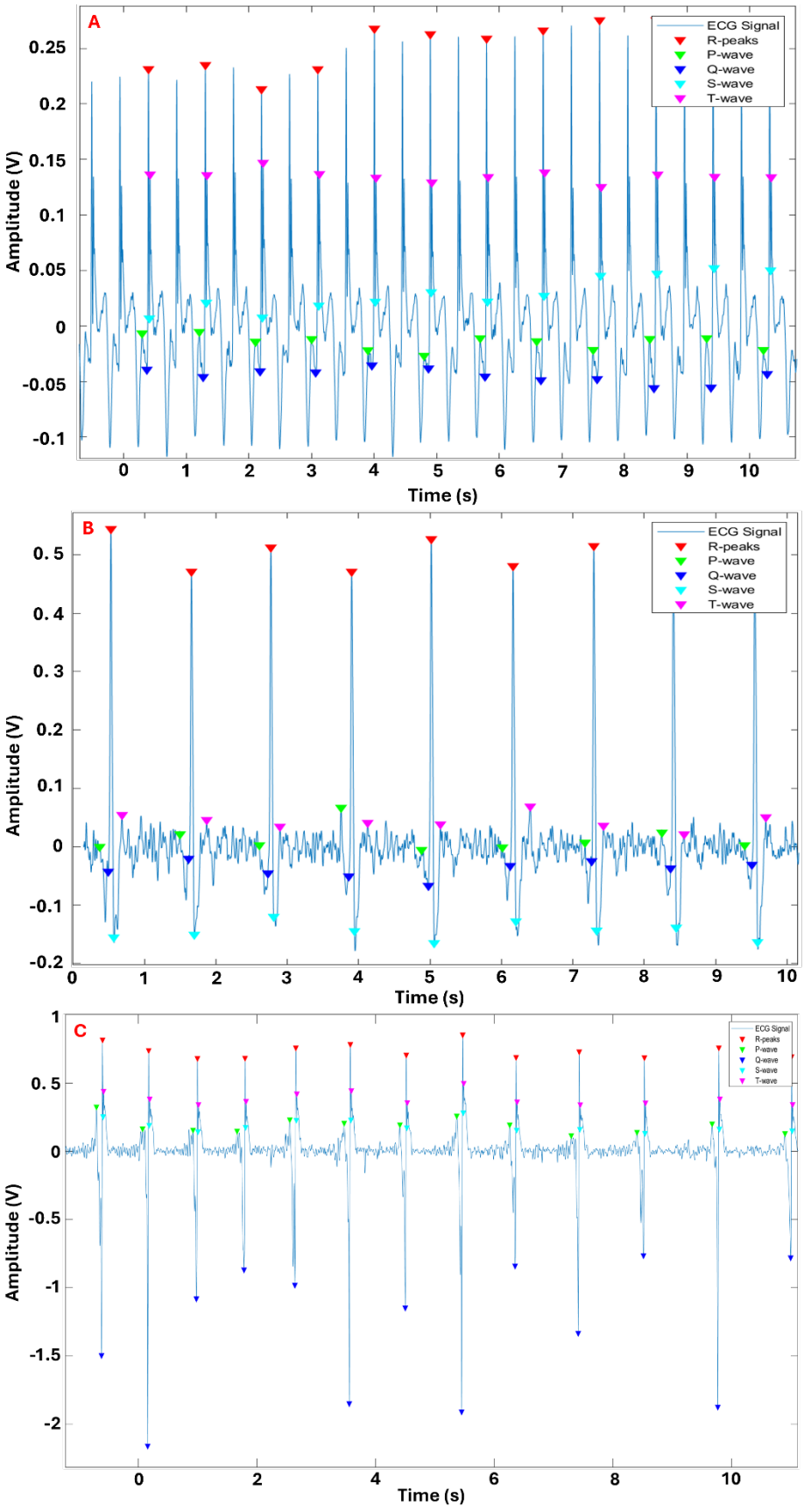
A
ECG Signal
R-peaks
P-wave
Q-wave
S-wave
T-wave
Amplitude (V)
Time (s)
B
ECG Signal
R-peaks
P-wave
Q-wave
S-wave
T-wave
Amplitude (V)
Time (s)
C
ECG Signal
R-peaks
P-wave
Q-wave
S-wave
T-wave
Amplitude (V)
Time (s)

Figure 9.2. ECG Graphs of 10 second Lapse for Treated and Untreated Larvae with PQRST Complex Labels. (A) Control group (B) Treated Group: 10 µM (C) Treated Group: 30 µM.

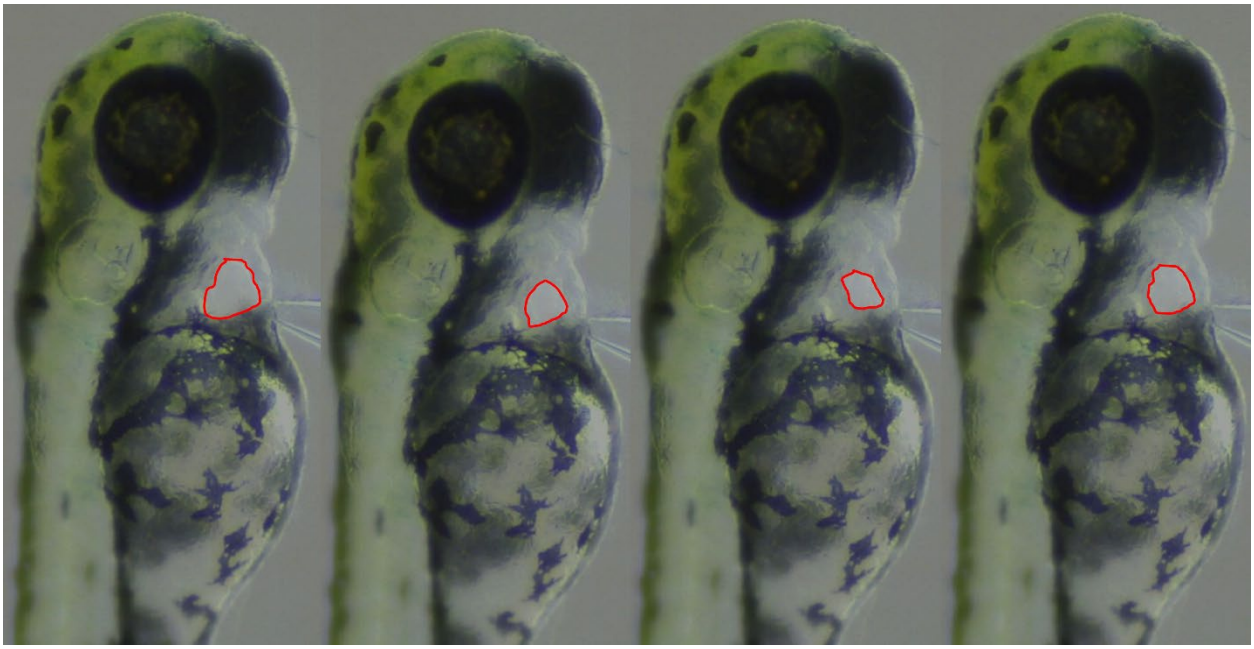

Figure 9.3. Heart Border Labeling from Video Recording of the Heart Beating.

9.4 Discussion.

Conducting electrophysiological studies in small animals, such as zebrafish, presents significant challenges because the standard techniques used in larger mammalian models are not directly applicable. For zebrafish, particularly, recording a clean ECG signal requires the use of a reverse lead II configuration. While this approach may seem straightforward, it is complicated by factors such as the animal's age, size, and even sex, all of which can influence the quality of the ECG recording. Additionally, variables like stress levels, physical condition, overall health, and temperature can further impact the signal-to-noise ratio (SNR), often reducing it to the point where the background noise overwhelms the actual ECG signal. In some cases, particularly with embryonic zebrafish, the electrical signal amplitude is significantly lower—up to three times less—than that of other commonly used animal models. This makes the use of pre-amplifiers to boost the signal necessary to achieve a usable

ECG recording. Also, increases the need to develop better ways of electrical interface between electrodes and zebrafish embryos as it is still the most critical part of ECG collection. These complexities underscore the need for tailored approaches and specialized equipment when performing electrophysiology on small animal models like zebrafish, to ensure accurate and reliable data collection.

9.5 Conclusion.

As previously discussed, acquiring accurate electrocardiogram (ECG) and electroencephalogram (EEG) signals from zebrafish embryos presents significant challenges due to the inherently low amplitude of these signals, which can be up to three times lower than those observed in mammalian models. This limitation necessitates the development and implementation of sophisticated, integrative devices that ensure precise sample positioning and stringent environmental control to enhance signal detection and fidelity.

Recent technological advancements have prompted a paradigm shift from traditional electrode-based ECG recording methods towards innovative approaches that utilize high-resolution video recordings of cardiac activity. These video datasets can be analyzed and translated into pseudo-ECG signals through advanced machine learning algorithms, offering a non-invasive and efficient alternative for monitoring cardiac function in zebrafish embryos.

Embracing these cutting-edge techniques has the potential to substantially increase the experimental throughput and scalability of studies utilizing zebrafish as a model organism. The ability to capture and analyze multiple aspects of cardiovascular function simultaneously not only improves the efficiency of data collection but also enhances the depth and quality of physiological insights attainable. This progression in methodological

approaches lays a robust foundation for more comprehensive investigations into cardiac development, function, and disease modeling, thereby advancing our understanding in the field of cardiovascular research.

CHAPTER 10

Summary and Prospective

10.1 Summary of Contributions.

This dissertation provides a number of contributions were the need of multimodal bio-signal acquisition systems is presented including (1)the elucidation of the effects of methamphetamine on arrhythmic phenotypes using an standard ECG recording methodology which is time consuming and tedious; (2) the ECG assessment of Doxorubicin-Induce Cardiomyopathy in adult zebrafish by comparing three different IP injection methodologies and (3) through the first approach for ECG and video assessment of Amiodarone effects in the developing heart of embryonic zebrafish. These previously mentioned work, serve as a starting point for the need to create integrative multimodal technology that can transform the standard studies into high throughput studies that completely take advantage of the zebrafish model by using large numbers simultaneously while using different methodologies to explain cardiovascular diseases or drug screening through different perspectives that can be easily correlated with. For this, (4) an integrative ECG recording device that involves an increased recording time was created to later improve it during its (5) second generation which includes multi-point ECG probes, and all-in-one cloud-based device. The same process is followed by the embryonic zebrafish model as the transition from ECG probing alone is changing and pointing towards machine learning applied to heart beating videos in order to try to derive pseudo-ECG from them.

10.2 Future Work.

There are a couple of tasks needed to be done in order to improve the previously described work:

- **System Optimization and Redesign**: The current second-generation Zebra II device, while effective as an All-In-One system, suffers from significant bulkiness and weight issues. There is a clear need to redesign and reorganize several components to reduce the overall size and weight without compromising functionality. This optimization will enhance the device's usability and portability.
- **Improving Signal Isolation During Simultaneous Recording**: Recording both ECG signals and videos from embryonic zebrafish has proven challenging due to electrical noise interference, leading to low reproducibility and feasibility issues. Developing a new platform that can precisely position the larva while effectively shielding it from external noise may offer a solution. Given the complications associated with ECG probing in this model, exploring alternative diagnostic tools may be necessary.
- **Integrating a Secondary Diagnostic Tool**: To enhance the multimodality of the Zebra II system, integrating a second diagnostic tool could be highly beneficial, following the approach used with the embryonic model. Echocardiography (ECHO) is a promising option for inclusion in next-generation devices, as it has shown considerable potential in popular studies for complementing ECG data and providing a more comprehensive assessment of cardiac function.

BIBLIOGRAPHY

[1] J. Zhang *et al.*, *Consecutive treatments of methamphetamine promote the development of cardiac pathological symptoms in zebrafish*. 2023.

[2] T. Le *et al.*, "A novel wireless ECG system for prolonged monitoring of multiple zebrafish for heart disease and drug screening studies," *Biosensors and Bioelectronics,* vol. 197, p. 113808, 2022/02/01/ 2022, doi: https://doi.org/10.1016/j.bios.2021.113808.

[3] A. M. Naderi *et al.*, "Deep learning-based framework for cardiac function assessment in embryonic zebrafish from heart beating videos," *Computers in Biology and Medicine,* vol. 135, p. 104565, 2021/08/01/ 2021, doi: https://doi.org/10.1016/j.compbiomed.2021.104565.

[4] R. S. T. Torres *et al.*, "Zebra II as A Novel System to Record Electrophysiological Signals in Zebrafish," *JoVE,* no. 210, p. e67066, 2024/08/16 2024, doi: doi:10.3791/67066.

[5] N. J. Pagidipati and T. A. Gaziano, "Estimating Deaths From Cardiovascular Disease: A Review of Global Methodologies of Mortality Measurement," *Circulation,* vol. 127, no. 6, pp. 749-756, 2013, doi: doi:10.1161/CIRCULATIONAHA.112.128413.

[6] S. S. Virani *et al.*, "Heart Disease and Stroke Statistics-2020 Update: A Report From the American Heart Association," (in eng), *Circulation,* vol. 141, no. 9, pp. e139-e596, Mar 3 2020, doi: 10.1161/cir.0000000000000757.

[7] C. W. Tsao *et al.*, "Heart Disease and Stroke Statistics—2022 Update: A Report From the American Heart Association," *Circulation,* vol. 145, no. 8, pp. e153-e639, 2022, doi: doi:10.1161/CIR.0000000000001052.

[8] N. Townsend *et al.*, "Epidemiology of cardiovascular disease in Europe," *Nature Reviews Cardiology,* vol. 19, no. 2, pp. 133-143, 2022/02/01 2022, doi: 10.1038/s41569-021-00607-3.

[9] J. Perk *et al.*, "European Guidelines on cardiovascular disease prevention in clinical practice (version 2012). The Fifth Joint Task Force of the European Society of Cardiology and Other Societies on Cardiovascular Disease Prevention in Clinical Practice (constituted by representatives of nine societies and by invited experts)," (in eng), *Eur Heart J,* vol. 33, no. 13, pp. 1635-701, Jul 2012, doi: 10.1093/eurheartj/ehs092.

[10] M. J. Pencina *et al.*, "Quantifying Importance of Major Risk Factors for Coronary Heart Disease," *Circulation,* vol. 139, no. 13, pp. 1603-1611, 2019/03/26 2019, doi: 10.1161/CIRCULATIONAHA.117.031855.

[11] J. Stewart, G. Manmathan, and P. Wilkinson, "Primary prevention of cardiovascular disease: A review of contemporary guidance and literature," (in eng), *JRSM Cardiovasc Dis,* vol. 6, p. 2048004016687211, Jan-Dec 2017, doi: 10.1177/2048004016687211.

[12] M. McClellan, N. Brown, R. M. Califf, and J. J. Warner, "Call to Action: Urgent Challenges in Cardiovascular Disease: A Presidential Advisory From the American Heart Association," *Circulation,* vol. 139, no. 9, pp. e44-e54, 2019, doi: doi:10.1161/CIR.0000000000000652.

[13] F. J. Lin, W. K. Tseng, W. H. Yin, H. I. Yeh, J. W. Chen, and C. C. Wu, "Residual Risk Factors to Predict Major Adverse Cardiovascular Events in Atherosclerotic Cardiovascular Disease Patients with and without Diabetes Mellitus," (in eng), *Sci Rep,* vol. 7, no. 1, p. 9179, Aug 23 2017, doi: 10.1038/s41598-017-08741-0.

[14] J. Rockberg, L. Jørgensen, B. Taylor, P. Sobocki, and G. Johansson, "Risk of mortality and recurrent cardiovascular events in patients with acute coronary syndromes on high intensity statin treatment," (in eng), *Prev Med Rep,* vol. 6, pp. 203-209, Jun 2017, doi: 10.1016/j.pmedr.2017.03.001.

[15] Y. Hammer *et al.*, "Guideline-Recommended Therapies and Clinical Outcomes According to the Risk for Recurrent Cardiovascular Events After an Acute Coronary Syndrome," (in eng), *J Am Heart Assoc,* vol. 7, no. 18, p. e009885, Sep 18 2018, doi: 10.1161/jaha.118.009885.

[16] K. M. Engebretsen, K. M. Kaczmarek, J. Morgan, and J. S. Holger, "High-dose insulin therapy in beta-blocker and calcium channel-blocker poisoning," (in eng), *Clin Toxicol (Phila),* vol. 49, no. 4, pp. 277-83, Apr 2011, doi: 10.3109/15563650.2011.582471.

[17] K. Thygesen *et al.*, "Fourth Universal Definition of Myocardial Infarction (2018)," *Circulation,* vol. 138, no. 20, pp. e618-e651, 2018/11/13 2018, doi: 10.1161/CIR.0000000000000617.

[18] A. Krishnan *et al.*, "A detailed comparison of mouse and human cardiac development," (in eng), *Pediatr Res,* vol. 76, no. 6, pp. 500-7, Dec 2014, doi: 10.1038/pr.2014.128.

[19] A. T. Chinwalla *et al.*, "Initial sequencing and comparative analysis of the mouse genome," *Nature,* vol. 420, no. 6915, pp. 520-562, 2002/12/01 2002, doi: 10.1038/nature01262.

[20] X. Kan *et al.*, "Deficiency of IL-12p35 improves cardiac repair after myocardial infarction by promoting angiogenesis," (in eng), *Cardiovasc Res,* vol. 109, no. 2, pp. 249-59, Feb 1 2016, doi: 10.1093/cvr/cvv255.

[21] V. K. Singh and T. M. Seed, "How necessary are animal models for modern drug discovery?," *Expert Opinion on Drug Discovery,* vol. 16, no. 12, pp. 1391-1397, 2021/12/02 2021, doi: 10.1080/17460441.2021.1972255.

[22] F. Simon, A. Oberhuber, and H. Schelzig, "Advantages and Disadvantages of Different Animal Models for Studying Ischemia/Reperfusion Injury of the Spinal Cord," *European Journal of Vascular and Endovascular Surgery,* vol. 49, no. 6, p. 744, 2015, doi: 10.1016/j.ejvs.2015.03.041.

[23] P. D. Anderson and H. I. Battle, "Effects of chloramphenicol on the development of the zebrafish, Brachydanio rerio," (in eng), *Can J Zool,* vol. 45, no. 2, pp. 191-204, Mar 1967, doi: 10.1139/z67-026.

[24] R. Rehwoldt and D. Karimian-Teherani, "Uptake and effect of cadmium on zebrafish," (in eng), *Bull Environ Contam Toxicol,* vol. 15, no. 4, pp. 442-6, Apr 1976, doi: 10.1007/bf01685069.

[25] J. F. Skidmore, "Resistance to zinc sulphate of the zebrafish (Brachydanio rerio Hamilton-Buchanan) at different phases of its life history," (in eng), *Ann Appl Biol,* vol. 56, no. 1, pp. 47-53, Aug 1965, doi: 10.1111/j.1744-7348.1965.tb01214.x.

[26] G. Streisinger, C. Walker, N. Dower, D. Knauber, and F. Singer, "Production of clones of homozygous diploid zebra fish (Brachydanio rerio)," (in eng), *Nature,* vol. 291, no. 5813, pp. 293-6, May 28 1981, doi: 10.1038/291293a0.

[27] J. S. Eisen, "Chapter 1 - History of Zebrafish Research," in *The Zebrafish in Biomedical Research*, S. C. Cartner, J. S. Eisen, S. C. Farmer, K. J. Guillemin, M. L. Kent, and G. E. Sanders Eds.: Academic Press, 2020, pp. 3-14.

[28] K. Howe *et al.*, "The zebrafish reference genome sequence and its relationship to the human genome," *Nature,* vol. 496, no. 7446, pp. 498-503, 2013, doi: 10.1038/nature12111.

[29] P. Giardoglou and D. Beis, "On Zebrafish Disease Models and Matters of the Heart," (in eng), *Biomedicines,* vol. 7, no. 1, Feb 28 2019, doi: 10.3390/biomedicines7010015.

[30] M. S. Dickover, R. Zhang, P. Han, and N. C. Chi, "Zebrafish cardiac injury and regeneration models: a noninvasive and invasive in vivo model of cardiac regeneration," (in eng), *Methods Mol Biol,* vol. 1037, pp. 463-73, 2013, doi: 10.1007/978-1-62703-505-7_27.

[31] R. Ryan, B. R. Moyse, and R. J. Richardson, "Zebrafish cardiac regeneration-looking beyond cardiomyocytes to a complex microenvironment," (in eng), *Histochem Cell Biol,* vol. 154, no. 5, pp. 533-548, Nov 2020, doi: 10.1007/s00418-020-01913-6.

[32] A. Asnani and R. T. Peterson, "The zebrafish as a tool to identify novel therapies for human cardiovascular disease," (in eng), *Dis Model Mech,* vol. 7, no. 7, pp. 763-7, Jul 2014, doi: 10.1242/dmm.016170.

[33] T. Y. Choi, T. I. Choi, Y. R. Lee, S. K. Choe, and C. H. Kim, "Zebrafish as an animal model for biomedical research," (in eng), *Exp Mol Med,* vol. 53, no. 3, pp. 310-317, Mar 2021, doi: 10.1038/s12276-021-00571-5.

[34] D. Bournele and D. Beis, "Zebrafish models of cardiovascular disease," (in eng), *Heart Fail Rev,* vol. 21, no. 6, pp. 803-813, Nov 2016, doi: 10.1007/s10741-016-9579-y.

[35] B. J. Haubner *et al.*, "Complete cardiac regeneration in a mouse model of myocardial infarction," (in eng), *Aging (Albany NY),* vol. 4, no. 12, pp. 966-77, Dec 2012, doi: 10.18632/aging.100526.

[36] M. Gemberling, T. J. Bailey, D. R. Hyde, and K. D. Poss, "The zebrafish as a model for complex tissue regeneration," (in eng), *Trends Genet,* vol. 29, no. 11, pp. 611-20, Nov 2013, doi: 10.1016/j.tig.2013.07.003.

[37] A. W. Seifert and K. Muneoka, "The blastema and epimorphic regeneration in mammals," (in eng), *Dev Biol,* vol. 433, no. 2, pp. 190-199, Jan 15 2018, doi: 10.1016/j.ydbio.2017.08.007.

[38] S. A. Brittijn *et al.*, "Zebrafish development and regeneration: new tools for biomedical research," (in eng), *Int J Dev Biol,* vol. 53, no. 5-6, pp. 835-50, 2009, doi: 10.1387/ijdb.082615sb.

[39] S. P. Singh, J. E. Holdway, and K. D. Poss, "Regeneration of amputated zebrafish fin rays from de novo osteoblasts," (in eng), *Dev Cell,* vol. 22, no. 4, pp. 879-86, Apr 17 2012, doi: 10.1016/j.devcel.2012.03.006.

[40] K. Kikuchi *et al.*, "Primary contribution to zebrafish heart regeneration by gata4+ cardiomyocytes," *Nature,* vol. 464, no. 7288, pp. 601-605, 2010/03/01 2010, doi: 10.1038/nature08804.

[41] C. Jopling, E. Sleep, M. Raya, M. Martí, A. Raya, and J. C. I. Belmonte, "Zebrafish heart regeneration occurs by cardiomyocyte dedifferentiation and proliferation," *Nature,* vol. 464, no. 7288, pp. 606-609, 2010/03/01 2010, doi: 10.1038/nature08899.

[42] K. L. Poon and T. Brand, "The zebrafish model system in cardiovascular research: A tiny fish with mighty prospects," *Global Cardiology Science and Practice,* vol. 2013, no. 1, 2013, doi: https://doi.org/10.5339/gcsp.2013.4.

[43] E. E. Patton, L. I. Zon, and D. M. Langenau, "Zebrafish disease models in drug discovery: from preclinical modelling to clinical trials," (in eng), *Nat Rev Drug Discov,* vol. 20, no. 8, pp. 611-628, Aug 2021, doi: 10.1038/s41573-021-00210-8.

[44] C. A. MacRae and R. T. Peterson, "Zebrafish as tools for drug discovery," *Nature Reviews Drug Discovery,* vol. 14, no. 10, pp. 721-731, 2015/10/01 2015, doi: 10.1038/nrd4627.

[45] D. J. Milan, T. A. Peterson, J. N. Ruskin, R. T. Peterson, and C. A. MacRae, "Drugs that induce repolarization abnormalities cause bradycardia in zebrafish," (in eng), *Circulation,* vol. 107, no. 10, pp. 1355-8, Mar 18 2003, doi: 10.1161/01.cir.0000061912.88753.87.

[46] E. de Pater *et al.*, "Distinct phases of cardiomyocyte differentiation regulate growth of the zebrafish heart," (in eng), *Development,* vol. 136, no. 10, pp. 1633-41, May 2009, doi: 10.1242/dev.030924.

[47] S. Lazic and I. C. Scott, "Mef2cb regulates late myocardial cell addition from a second heart field-like population of progenitors in zebrafish," (in eng), *Dev Biol,* vol. 354, no. 1, pp. 123-33, Jun 1 2011, doi: 10.1016/j.ydbio.2011.03.028.

[48] S. Burkhard, V. van Eif, L. Garric, V. M. Christoffels, and J. Bakkers, "On the Evolution of the Cardiac Pacemaker," (in eng), *J Cardiovasc Dev Dis,* vol. 4, no. 2, Apr 27 2017, doi: 10.3390/jcdd4020004.

[49] I. P. Temple, S. Inada, H. Dobrzynski, and M. R. Boyett, "Connexins and the atrioventricular node," (in eng), *Heart Rhythm,* vol. 10, no. 2, pp. 297-304, Feb 2013, doi: 10.1016/j.hrthm.2012.10.020.

[50] Y. Zhao, M. Yun, S. A. Nguyen, M. Tran, and T. P. Nguyen, "In Vivo Surface Electrocardiography for Adult Zebrafish," (in eng), *J Vis Exp,* no. 150, Aug 1 2019, doi: 10.3791/60011.

[51] B. P. Sampurna, G. Audira, S. Juniardi, Y.-H. Lai, and C.-D. Hsiao, "A Simple ImageJ-Based Method to Measure Cardiac Rhythm in Zebrafish Embryos," *Inventions*, vol. 3, no. 2*,* doi: 10.3390/inventions3020021.

[52] D. S. Peal *et al.*, "Novel chemical suppressors of long QT syndrome identified by an in vivo functional screen," (in eng), *Circulation,* vol. 123, no. 1, pp. 23-30, Jan 4 2011, doi: 10.1161/circulationaha.110.003731.

[53] Y. Zhao *et al.*, "Adult zebrafish ventricular electrical gradients as tissue mechanisms of ECG patterns under baseline vs. oxidative stress," (in eng), *Cardiovasc Res,* vol. 117, no. 8, pp. 1891-1907, Jul 7 2021, doi: 10.1093/cvr/cvaa238.

[54] L. W. Wang *et al.*, "Standardized echocardiographic assessment of cardiac function in normal adult zebrafish and heart disease models," *Disease Models & Mechanisms,* vol. 10, no. 1, pp. 63-76, 2017, doi: 10.1242/dmm.026989.

[55] H. C. Yalcin, A. Amindari, J. T. Butcher, A. Althani, and M. Yacoub, "Heart function and hemodynamic analysis for zebrafish embryos," *Developmental Dynamics,* vol. 246, no. 11, pp. 868-880, 2017, doi: https://doi.org/10.1002/dvdy.24497.

[56] R. J. Wessells and R. Bodmer, "Screening assays for heart function mutants in Drosophila," *BioTechniques,* vol. 37, no. 1, pp. 58-66, 2004/07/01 2004, doi: 10.2144/04371ST01.

[57] O. Ishaq, S. K. Sadanandan, and C. Wählby, "Deep Fish: Deep Learning–Based Classification of Zebrafish Deformation for High-Throughput Screening," *SLAS*

Discovery, vol. 22, no. 1, pp. 102-107, 2017/01/01/ 2017, doi: https://doi.org/10.1177/1087057116667894.

[58] W. Wu, X. Liu, M. Xu, J.-R. Peng, and R. Setiono, "A Hybrid SOM-SVM Approach for the Zebrafish Gene Expression Analysis," *Genomics, Proteomics & Bioinformatics,* vol. 3, no. 2, pp. 84-93, 2005, doi: 10.1016/S1672-0229(05)03013-5.

[59] H. Zhang, W. Li, Y. Xie, W. J. Wang, L. L. Li, and S. Y. Yang, "Rapid and accurate assessment of seizure liability of drugs by using an optimal support vector machine method," (in eng), *Toxicol In Vitro,* vol. 25, no. 8, pp. 1848-54, Dec 2011, doi: 10.1016/j.tiv.2011.05.015.

[60] O. Mirat, J. R. Sternberg, K. E. Severi, and C. Wyart, "ZebraZoom: an automated program for high-throughput behavioral analysis and categorization," (in eng), *Front Neural Circuits,* vol. 7, p. 107, 2013, doi: 10.3389/fncir.2013.00107.

[61] R. Mikut *et al.*, "Automated processing of zebrafish imaging data: a survey," (in eng), *Zebrafish,* vol. 10, no. 3, pp. 401-21, Sep 2013, doi: 10.1089/zeb.2013.0886.

[62] O. Ronneberger *et al.*, "ViBE-Z: a framework for 3D virtual colocalization analysis in zebrafish larval brains," (in eng), *Nat Methods,* vol. 9, no. 7, pp. 735-42, Jun 17 2012, doi: 10.1038/nmeth.2076.

[63] M. L. Cordero-Maldonado *et al.*, "Deep learning image recognition enables efficient genome editing in zebrafish by automated injections," (in eng), *PLoS One,* vol. 14, no. 1, p. e0202377, 2019, doi: 10.1371/journal.pone.0202377.

[64] R. Sawaki, D. Sato, H. Nakayama, Y. Nakagawa, and Y. Shimada, "ZF-AutoML: An Easy Machine-Learning-Based Method to Detect Anomalies in Fluorescent-Labelled Zebrafish," *Inventions*, vol. 4, no. 4, doi: 10.3390/inventions4040072.

[65] C. G. Kevil *et al.*, "Methamphetamine Use and Cardiovascular Disease," *Arteriosclerosis, Thrombosis, and Vascular Biology,* vol. 39, no. 9, pp. 1739-1746, 2019, doi: doi:10.1161/ATVBAHA.119.312461.

[66] D. J. Heal, S. L. Smith, J. Gosden, and D. J. Nutt, "Amphetamine, past and present--a pharmacological and clinical perspective," (in eng), *J Psychopharmacol,* vol. 27, no. 6, pp. 479-96, Jun 2013, doi: 10.1177/0269881113482532.

[67] M. G. Kirkpatrick, E. W. Gunderson, C. E. Johanson, F. R. Levin, R. W. Foltin, and C. L. Hart, "Comparison of intranasal methamphetamine and d-amphetamine self-administration by humans," (in eng), *Addiction,* vol. 107, no. 4, pp. 783-91, Apr 2012, doi: 10.1111/j.1360-0443.2011.03706.x.

[68] S. D. Robertson, H. J. Matthies, and A. Galli, "A closer look at amphetamine-induced reverse transport and trafficking of the dopamine and norepinephrine transporters," (in eng), *Mol Neurobiol,* vol. 39, no. 2, pp. 73-80, Apr 2009, doi: 10.1007/s12035-009-8053-4.

[69] A. E. Fleckenstein, T. J. Volz, E. L. Riddle, J. W. Gibb, and G. R. Hanson, "New insights into the mechanism of action of amphetamines," (in eng), *Annu Rev Pharmacol Toxicol,* vol. 47, pp. 681-98, 2007, doi: 10.1146/annurev.pharmtox.47.120505.105140.

[70] M. W. Warren, F. H. Kobeissy, M. C. Liu, R. L. Hayes, M. S. Gold, and K. K. W. Wang, "Concurrent calpain and caspase-3 mediated proteolysis of αII-spectrin and tau in rat brain after methamphetamine exposure: A similar profile to traumatic brain injury," *Life Sciences,* vol. 78, no. 3, pp. 301-309, 2005/12/05/ 2005, doi: https://doi.org/10.1016/j.lfs.2005.04.058.

[71] S. A. Lloyd, B. Corkill, M. C. Bruster, R. L. Roberts, and R. A. Shanks, "Chronic methamphetamine exposure significantly decreases microglia activation in the arcuate nucleus," (in eng), *J Chem Neuroanat,* vol. 82, pp. 5-11, Jul 2017, doi: 10.1016/j.jchemneu.2017.03.001.

[72] P. Melo *et al.*, "Methamphetamine mimics the neurochemical profile of aging in rats and impairs recognition memory," (in eng), *Neurotoxicology,* vol. 33, no. 3, pp. 491-9, Jun 2012, doi: 10.1016/j.neuro.2012.03.002.

[73] S. Won, R. A. Hong, R. V. Shohet, T. B. Seto, and N. I. Parikh, "Methamphetamine-associated cardiomyopathy," (in eng), *Clin Cardiol,* vol. 36, no. 12, pp. 737-42, Dec 2013, doi: 10.1002/clc.22195.

[74] K. J. Varner, B. A. Ogden, J. Delcarpio, and S. Meleg-Smith, "Cardiovascular responses elicited by the "binge" administration of methamphetamine," (in eng), *J Pharmacol Exp Ther,* vol. 301, no. 1, pp. 152-9, Apr 2002, doi: 10.1124/jpet.301.1.152.

[75] J. Li *et al.*, "Methamphetamine use associated with monomorphic ventricular tachycardia," (in eng), *J Addict Med,* vol. 8, no. 6, pp. 470-3, Nov-Dec 2014, doi: 10.1097/adm.0000000000000069.

[76] W. Haning and D. Goebert, "Electrocardiographic abnormalities in methamphetamine abusers," (in eng), *Addiction,* vol. 102 Suppl 1, pp. 70-5, Apr 2007, doi: 10.1111/j.1360-0443.2006.01776.x.

[77] E. D. Paratz, N. J. Cunningham, and A. I. MacIsaac, "The Cardiac Complications of Methamphetamines," *Heart, Lung and Circulation,* vol. 25, no. 4, pp. 325-332, 2016/04/01/ 2016, doi: https://doi.org/10.1016/j.hlc.2015.10.019.

[78] M. N. Islam *et al.*, "Cardiac lesions and their reversibility after long term administration of methamphetamine," (in eng), *Forensic Sci Int,* vol. 75, no. 1, pp. 29-43, Aug 28 1995, doi: 10.1016/0379-0738(95)01765-b.

[79] J. E. Lopez, K. Yeo, G. Caputo, M. Buonocore, and S. Schaefer, "Recovery of methamphetamine associated cardiomyopathy predicted by late gadolinium enhanced cardiovascular magnetic resonance," (in eng), *J Cardiovasc Magn Reson,* vol. 11, no. 1, p. 46, Nov 11 2009, doi: 10.1186/1532-429x-11-46.

[80] H. Kuribara and Y. Uchihashi, "Dopamine antagonists can inhibit methamphetamine sensitization, but not cocaine sensitization, when assessed by ambulatory activity in mice," (in eng), *J Pharm Pharmacol,* vol. 45, no. 12, pp. 1042-5, Dec 1993, doi: 10.1111/j.2042-7158.1993.tb07177.x.

[81] K. A. Johnson and D. M. Lovinger, "Presynaptic G Protein-Coupled Receptors: Gatekeepers of Addiction?," (in eng), *Front Cell Neurosci,* vol. 10, p. 264, 2016, doi: 10.3389/fncel.2016.00264.

[82] J. Wang, C. Gareri, and H. A. Rockman, "G-Protein-Coupled Receptors in Heart Disease," (in eng), *Circ Res,* vol. 123, no. 6, pp. 716-735, Aug 31 2018, doi: 10.1161/circresaha.118.311403.

[83] N. Kumari, S. Reabroi, and B. J. North, "Unraveling the Molecular Nexus between GPCRs, ERS, and EMT," (in eng), *Mediators Inflamm,* vol. 2021, p. 6655417, 2021, doi: 10.1155/2021/6655417.

[84] U. Sriram *et al.*, "Methamphetamine induces trace amine-associated receptor 1 (TAAR1) expression in human T lymphocytes: role in immunomodulation," (in eng), *J Leukoc Biol,* vol. 99, no. 1, pp. 213-23, Jan 2016, doi: 10.1189/jlb.4A0814-395RR.

[85] B. Borowsky *et al.*, "Trace amines: identification of a family of mammalian G protein-coupled receptors," (in eng), *Proc Natl Acad Sci U S A,* vol. 98, no. 16, pp. 8966-71, Jul 31 2001, doi: 10.1073/pnas.151105198.

[86] H. Cao *et al.*, "Wearable multi-channel microelectrode membranes for elucidating electrophysiological phenotypes of injured myocardium," *Integrative Biology (United Kingdom),* Article vol. 6, no. 8, pp. 789-795, 2014, doi: 10.1039/c4ib00052h.

[87] I. Miranda *et al.*, "Properties and Applications of PDMS for Biomedical Engineering: A Review," (in eng), *J Funct Biomater,* vol. 13, no. 1, Dec 21 2021, doi: 10.3390/jfb13010002.

[88] E. Tackie-Yarboi *et al.*, "Combining Neurobehavioral Analysis and In Vivo Photoaffinity Labeling to Understand Protein Targets of Methamphetamine in Casper Zebrafish," (in eng), *ACS Chem Neurosci,* vol. 11, no. 17, pp. 2761-2773, Sep 2 2020, doi: 10.1021/acschemneuro.0c00416.

[89] F. Yu, R. Li, E. Parks, W. Takabe, and T. K. Hsiai, "Electrocardiogram signals to assess zebrafish heart regeneration: implication of long QT intervals," (in eng), *Ann Biomed Eng,* vol. 38, no. 7, pp. 2346-57, Jul 2010, doi: 10.1007/s10439-010-9993-6.

[90] H. C. BAZETT, "AN ANALYSIS OF THE TIME-RELATIONS OF ELECTROCARDIOGRAMS," *Annals of Noninvasive Electrocardiology,* vol. 2, no. 2, pp. 177-194, 1997, doi: https://doi.org/10.1111/j.1542-474X.1997.tb00325.x.

[91] V. Sander, G. Suñe, C. Jopling, C. Morera, and J. C. Izpisua Belmonte, "Isolation and in vitro culture of primary cardiomyocytes from adult zebrafish hearts," (in eng), *Nat Protoc,* vol. 8, no. 4, pp. 800-9, Apr 2013, doi: 10.1038/nprot.2013.041.

[92] A. Bradaia *et al.*, "The selective antagonist EPPTB reveals TAAR1-mediated regulatory mechanisms in dopaminergic neurons of the mesolimbic system," (in eng), *Proc Natl Acad Sci U S A,* vol. 106, no. 47, pp. 20081-6, Nov 24 2009, doi: 10.1073/pnas.0906522106.

[93] R. D. Harvey and C. E. Clancy, "Mechanisms of cAMP compartmentation in cardiac myocytes: experimental and computational approaches to understanding," (in eng), *J Physiol,* vol. 599, no. 20, pp. 4527-4544, Oct 2021, doi: 10.1113/jp280801.

[94] C. W. Schindler, J. W. Zheng, S. R. Tella, and S. R. Goldberg, "Pharmacological mechanisms in the cardiovascular effects of methamphetamine in conscious squirrel monkeys," (in eng), *Pharmacol Biochem Behav,* vol. 42, no. 4, pp. 791-6, Aug 1992, doi: 10.1016/0091-3057(92)90031-a.

[95] J. Fang, D. Zhu, and C. Luo, "An in vivo assessment: cardiotoxicity induced by three kinds of addictive drugs (methamphetamine, ketamine, and methadone) in zebrafish embryos," *International Journal of Public Health and Safety,* vol. 1, no. 3, pp. 1-4, 2016.

[96] W. Kobinger and L. Pichler, "Differentiation of drugs acting centrally upon the cardiovascular system by means of sympathetic and vagal responses," (in eng), *Clin Exp Hypertens (1978),* vol. 1, no. 2, pp. 229-49, 1978, doi: 10.3109/10641967809068606.

[97] M. E. Field *et al.*, "P-Wave Amplitude and PR Changes in Patients With Inappropriate Sinus Tachycardia: Findings Supportive of a Central Mechanism," (in eng), *J Am Heart Assoc,* vol. 7, no. 9, Apr 19 2018, doi: 10.1161/jaha.118.008528.

[98] F. Sessa *et al.*, "Heart rate variability as predictive factor for sudden cardiac death," (in eng), *Aging (Albany NY),* vol. 10, no. 2, pp. 166-177, Feb 23 2018, doi: 10.18632/aging.101386.

[99] A. E. Draghici and J. A. Taylor, "The physiological basis and measurement of heart rate variability in humans," (in eng), *J Physiol Anthropol,* vol. 35, no. 1, p. 22, Sep 28 2016, doi: 10.1186/s40101-016-0113-7.

[100] B. L. Henry, A. Minassian, and W. Perry, "Effect of methamphetamine dependence on heart rate variability," (in eng), *Addict Biol,* vol. 17, no. 3, pp. 648-58, May 2012, doi: 10.1111/j.1369-1600.2010.00270.x.

[101] P. K. V. Reddy, T. M. H. Ng, E. E. Oh, G. Moady, and U. Elkayam, "Clinical Characteristics and Management of Methamphetamine-Associated Cardiomyopathy: State-of-the-Art Review," (in eng), *J Am Heart Assoc,* vol. 9, no. 11, p. e016704, Jun 2 2020, doi: 10.1161/jaha.120.016704.

[102] S. M. Pikkujämsä *et al.*, "Heart rate variability and baroreflex sensitivity in hypertensive subjects with and without metabolic features of insulin resistance syndrome," (in eng), *Am J Hypertens,* vol. 11, no. 5, pp. 523-31, May 1998, doi: 10.1016/s0895-7061(98)00035-1.

[103] E. Bazmi, F. Mousavi, L. Giahchin, T. Mokhtari, and B. Behnoush, "Cardiovascular Complications of Acute Amphetamine Abuse: Cross-sectional study," (in eng), *Sultan Qaboos Univ Med J,* vol. 17, no. 1, pp. e31-e37, Feb 2017, doi: 10.18295/squmj.2016.17.01.007.

[104] A. Sinha, O. Lewis, R. Kumar, S. L. Yeruva, and B. H. Curry, "Amphetamine Abuse Related Acute Myocardial Infarction," (in eng), *Case Rep Cardiol,* vol. 2016, p. 7967851, 2016, doi: 10.1155/2016/7967851.

[105] Q. Wang, T. Michiue, T. Ishikawa, B. L. Zhu, and H. Maeda, "Combined analyses of creatine kinase MB, cardiac troponin I and myoglobin in pericardial and cerebrospinal fluids to investigate myocardial and skeletal muscle injury in medicolegal autopsy cases," (in eng), *Leg Med (Tokyo),* vol. 13, no. 5, pp. 226-32, Sep 2011, doi: 10.1016/j.legalmed.2011.05.002.

[106] S. Ahnve, "Correction of the QT interval for heart rate: review of different formulas and the use of Bazett's formula in myocardial infarction," *American heart journal,* vol. 109, no. 3, pp. 568-574, 1985.

[107] R. Liang *et al.*, "Effect of methamphetamine on potassium and L-type calcium currents in rat ventricular myocytes," (in eng), *Toxicol Mech Methods,* vol. 20, no. 8, pp. 458-65, Oct 2010, doi: 10.3109/15376516.2010.497979.

[108] P. Debonnaire *et al.*, "QRS Fragmentation and QTc Duration Relate to Malignant Ventricular Tachyarrhythmias and Sudden Cardiac Death in Patients with Hypertrophic Cardiomyopathy," (in eng), *J Cardiovasc Electrophysiol,* vol. 26, no. 5, pp. 547-55, May 2015, doi: 10.1111/jce.12629.

[109] L. M. Ryerson and R. M. Giuffre, "QT intervals in metabolic dilated cardiomyopathy," (in eng), *Can J Cardiol,* vol. 22, no. 3, pp. 217-20, Mar 1 2006, doi: 10.1016/s0828-282x(06)70899-6.

[110] Y. H. Qu *et al.*, "Remodeling of ion channel expression may contribute to electrophysiological consequences caused by methamphetamine in vitro and in vivo,"

(in eng), *Biochem Biophys Res Commun,* vol. 443, no. 2, pp. 441-6, Jan 10 2014, doi: 10.1016/j.bbrc.2013.11.114.

[111] S. Jayanthi, O. V. Torres, B. Ladenheim, and J. L. Cadet, "A Single Prior Injection of Methamphetamine Enhances Methamphetamine Self-Administration (SA) and Blocks SA-Induced Changes in DNA Methylation and mRNA Expression of Potassium Channels in the Rat Nucleus Accumbens," (in eng), *Mol Neurobiol,* vol. 57, no. 3, pp. 1459-1472, Mar 2020, doi: 10.1007/s12035-019-01830-3.

[112] K. Sugimoto *et al.*, "Methamphetamine directly accelerates beating rate in cardiomyocytes by increasing Ca(2+) entry via L-type Ca(2+) channel," (in eng), *Biochem Biophys Res Commun,* vol. 390, no. 4, pp. 1214-20, Dec 25 2009, doi: 10.1016/j.bbrc.2009.10.124.

[113] A. Scholz, "Mechanisms of (local) anaesthetics on voltage-gated sodium and other ion channels," (in eng), *Br J Anaesth,* vol. 89, no. 1, pp. 52-61, Jul 2002, doi: 10.1093/bja/aef163.

[114] P. Sun *et al.*, "Micro-Electrocardiograms to Study Post-Ventricular Amputation of Zebrafish Heart," *Annals of Biomedical Engineering,* vol. 37, no. 5, pp. 890-901, 2009/05/01 2009, doi: 10.1007/s10439-009-9668-3.

[115] R. Dziaman, B. Kłyszejko, and G. Hajek, "The effect of MS-222 on the cardiac and respiratory function and behaviour of common carp, Cyprinus carpio L., during general anaesthesia," *Acta Ichthyologica et Piscatoria,* vol. 35, pp. 125-131, 2005.

[116] J. P. Owen and R. N. Kelsh, "A suitable anaesthetic protocol for metamorphic zebrafish," (in eng), *PLoS One,* vol. 16, no. 3, p. e0246504, 2021, doi: 10.1371/journal.pone.0246504.

[117] C. H. Kwon and S. H. Kim, "Intraoperative management of critical arrhythmia," (in eng), *Korean J Anesthesiol,* vol. 70, no. 2, pp. 120-126, Apr 2017, doi: 10.4097/kjae.2017.70.2.120.

[118] I. Hoyer and P. A. van Zwieten, "The centrally induced fall in blood pressure after the infusion of amphetamine and related drugs into the vertebral artery of the cat," (in eng), *J Pharm Pharmacol,* vol. 23, no. 11, pp. 892-3, Nov 1971, doi: 10.1111/j.2042-7158.1971.tb10214.x.

[119] D. B. Vaupel *et al.*, "Delayed emergence of methamphetamine's enhanced cardiovascular effects in nonhuman primates during protracted methamphetamine abstinence," (in eng), *Drug Alcohol Depend,* vol. 159, pp. 181-9, Feb 1 2016, doi: 10.1016/j.drugalcdep.2015.12.008.

[120] B. S. Muntean *et al.*, "A Comparative Study of Embedded and Anesthetized Zebrafish in vivo on Myocardiac Calcium Oscillation and Heart Muscle Contraction," (in eng), *Front Pharmacol,* vol. 1, p. 139, 2010, doi: 10.3389/fphar.2010.00139.

[121] M. Casanovas *et al.*, "Methamphetamine Blocks Adenosine A(2A) Receptor Activation via Sigma 1 and Cannabinoid CB(1) Receptors," (in eng), *Int J Mol Sci,* vol. 22, no. 5, Mar 9 2021, doi: 10.3390/ijms22052743.

[122] M. Fehler, K. J. Broadley, W. R. Ford, and E. J. Kidd, "Identification of trace-amine-associated receptors (TAAR) in the rat aorta and their role in vasoconstriction by β-phenylethylamine," (in eng), *Naunyn Schmiedebergs Arch Pharmacol,* vol. 382, no. 4, pp. 385-98, Oct 2010, doi: 10.1007/s00210-010-0554-1.

[123] K. J. Broadley, M. Fehler, W. R. Ford, and E. J. Kidd, "Functional evaluation of the receptors mediating vasoconstriction of rat aorta by trace amines and

amphetamines," (in eng), *Eur J Pharmacol,* vol. 715, no. 1-3, pp. 370-80, Sep 5 2013, doi: 10.1016/j.ejphar.2013.04.034.

[124] C. S. Abdullah *et al.*, "Methamphetamine induces cardiomyopathy by Sigmar1 inhibition-dependent impairment of mitochondrial dynamics and function," (in eng), *Commun Biol,* vol. 3, no. 1, p. 682, Nov 17 2020, doi: 10.1038/s42003-020-01408-z.

[125] H. Chavva *et al.*, "Methamphetamine-induced changes in myocardial gene transcription are sex-dependent," (in eng), *BMC Genomics,* vol. 22, no. 1, p. 259, Apr 12 2021, doi: 10.1186/s12864-021-07561-x.

[126] N. B. Miner, J. S. Elmore, M. H. Baumann, T. J. Phillips, and A. Janowsky, "Trace amine-associated receptor 1 regulation of methamphetamine-induced neurotoxicity," (in eng), *Neurotoxicology,* vol. 63, pp. 57-69, Dec 2017, doi: 10.1016/j.neuro.2017.09.006.

[127] K. Ravid, L. I. Smith-Mungo, Z. Zhao, K. M. Thomas, and H. M. Kagan, "Upregulation of lysyl oxidase in vascular smooth muscle cells by cAMP: role for adenosine receptor activation," (in eng), *J Cell Biochem,* vol. 75, no. 1, pp. 177-85, Oct 1 1999, doi: 10.1002/(sici)1097-4644(19991001)75:1<177::aid-jcb18>3.3.co;2-n.

[128] M. Grimm and J. H. Brown, "Beta-adrenergic receptor signaling in the heart: role of CaMKII," (in eng), *J Mol Cell Cardiol,* vol. 48, no. 2, pp. 322-30, Feb 2010, doi: 10.1016/j.yjmcc.2009.10.016.

[129] P. D. Swaminathan, A. Purohit, T. J. Hund, and M. E. Anderson, "Calmodulin-dependent protein kinase II: linking heart failure and arrhythmias," (in eng), *Circ Res,* vol. 110, no. 12, pp. 1661-77, Jun 8 2012, doi: 10.1161/circresaha.111.243956.

[130] D. M. Hedges *et al.*, "Methamphetamine Induces Dopamine Release in the Nucleus Accumbens Through a Sigma Receptor-Mediated Pathway," (in eng), *Neuropsychopharmacology,* vol. 43, no. 6, pp. 1405-1414, May 2018, doi: 10.1038/npp.2017.291.

[131] F. Limanaqi, S. Gambardella, F. Biagioni, C. L. Busceti, and F. Fornai, "Epigenetic Effects Induced by Methamphetamine and Methamphetamine-Dependent Oxidative Stress," (in eng), *Oxid Med Cell Longev,* vol. 2018, p. 4982453, 2018, doi: 10.1155/2018/4982453.

[132] S. Hernandez-Lopez *et al.*, "D2 dopamine receptors in striatal medium spiny neurons reduce L-type Ca2+ currents and excitability via a novel PLC[beta]1-IP3-calcineurin-signaling cascade," (in eng), *J Neurosci,* vol. 20, no. 24, pp. 8987-95, Dec 15 2000, doi: 10.1523/jneurosci.20-24-08987.2000.

[133] O. Monfredi and M. R. Boyett, "Sick sinus syndrome and atrial fibrillation in older persons—a view from the sinoatrial nodal myocyte," *Journal of molecular and cellular cardiology,* vol. 83, pp. 88-100, 2015.

[134] V. Adan and L. A. Crown, "Diagnosis and treatment of sick sinus syndrome," *American family physician,* vol. 67, no. 8, pp. 1725-1732, 2003.

[135] M. Semelka, J. Gera, and S. Usman, "Sick sinus syndrome: a review," *American family physician,* vol. 87, no. 10, pp. 691-696, 2013.

[136] M. L. Bakker *et al.*, "T-box transcription factor TBX3 reprogrammes mature cardiac myocytes into pacemaker-like cells," *Cardiovasc Res,* vol. 94, no. 3, pp. 439-449, 2012, doi: 10.1093/cvr/cvs120.

[137] M. Choudhury *et al.*, "TBX18 overexpression enhances pacemaker function in a rat subsidiary atrial pacemaker model of sick sinus syndrome," *The Journal of Physiology,* vol. 596, no. 24, pp. 6141-6155, 2018.

[138] J. Yan *et al.*, "Aging-associated sinus arrest and sick sinus syndrome in adult zebrafish," *PloS one,* vol. 15, no. 5, p. e0232457, 2020.

[139] R. Arnaout *et al.*, "Zebrafish model for human long QT syndrome," *Proceedings of the National Academy of Sciences,* vol. 104, no. 27, pp. 11316-11321, 2007, doi: doi:10.1073/pnas.0702724104.

[140] C. D. Koopman *et al.*, "The zebrafish grime mutant uncovers an evolutionarily conserved role for Tmem161b in the control of cardiac rhythm," *Proceedings of the National Academy of Sciences,* vol. 118, no. 9, p. e2018220118, 2021.

[141] C. E. Genge *et al.*, "The Zebrafish Heart as a Model of Mammalian Cardiac Function," in *Reviews of Physiology, Biochemistry and Pharmacology, Vol. 171*, B. Nilius, P. de Tombe, T. Gudermann, R. Jahn, R. Lill, and O. H. Petersen Eds. Cham: Springer International Publishing, 2016, pp. 99-136.

[142] P. Nemtsas, E. Wettwer, T. Christ, G. Weidinger, and U. Ravens, "Adult zebrafish heart as a model for human heart? An electrophysiological study," *Journal of Molecular and Cellular Cardiology,* vol. 48, no. 1, pp. 161-171, 2010/01/01/ 2010, doi: https://doi.org/10.1016/j.yjmcc.2009.08.034.

[143] M. H. Lin *et al.*, "Development of a rapid and economic in vivo electrocardiogram platform for cardiovascular drug assay and electrophysiology research in adult zebrafish," *Scientific Reports,* Article vol. 8, no. 1, 2018, Art no. 15986, doi: 10.1038/s41598-018-33577-7.

[144] G. H. Chaudhari, K. S. Chennubhotla, K. Chatti, and P. Kulkarni, "Optimization of the adult zebrafish ECG method for assessment of drug-induced QTc prolongation," *Journal of Pharmacological and Toxicological Methods,* vol. 67, no. 2, pp. 115-120, 2013/03/01/ 2013, doi: https://doi.org/10.1016/j.vascn.2013.01.007.

[145] C. C. Liu, L. Li, Y. W. Lam, C. W. Siu, and S. H. Cheng, "Improvement of surface ECG recording in adult zebrafish reveals that the value of this model exceeds our expectation," *Scientific Reports,* Article vol. 6, 2016, Art no. 25073, doi: 10.1038/srep25073.

[146] M. R. Stoyek, E. A. Rog-Zielinska, and T. A. Quinn, "Age-associated changes in electrical function of the zebrafish heart," *Progress in Biophysics and Molecular Biology,* vol. 138, pp. 91-104, 2018/10/01/ 2018, doi: https://doi.org/10.1016/j.pbiomolbio.2018.07.014.

[147] M. Lenning *et al.*, "Real-time monitoring and analysis of zebrafish electrocardiogram with anomaly detection," *Sensors (Switzerland),* Article vol. 18, no. 1, 2018, Art no. 61, doi: 10.3390/s18010061.

[148] F. Yu *et al.*, "Flexible microelectrode arrays to interface epicardial electrical signals with intracardial calcium transients in zebrafish hearts," *Biomedical Microdevices,* vol. 14, no. 2, pp. 357-366, 2012/04/01 2012, doi: 10.1007/s10544-011-9612-9.

[149] S.-J. Cho *et al.*, "Zebrafish as an animal model in epilepsy studies with multichannel EEG recordings," *Scientific Reports,* vol. 7, no. 1, p. 3099, 2017/06/08 2017, doi: 10.1038/s41598-017-03482-6.

[150] T. Le *et al.*, "Continuous Electrocardiogram Monitoring in Zebrafish with Prolonged Mild Anesthesia," in *2020 42nd Annual International Conference of the IEEE*

Engineering in Medicine & Biology Society (EMBC), 20-24 July 2020 2020, pp. 2610-2613, doi: 10.1109/EMBC44109.2020.9175576.

[151] J. E. Tisdale *et al.*, "Drug-induced arrhythmias: a scientific statement from the American Heart Association," *Circulation,* vol. 142, no. 15, pp. e214-e233, 2020.

[152] S. Nagasawa *et al.*, "Relationship between KCNQ1 (LQT1) and KCNH2 (LQT2) gene mutations and sudden death during illegal drug use," *Scientific reports,* vol. 8, no. 1, p. 8443, 2018.

[153] T. Le *et al.*, "Acquisition, processing and analysis of electrocardiogram in awake zebrafish," *IEEE sensors journal,* vol. 19, no. 11, pp. 4283-4289, 2019.

[154] F. Shaffer and J. P. Ginsberg, "An overview of heart rate variability metrics and norms," *Frontiers in public health,* vol. 5, p. 258, 2017.

[155] P. Bulić, G. Kojek, and A. Biasizzo, "Data Transmission Efficiency in Bluetooth Low Energy Versions," *Sensors,* vol. 19, no. 17, p. 3746, 2019. [Online]. Available: https://www.mdpi.com/1424-8220/19/17/3746.

[156] M. Maricondi-Massari, A. Kalinin, M. Glass, and F. Rantin, "The effects of temperature on oxygen uptake, gill ventilation and ECG waveforms in the Nile tilapia, Oreochromis niloticus," *Journal of Thermal Biology,* vol. 23, no. 5, pp. 283-290, 1998.

[157] M. Matthews and Z. M. Varga, "Anesthesia and euthanasia in zebrafish," *ILAR journal,* vol. 53, no. 2, pp. 192-204, 2012.

[158] A. L. George, "Inherited disorders of voltage-gated sodium channels," *The Journal of clinical investigation,* vol. 115, no. 8, pp. 1990-1999, 2005.

[159] A. Mente *et al.*, "PURE, EPIDREAM and ONTARGET/TRANSCEND Investigators. Associations of urinary sodium excretion with cardiovascular events in individuals

with and without hypertension: a pooled analysis of data from four studies," *Lancet,* vol. 388, no. 10043, pp. 465-475, 2016.

[160] C. ANTZELEVITCH, "Brugada Syndrome," *Pacing and Clinical Electrophysiology,* vol. 29, no. 10, pp. 1130-1159, 2006, doi: https://doi.org/10.1111/j.1540-8159.2006.00507.x.

[161] Y. Mizusawa and A. A. Wilde, "Brugada syndrome," *Circulation: Arrhythmia and Electrophysiology,* vol. 5, no. 3, pp. 606-616, 2012.

[162] D. Darbar *et al.*, "Cardiac sodium channel (SCN5A) variants associated with atrial fibrillation," *Circulation,* vol. 117, no. 15, pp. 1927-1935, 2008.

[163] M. Liu, K.-C. Yang, and S. C. Dudley Jr, "Cardiac sodium channel mutations: why so many phenotypes?," *Nature Reviews Cardiology,* vol. 11, no. 10, pp. 607-615, 2014.

[164] W. P. McNair *et al.*, "SCN5A mutations associate with arrhythmic dilated cardiomyopathy and commonly localize to the voltage-sensing mechanism," *Journal of the American College of Cardiology,* vol. 57, no. 21, pp. 2160-2168, 2011.

[165] T. P. Nguyen, D. W. Wang, T. H. Rhodes, and A. L. George Jr, "Divergent biophysical defects caused by mutant sodium channels in dilated cardiomyopathy with arrhythmia," *Circulation research,* vol. 102, no. 3, pp. 364-371, 2008.

[166] H. Zulkifly, G. Y. H. Lip, and D. A. Lane, "Epidemiology of atrial fibrillation," *International Journal of Clinical Practice,* vol. 72, no. 3, p. e13070, 2018, doi: https://doi.org/10.1111/ijcp.13070.

[167] C. Ferreira, R. Providência, M. J. Ferreira, and L. M. Gonçalves, "Atrial Fibrillation and Non-cardiovascular Diseases: A Systematic Review," (in eng

por), *Arq Bras Cardiol,* vol. 105, no. 5, pp. 519-26, Nov 2015, doi: 10.5935/abc.20150142.

[168] Z. Hu, L. Ding, and Y. Yao, "Atrial fibrillation: mechanism and clinical management," (in eng), *Chin Med J (Engl),* vol. 136, no. 22, pp. 2668-2676, Nov 20 2023, doi: 10.1097/cm9.0000000000002906.

[169] S. Babapoor-Farrokhran, R. T. Rasekhi, D. Gill, S. Babapoor, and A. Amanullah, "Arrhythmia in COVID-19," *SN Comprehensive Clinical Medicine,* vol. 2, no. 9, pp. 1430-1435, 2020/09/01 2020, doi: 10.1007/s42399-020-00454-2.

[170] C. D. Koopman *et al.*, "The zebrafish grime mutant uncovers an evolutionarily conserved role for Tmem161b in the control of cardiac rhythm," *Proceedings of the National Academy of Sciences,* vol. 118, no. 9, p. e2018220118, 2021, doi: doi:10.1073/pnas.2018220118.

[171] D. J. Milan, I. L. Jones, P. T. Ellinor, and C. A. MacRae, "In vivo recording of adult zebrafish electrocardiogram and assessment of drug-induced QT prolongation," (in eng), *Am J Physiol Heart Circ Physiol,* vol. 291, no. 1, pp. H269-73, Jul 2006, doi: 10.1152/ajpheart.00960.2005.

[172] Y. Octavia, C. G. Tocchetti, K. L. Gabrielson, S. Janssens, H. J. Crijns, and A. L. Moens, "Doxorubicin-induced cardiomyopathy: from molecular mechanisms to therapeutic strategies," (in eng), *J Mol Cell Cardiol,* vol. 52, no. 6, pp. 1213-25, Jun 2012, doi: 10.1016/j.yjmcc.2012.03.006.

[173] P. K. Singal and N. Iliskovic, "Doxorubicin-induced cardiomyopathy," (in eng), *N Engl J Med,* vol. 339, no. 13, pp. 900-5, Sep 24 1998, doi: 10.1056/nejm199809243391307.

[174] A. Z. Luu, B. Chowdhury, M. Al-Omran, H. Teoh, D. A. Hess, and S. Verma, "Role of Endothelium in Doxorubicin-Induced Cardiomyopathy," (in eng), *JACC Basic Transl Sci,* vol. 3, no. 6, pp. 861-870, Dec 2018, doi: 10.1016/j.jacbts.2018.06.005.

[175] F. Yu Anthony, T. Chan Angel, and M. Steingart Richard, "Cardiac Magnetic Resonance and Cardio-Oncology," *Journal of the American College of Cardiology,* vol. 73, no. 7, pp. 792-794, 2019/02/26 2019, doi: 10.1016/j.jacc.2018.11.045.

[176] N. Koleini, B. E. Nickel, A. L. Edel, R. R. Fandrich, A. Ravandi, and E. Kardami, "Oxidized phospholipids in Doxorubicin-induced cardiotoxicity," *Chemico-Biological Interactions,* vol. 303, pp. 35-39, 2019/04/25/ 2019, doi: https://doi.org/10.1016/j.cbi.2019.01.032.

[177] S. Sritharan and N. Sivalingam, "A comprehensive review on time-tested anticancer drug doxorubicin," (in eng), *Life Sci,* vol. 278, p. 119527, Aug 1 2021, doi: 10.1016/j.lfs.2021.119527.

[178] J. V. McGowan, R. Chung, A. Maulik, I. Piotrowska, J. M. Walker, and D. M. Yellon, "Anthracycline Chemotherapy and Cardiotoxicity," (in eng), *Cardiovasc Drugs Ther,* vol. 31, no. 1, pp. 63-75, Feb 2017, doi: 10.1007/s10557-016-6711-0.

[179] K. Johnson-Arbor and R. Dubey, *Doxorubicin*. Treasure Island (Fl): StatPearls Publishing (Internet), 2023.

[180] X. Ma, Y. Ding, Y. Wang, and X. Xu, "A Doxorubicin-induced Cardiomyopathy Model in Adult Zebrafish," (in eng), *J Vis Exp,* no. 136, Jun 7 2018, doi: 10.3791/57567.

[181] X. Xu, H. Zhang, J. Li, M. Moossavi, and F. Yan, "An Intraperitoneal Injection Technique in Adult Zebrafish that Minimizes Body Damage and Associated Mortality," *JoVE,* no. 205, p. e66500, 2024/03/29 2024, doi: doi:10.3791/66500.

[182] C. A. Lessman, "The developing zebrafish (Danio rerio): a vertebrate model for high-throughput screening of chemical libraries," (in eng), *Birth Defects Res C Embryo Today,* vol. 93, no. 3, pp. 268-80, Sep 2011, doi: 10.1002/bdrc.20212.

[183] E. W. Mackay, A. Apschner, and S. Schulte-Merker, "A bone to pick with zebrafish," (in eng), *Bonekey Rep,* vol. 2, p. 445, Nov 13 2013, doi: 10.1038/bonekey.2013.179.

[184] J. M. Taylor *et al.*, "Hybrid optical gating for long-term 3D time-lapse imaging of the beating embryonic zebrafish heart," *bioRxiv,* p. 526830, 2019, doi: 10.1101/526830.

[185] M. Merlo, A. Cannata, M. Gobbo, D. Stolfo, P. M. Elliott, and G. Sinagra, "Evolving concepts in dilated cardiomyopathy," *European journal of heart failure,* vol. 20, no. 2, pp. 228-239, 2018.

[186] R. E. Hershberger, D. J. Hedges, and A. Morales, "Dilated cardiomyopathy: the complexity of a diverse genetic architecture," *Nature reviews cardiology,* vol. 10, no. 9, pp. 531-547, 2013.

[187] F. C. Wheeler, L. Fernandez, K. M. Carlson, M. J. Wolf, H. A. Rockman, and D. A. Marchuk, "QTL mapping in a mouse model of cardiomyopathy reveals an ancestral modifier allele affecting heart function and survival," *Mammalian genome,* vol. 16, pp. 414-423, 2005.

[188] T. Hoage, Y. Ding, and X. Xu, "Quantifying cardiac functions in embryonic and adult zebrafish," *Methods Mol Biol,* vol. 843, pp. 11-20, 2012, doi: 10.1007/978-1-61779-523-7_2.

[189] Z. Chen, W. Huang, T. Dahme, W. Rottbauer, M. J. Ackerman, and X. Xu, "Depletion of zebrafish essential and regulatory myosin light chains reduces cardiac function through distinct mechanisms," *Cardiovasc Res,* vol. 79, no. 1, pp. 97-108, 2008.

[190] S. Nasrat, D. Marcato, S. Hirth, M. Reischl, and C. Pylatiuk, "Semi-automated detection of fractional shortening in zebrafish embryo heart videos," *Current Directions in Biomedical Engineering,* vol. 2, no. 1, pp. 233-236, 2016.

[191] A. A. Akerberg, C. E. Burns, C. G. Burns, and C. Nguyen, "Deep learning enables automated volumetric assessments of cardiac function in zebrafish," *Disease models & mechanisms,* vol. 12, no. 10, p. dmm040188, 2019.

[192] W.-Y. Huang, J. Aramburu, P. S. Douglas, and S. Izumo, "Transgenic expression of green fluorescence protein can cause dilated cardiomyopathy," *Nature medicine,* vol. 6, no. 5, pp. 482-483, 2000.

[193] O. Ronneberger, P. Fischer, and T. Brox, "U-net: Convolutional networks for biomedical image segmentation," in *Medical image computing and computer-assisted intervention–MICCAI 2015: 18th international conference, Munich, Germany, October 5-9, 2015, proceedings, part III 18*, 2015: Springer, pp. 234-241.

[194] C. Decourt and L. Duong, "Semi-supervised generative adversarial networks for the segmentation of the left ventricle in pediatric MRI," *Computers in Biology and Medicine,* vol. 123, p. 103884, 2020.

[195] J. Canny, "A computational approach to edge detection," *IEEE Transactions on pattern analysis and machine intelligence,* no. 6, pp. 679-698, 1986.

[196] G. Stockman and L. G. Shapiro, *Computer vision*. Prentice Hall PTR, 2001.

[197] N. Otsu, "A threshold selection method from gray-level histograms," *Automatica,* vol. 11, no. 285-296, pp. 23-27, 1975.

[198] K. Zuiderveld, "Contrast limited adaptive histogram equalization," in *Graphics gems IV*, 1994, pp. 474-485.

[199] S. Jadon, "A survey of loss functions for semantic segmentation," in *2020 IEEE conference on computational intelligence in bioinformatics and computational biology (CIBCB)*, 2020: IEEE, pp. 1-7.

[200] J. M. Bland and D. Altman, "Statistical methods for assessing agreement between two methods of clinical measurement," *The lancet,* vol. 327, no. 8476, pp. 307-310, 1986.

[201] Y. Bromberg, "Chapter 15: disease gene prioritization," (in eng), *PLoS Comput Biol,* vol. 9, no. 4, p. e1002902, Apr 2013, doi: 10.1371/journal.pcbi.1002902.

[202] S. J. Cho, T. S. Nam, D. Byun, S. Y. Choi, M. K. Kim, and S. Kim, "Zebrafish needle EMG: a new tool for high-throughput drug screens," (in eng), *J Neurophysiol,* vol. 114, no. 3, pp. 2065-70, Sep 2015, doi: 10.1152/jn.00538.2015.

[203] B. P. Grone and S. C. Baraban, "Animal models in epilepsy research: legacies and new directions," *Nature Neuroscience,* vol. 18, no. 3, pp. 339-343, 2015/03/01 2015, doi: 10.1038/nn.3934.

[204] F. Yang, C. Gao, P. Wang, G. J. Zhang, and Z. Chen, "Fish-on-a-chip: microfluidics for zebrafish research," (in eng), *Lab Chip,* vol. 16, no. 7, pp. 1106-25, Apr 7 2016, doi: 10.1039/c6lc00044d.

[205] A. J. Sehnert and D. Y. R. Stainier, "A window to the heart: can zebrafish mutants help us understand heart disease in humans?," *Trends in Genetics,* vol. 18, no. 10, pp. 491-494, 2002/10/01/ 2002, doi: https://doi.org/10.1016/S0168-9525(02)02766-X.

[206] C. T. Nguyen, Q. Lu, Y. Wang, and J.-N. Chen, "Zebrafish as a model for cardiovascular development and disease," (in eng), *Drug Discov Today Dis Models,* vol. 5, no. 3, pp. 135-140, Fall 2008, doi: 10.1016/j.ddmod.2009.02.003.

[207] T. J. Chico, P. W. Ingham, and D. C. Crossman, "Modeling cardiovascular disease in the zebrafish," (in eng), *Trends Cardiovasc Med,* vol. 18, no. 4, pp. 150-5, May 2008, doi: 10.1016/j.tcm.2008.04.002.

[208] T. Dahme, H. A. Katus, and W. Rottbauer, "Fishing for the genetic basis of cardiovascular disease," (in eng), *Dis Model Mech,* vol. 2, no. 1-2, pp. 18-22, Jan-Feb 2009, doi: 10.1242/dmm.000687.

[209] J. Bakkers, "Zebrafish as a model to study cardiac development and human cardiac disease," (in eng), *Cardiovasc Res,* vol. 91, no. 2, pp. 279-288, 2011, doi: 10.1093/cvr/cvr098.

[210] D. Y. R. Stainier, "Zebrafish genetics and vertebrate heart formation," *Nature Reviews Genetics,* vol. 2, no. 1, pp. 39-48, 2001/01/01 2001, doi: 10.1038/35047564.

[211] D. Staudt and D. Stainier, "Uncovering the molecular and cellular mechanisms of heart development using the zebrafish," (in eng), *Annu Rev Genet,* vol. 46, pp. 397-418, 2012, doi: 10.1146/annurev-genet-110711-155646.

[212] B. Pelster and W. W. Burggren, "Disruption of hemoglobin oxygen transport does not impact oxygen-dependent physiological processes in developing embryos of zebra fish (Danio rerio)," (in eng), *Circ Res,* vol. 79, no. 2, pp. 358-62, Aug 1996, doi: 10.1161/01.res.79.2.358.

[213] T. Schwerte, C. Prem, A. Mairösl, and B. Pelster, "Development of the sympatho-vagal balance in the cardiovascular system in zebrafish (Danio rerio) characterized by power spectrum and classical signal analysis," (in eng), *J Exp Biol,* vol. 209, no. Pt 6, pp. 1093-100, Mar 2006, doi: 10.1242/jeb.02117.

[214] C. G. Burns, D. J. Milan, E. J. Grande, W. Rottbauer, C. A. MacRae, and M. C. Fishman, "High-throughput assay for small molecules that modulate zebrafish embryonic heart rate," *Nature Chemical Biology,* vol. 1, no. 5, pp. 263-264, 2005/10/01 2005, doi: 10.1038/nchembio732.

[215] A. S. Forouhar, J. R. Hove, C. Calvert, J. Flores, H. Jadvar, and M. Gharib, "Electrocardiographic Characterization of Embryonic Zebrafish," in *The 26th Annual International Conference of the IEEE Engineering in Medicine and Biology Society*, 1-5 Sept. 2004 2004, vol. 2, pp. 3615-3617, doi: 10.1109/IEMBS.2004.1404016.

[216] P. K. Chan, C. C. Lin, and S. H. Cheng, "Noninvasive technique for measurement of heartbeat regularity in zebrafish (Danio rerio) embryos," *BMC Biotechnology,* vol. 9, no. 1, p. 11, 2009/02/19 2009, doi: 10.1186/1472-6750-9-11.

[217] M. Liebling *et al.*, "Rapid three-dimensional imaging and analysis of the beating embryonic heart reveals functional changes during development," (in eng), *Dev Dyn,* vol. 235, no. 11, pp. 2940-8, Nov 2006, doi: 10.1002/dvdy.20926.

[218] Y. M. Bradford *et al.*, "Zebrafish information network, the knowledgebase for Danio rerio research," *Genetics,* vol. 220, no. 4, p. iyac016, 2022, doi: 10.1093/genetics/iyac016.

[219] C. B. Kimmel, W. W. Ballard, S. R. Kimmel, B. Ullmann, and T. F. Schilling, "Stages of embryonic development of the zebrafish," (in eng), *Dev Dyn,* vol. 203, no. 3, pp. 253-310, Jul 1995, doi: 10.1002/aja.1002030302.

[220] F. Yu *et al.*, "Evolving cardiac conduction phenotypes in developing zebrafish larvae: implications to drug sensitivity," (in eng), *Zebrafish,* vol. 7, no. 4, pp. 325-31, Dec 2010, doi: 10.1089/zeb.2010.0658.

[221] H.-C. Lee *et al.*, "Amiodarone Induces Overexpression of Similar to Versican b to Repress the EGFR/Gsk3b/Snail Signaling Axis during Cardiac Valve Formation of Zebrafish Embryos," *PLOS ONE,* vol. 10, no. 12, p. e0144751, 2015, doi: 10.1371/journal.pone.0144751.

[222] Y.-H. Chen *et al.*, "The toxic effect of Amiodarone on valve formation in the developing heart of zebrafish embryos," *Reproductive Toxicology,* vol. 33, no. 2, pp. 233-244, 2012/04/01/ 2012, doi: https://doi.org/10.1016/j.reprotox.2011.12.008.